Discrete Modeling of Heat Conduction in Granular Media

by

Watson L. Vargas-Escobar

B.S. in Ch. E., University of America, Colombia 1992

M.Sc. in Ch. E., Colombia National University, 1995

Submitted to the Graduate Faculty
of the School of Engineering
in partial fulfillment of
the requirement for the degree of
Doctor
of
Philosophy

University of Pittsburgh

2002

The author grants permission
to reproduce single copies.

_____

Signed

"We are obliged by the deepest drives of the human spirit to make ourselves more than animated dust, and we must have a story to tell about where we come from, and why we are here."

E. O. Wilson(1998)

COMMITTEE SIGNATURE PAGE

This dissertation was presented

by

Watson L. Vargas-Escobar

It was defended on

March 7, 2002

and approved by

Committee Chair
Joseph. J. McCarthy, Ph.D.

Committee Member
Luis E. Vallejo, Ph.D.

Committee Member
J. Karl Johnson , Ph.D.

Committee Member
Robert S. Parker, Ph.D.

ACKNOWLEDGMENTS

To my wife Rubby; for understanding that science, family, conversation, the practical, the abstract, the trivial and the deep are all one and the same –*life*.

ABSTRACT

Signature _____

J. J. McCarthy, Ph.D.

Discrete Modeling of Heat Conduction in Granular Media

Watson L. Vargas-Escobar , Ph.D.

University of Pittsburgh

This thesis addresses heat conduction in granular systems both under static and slow flow conditions with and without the presence of a stagnant interstitial fluid. A novel discrete simulation technique for granular heat transfer, the Thermal Particle Dynamics (TPD) method has been developed. By modeling particle-particle interactions, bed heterogeneities – *e.g.*, mechanical and thermal – are directly accounted for and transient temperature distributions are obtained at the particle level. This technique, based on the Discrete Element Method, not only sheds light on fundamental issues in heat conduction in particulate systems, but also provides a valuable test-bed for existing continuous theories. Computational results, as well as supporting experiments coupled with existing theoretical models are used to probe the validity of the proposed simulation technique.

Studies on heat conduction through static beds of particles indicate that stress and contact heterogeneities – due primarily to the existence of localized "chains" of particles which

support the majority of an imposed load (stress chains) – may cause dramatic changes in the way that heat is transported by conduction. It is found that by matching the microstructure of an experimental system only qualitatively, quantitatively accurate estimates of effective properties are possible, without requiring adjustable parameters. One key result in this study reveals that an important consideration has been missing from previous granular conduction studies – the stress distribution in the particle bed. Extensions of TPD to incorporate the ability to model heat transfer in particulate systems in the presence of an interstitial fluid indicate that a good qualitative and quantitative agreement between measured and calculated values of the effective thermal conductivity for a wide variety of materials in the presence of both liquid and/or gas are possible.

Simulation results for slow granular flows – e.g., a simple shear cell and a rotating drum – indicate that in both cases there is an enhancement of the effective thermal conductivity with increase in the shear/rotation rate due to enhanced mixing of the particles. These results are in agreement with previous theoretical and experimental investigations. In contrast to the behavior found at high shear rates, where the thermal conductivity is proportional to the shear rate, a complex non-linear relation is found for the effective conductivity in granular flows at low shear rates. This observation has not been previously reported. It is argued that a balance between heat conduction and convection is necessary to explain these observations.

DESCRIPTORS

Particle dynamics	Discrete modeling
Heat conduction	Granular media
Effective conductivity	Contact conductance

TABLE OF CONTENTS

Page

LIST OF FIGURES

LIST OF TABLES

NOMENCLATURE

a contact radius $[m]$

c specific heat $[J\,kg^{-1}K^{-1}]$

E Young modulus $[GPa]$

f normalized force, filling degree

F_{ij} fabric tensor

F_n normal force $[N]$

F_t tangential force $[N]$

g gravity $[9.8ms^{-2}]$

I_s intensity of segregation

H wall separation in simple shear cell $[m]$

H_c contact conductance $[Wm^{-2}K^{-1}]$

k thermal conductivity $[Wm^{-1}K^{-1}]$

K_{ij} effective thermal conductivity tensor

k_{mix} rate of mixing constant $[s^{-1}]$

L characteristic length $[m]$

$n_i\,n_j$ vector components

N number of contacts

N_{ij} fabric tensor

Q heat transfer $[Wm^{-1}]$

r particle radius $[m]$

t time $[s]$

T temperature $[^oK]$

U wall velocity $[m\,s^{-1}]$

$u,\ v,\ w$ velocities $[m\,s^{-1}]$

V volume $[m^{-3}]$

$\bar{Z}$ mean coordination number

greek symbols

α thermal diffusivity $[m^2 s^{-1}]$

β arch of length $[m]$

δ overlap $[m]$

ϵ void fraction

ν solid fraction

ρ density $[kg\, m^{-3}]$

Ω rotation rate $[rev\, s^{-1}]$

Θ dimensionless temperature

Υ granular temperature $[m^2 s^{-2}]$

Subscripts

11

12   tensor indexes in fabric tensor

22

c contact

e effective

f fluid

g gas

i particle i

j particle j

l liquid

p particle

s solid

$\perp$ perpendicular

$\parallel$ parallel

ABBREVIATIONS

DEM Discrete Element Method,

MD Molecular Dynamics,

PD Particle Dynamics,

TPD Thermal Particle Dynamics,

1.0   INTRODUCTION

Heterogeneous media, which involve discrete particles, are frequently encountered in different fields of science and industry. These systems may be suspensions, composites, bulk solids, fluidized beds, packed beds, soil, etc. These materials often behave differently from ordinary single phase systems, and their physicochemical and transport properties are of interest in the analysis, design and optimization of industrial processes and in the understanding of natural phenomena. While particle phenomena has been an area of active research since the time of Reynolds [1]*, a solid fundamental understanding of transport in particulate systems is not yet complete. Heat conduction, in particular, is a relevant topic in many different disciplines where knowledge of the thermal conduction phenomena is essential for the analysis of the associated heat transport processes.

At present, some of the most common methods used to study these systems are based on a continuous macroscopic description, which requires the use of effective properties. Unfortunately, the determination of these effective properties is experimentally difficult and sometimes imprecise. Most importantly, the discrete nature of granular media, the fluctuations in the inter-grain force network, and the nonlinear nature of the contact interactions cast doubt on the applicability of the classical methods of homogenization to describe the collective behavior of particles [2].

Although, it is intuitive that the behavior of granular materials depends on phenomena that occur at the particle level, the exact nature of this dependence is yet not well understood [3]. A survey of the literature shows that a description of the heat transport problem from a microscopic or even discrete point of view is possible. In particular, atomic-level molecular dynamics (MD) simulations have shown that this technique is well suited for the study

---

*Bracketed references placed superior to the line of text refer to the bibliography.

of nanoscale phenomena [4, 5, 6, 7]. The problem however, is especially difficult due to the fact that the microstructure of the media, whose description is quite difficult even in the simplest case, may change due to external forces or flow [8].

In this work, an extension of the well-known Particle Dynamics (PD) technique, which we call *Thermal* Particle Dynamics(**TPD**) is introduced. TPD incorporates not only contact mechanics considerations (as does a traditional PD simulation), but also contact conductance models. This concept is similar, in spirit, to recent work by Hunt [9] – who incorporates gas-solid heat transfer into a hard-particle PD model; and Zhuang, Didwania, and Goddard [10] – who include contact conductance considerations into a quasi-static model geared toward measuring granular fabric and effective electrical conductivities. In contrast to both of these previous works, this new simulation technique is capable of yielding particle-level temperatures in static beds of particles and in slow granular flows while maintaining the versatility of a traditional (soft-particle) PD simulation.

This new method has the advantage of being extensible in a variety of ways: incorporation of numerous contact mechanics/conductance models to account for particle roughness, plastic deformation, etc.; inclusion of interstitial fluid effects. In its present form, this technique allows quite detailed temperature measurements which may be useful in evaluating the performance of a variety of applications.

This document is organized as follows. Chapter 2 presents a general overview of the relevant literature. Previous work on heat transfer in granular media, both fundamental and applied, are examined. Also included is a review of microstructure in granular media and a method to quantify this microstructure, namely the fabric tensor. A discussion on contact conductance theories is also covered. Finally, a discussion on heat transfer in slow granular flows is presented. Chapter 3 describes the Thermal Particle Dynamics (**TPD**) technique implementation, beginning with the introduction of the general method and then

extending this same method to incorporate stagnant interstitial fluids. For the sake of complitness, a brief introduction to Particle Dynamics (**PD**) is also covered in this chapter. Applications of the **TPD** technique to static beds of particles is the focus of Chapter 4. Studies under vacuum conditions are presented first, followed by studies that include the presence of stagnant interstitial fluids. Chapter 5 covers dynamic applications of **TPD** in slow granular flows. In particular, a simple shear flow cell and a rotating tumbler, are examined. Chapter 6 closes with a brief summary and discussion of the implications of this work and provides an outlook on future extensions.

2.0   BACKGROUND

Granular materials exhibit a vast array of unusual phenomena which has sparked considerable recent interest [9, 11, 12, 13, 14, 15, 16]. A primary cause of much of this behavior can be traced to the unique nature of particle-particle interactions. Unlike molecular interactions – in the companion cases of fluids or "continuous" solids – particle interactions often introduce new length scales which may create difficulty for continuum modeling of these systems [17]. In particular, particle contact inhomogeneities caused by stress chains[13, 18, 19] have been shown to have a profound effect on the pressure distribution in stacked grains [20], the propagation of sound in granular materials [21], and agglomerate breakage [22]. Stress chains occur in all but the most perfect of crystalline particle packings and often span many particle diameters (even orders of magnitude larger distances than the particle diameter, in certain instances [23]).

Traditional research in the area of granular heat transfer, using the effective medium approximation (EMA), generally provides accurate solutions of steady, averaged temperature profiles using detailed characterization of the microstructure (*e.g.*, for composites/porous materials see Refs. [24, 25]; for granular materials see Refs. [10, 26]) or restrictive simplifying assumptions (e.g., that the material is statistically homogeneous). However, even the simplest case – conduction through the solid phase – presents problems under transient conditions [27, 28, 29] and for the determination of proper boundary conditions [30, 31, 32, 33]. Moreover, it is difficult to discern how or if these methods can be made amenable to situations where the microstructure may change with time in a way which is not known *a priori* – *i.e.*, in a granular flow.

In what follows, a summary of the continuous modeling of heterogeneous media is presented, followed by a discussion of the determination of effective properties and its relation

to microstructural parameters. Heat transfer in packed beds is also presented. Then the role of contact conductance for the description of heat transfer phenomena in particulate matter is addressed. Finally, a discussion of prototypical granular flows closes this chapter.

2.1 Continuous modeling of heterogeneous media

In a traditional continuum approach, the partial differential equations governing the transport process under consideration are solved, subject to the appropriate boundary and initial conditions [34], by means of analytical or numerical techniques. When applicable, the continuous approach provides the simplest method of description. From a continuum point of view, two main theories are used to describe transport processes, *the micro-transport theory* and the so called *macro-transport theory*. In what follows a brief review of these two theories is presented.

2.1.1 Microscopic description

The microscopic approach is exemplified in the textbook by Bird *et al.* [35]. This theory calls for an *a priori* knowledge of the phenomenological coefficients (i.e., thermal diffusivity) in order to solve the partial differential equations. Various methods have been developed for relating the macro-transport behavior and properties of a system to its microstructure or micro-transport characteristics (see Slattery [36] for a review). These methods include *homogenization techniques, statistical averaging, ensemble averaging, volume averaging* and *effective medium approaches* among others [8, 25, 34, 37].

Most common among these methods is the *effective medium approach.* In this approach, the heterogeneous system is replaced by a homogeneous effective medium whose conductance between neighboring particles or sites is the same [27, 29, 38]. In a microscopically heterogeneous medium, however, the properties are expected to vary from point to point.

Provided this microscopic variation is sufficiently rapid compared to a relevant macroscopic length scale (i.e., the length of the bed) and has spatially independent mean, it is expected that, for purposes of calculating scalar transport, the medium can be represented by an effective homogeneous system with locally uniform properties [29].

The heat transport in a heterogeneous system is described, according to the EMA approach, by the classical continuum equation

$$\frac{\partial T}{\partial t} = \alpha_{eff}\nabla^2 T \qquad (2\text{-}1)$$

where T is the mean temperature of the system and α_{eff} is the effective thermal diffusivity. Strictly speaking, one cannot define the effective thermal diffusivity as a characteristic property of a heterogeneous material since Eq. 2-1 in which the thermal diffusivity appears as a characteristic constant applies only to "homogeneous" systems [39, 40, 41].

The main advantage of considering a heterogeneous material as homogeneous is that all the tools and methods developed for continuous and homogeneous systems can be used. The idea has a sound mathematical basis and can be used with confidence in most common applications. Unfortunately, for unsteady processes such confidence is not possible, specially at shorter times or for steep gradients of the temperature field [29, 42]. For rapid variations, according to Goddard [29] and Quintard *et al.* [43], it is expected that this approximation will fail, due to the thermal relaxation time introduced by the finite heat propagation velocity. The concept of a finite heat propagation velocity has been the subject of numerous studies in which its thermodynamic and experimental validity has been assessed [44, 45, 46, 47]. Several theoretical studies [27, 29, 48, 49, 50, 51] and experimental observations [42, 52, 53] have shown that continuous theories are unable to capture the behavior of heterogeneous systems under transient conditions. A typical example where an effective approach

may not be applicable is Combustion Synthesis (CS) for the manufacture of advanced materials. In this process, temporal gradients of temperature on the order of $150 \times 10^3 \ [^oC/s]$ are common [54, 52, 55, 56].

2.1.2 Macroscopic description

In the macroscopic description of heat transfer in heterogeneous media, the diffusion process in the medium is analyzed using an up-scaling method, in which the local phenomena at the microscopic level are described at the macroscopic scale by an effective thermal dispersion tensor [57]. The theory of macro-transport processes, as described by Brenner and collaborators [34, 48, 49, 58], represents a new paradigm among the traditional approaches of continuous theories, for rigorously obtaining macro-scale properties of heterogeneous systems. Based on the concept of moments, this mathematical technique was first developed by Aris [59], extended by Horn [60] and later generalized by Brenner [58, 61]. This paradigm extends the intuitive observations originally presented by Taylor [62, 63] on so-called Taylor dispersion which accounts for the diffusion of fluid molecules across streamlines. For a complete description of the foundations of the theory, and specific applications the reader is referred to the textbook by Brenner and Edwards [34].

Despite the introduction of this new formalism for heat transfer, Batycky and Brenner [48, 49] – using the so called macro-scale formulation scheme – found that it is (still) necessary to use fictitious initial conditions in order to capture transient heat conduction phenomena in a composite medium, at short times. Batycky and Brenner solved several elementary transient heat conduction problems and demonstrated that when the system losses heat a fictitious initial temperature is required in order to describe the behavior. This fact seems not to be surprising since many studies, as indicated in the previous section, have indicated that matching a heterogeneous medium with an homogeneous one induces *memory effects* –a "time-lag" or history effect– due to internal relaxation processes [27, 29, 50, 64, 65, 66]. It

is well known, however, that the effective medium approximation is valid for fairly long times, once the transient part has been dropped [48, 53].

2.1.3 Effective conductivity of heterogeneous media

Effective properties are the key factor for modeling heterogeneous media using either of the continuum approaches described above. Consequently, a large body of literature has been devoted to this single topic. In particular, for porous and/or granular materials there are generally three methods to obtain the effective conductivity; from a theoretical standpoint it is possible to either idealize the system as being composed of ordered arrays that can be described in terms of a repeating unit cell [67, 68] or simulating disordered arrangements by statistical means, using correlation functions. The last method involves using empirical correlations.

The first theoretical approach of the two mentioned above, yields estimated values of the effective properties of the granular or porous material. This technique uses the solution for some simple unit of the composite (for example, a single particle within a matrix) to scale up to a macroscopic value (for a numerical study that uses this approach see Lee *et al.* [69]). Alternatively, an exact value of the effective conductivity can be obtained for a certain class of problems where there is a well known, periodic micro-structure (e.g., a close-packed bed of spheres in a matrix [67]). In either case, knowledge of the basic cell solution – or contact conductance problem (see Section 2.3.2) – needs to be known.

Rigorous bounding methods, a statistical technique, relies on differing levels of information about the micro-structure. The most simple example of applying this technique is attributed to Maxwell [70]. In Maxwell's solution, an upper bound is calculated from the

assumption that the phases are everywhere in parallel relative to the direction of the heat flow, such that

$$k_{e_U} = \epsilon \cdot (k_f) + (1 - \epsilon) \cdot k_s, \qquad (2\text{-}2)$$

where k_{e_U} is the upper bound on the effective conductivity, ϵ is the void fraction, and k_f, k_s are the conductivities of the fluid and the solid, respectively. The lower bound in this case corresponds to all phases being in series, such that

$$k_{e_L} = \frac{k_s \cdot k_f}{\epsilon \cdot k_s + (1 - \epsilon) \cdot k_f}. \qquad (2\text{-}3)$$

The bounds become considerably more precise if more detailed knowledge of the micro-structure is available; however, quantifying micro-structure is an entire field of study in its own right [24] and won't be discussed here. Extensive reviews of the literature on this subject along with a number of correlations and their range of applicability are provided by Torquato [25], Kaviany [71], Cheng and Hsu [72], and Tavman [73]. A comprehensive review of the estimation of effective conductivity in the context of suspensions and structured liquids is provided by Dutta and Mashelkar [74].

Application of many of the expressions for the effective conductivity obtained using either of the methods described above is limited because of the difficulty involved in determining the statistical quantities therein [25]. Thus, numerous analytical and empirical models have been developed for calculating the effective thermal conductivity of packed beds with and without the presence of a stagnant fluid [71,72]. However, none of these correlations give consistent values of the fitting parameters when applied to heterogeneous systems [75]. Although thermal contact conductance is recognized as important, its effects are not included in most of the correlations reviewed. Recently, Molerus [76] has shown, by

analyzing experimental measurements published in the literature, that contact conductance is the decisive factor for the heat transfer between particles in contact or between a heating surface and a particle in a moving bed of particles filled with a stagnant fluid.

For granular materials under loading, the magnitude of the effective conductivity depends on the surface roughness, the type of material, and the interface pressure. In particular, the effective conductivity is strongly influenced by the contact mechanics of the surfaces in contact. The contact area varies according to the deformations which can be elastic, plastic or elasto-plastic [77]. For elastic deformations of the asperities in the contact area between cylinders and spheres under loading, Buonanno and Carotenuto [77,78] have shown that the effective conductivity not only depends on the dimensions of the contact area, but also on the orientation of these areas compared to the temperature gradient. The effects of contact deformation on the estimation of effective conductivity, have also been studied by Zinchenko [79], Wu *et al.* [80] and Siu *et al.* [81].

2.2 Microstructural Fabric and Effective Thermal Conductivity

The microstructure of a granular medium is the main feature that differentiates these heterogeneous materials from their homogeneous counterparts. Description of the microstructure is therefore an important element in determining the effective properties of heterogeneous media [82,83]. In continuum modeling of granular mechanics, it has been long realized that microstructural details (specifically, the anisotropy of the packing) is one of the fundamental aspects to be taken into account for a better understanding of the properties of the granular media [26,84]. The structural anisotropy of granular packings may

be quantified by a fabric tensor, F_{ij} [26, 85, 86], based on contact-plane normal vectors, $\mathbf{n}$, where

$$F_{ij} = \int_{\Omega} n_i n_j E(\mathbf{n}) d\Omega \qquad (i, j = 1, 2, 3), \tag{2-4}$$

in which $n_i (i = 1, 2, 3)$ are the components of the vector $\mathbf{n}$, Ω is the solid angle representing the surface of the particle, and $E(\mathbf{n})$ is the probability distribution of contact normals which satisfies

$$\int_{\Omega} E(\mathbf{n}) d\Omega = 1 \quad and \quad E(\mathbf{n}) = E(-\mathbf{n}). \tag{2-5}$$

The distribution function of inter-particle contacts, $E(\mathbf{n})$, may then be approximated as a truncated expansion in terms of the fabric tensor, F_{ij} [87, 88] to yield

$$E(\mathbf{n}) = \frac{1}{\Omega_{max}} [1 + F_{ij} n_i n_j], \tag{2-6}$$

where Ω_{max} is 4π for three dimensional systems, and 2π for two dimensional systems.

The fabric tensor, F_{ij}, may then be written for the three dimensional system as

$$F_{ij} = \frac{15}{2} [N_{ij} - \frac{1}{5} \delta_{ij}], \tag{2-7}$$

and for the two dimensional system as

$$F_{ij} = 4 [N_{ij} - \frac{1}{4} \delta_{ij}], \tag{2-8}$$

where

$$N_{ij} = \langle n_i n_j \rangle, \tag{2-9}$$

δ_{ij} is the Kronecker delta, and $\langle . \rangle$ designates an ensemble average, i.e. $\langle n_i n_j \rangle = \frac{1}{N} \sum_{c=1}^{N} n_i n_j$, with N being the total number of contacts.

In a two dimensional system $\mathbf{n}$ may be expressed in terms of $\cos(\theta)$ and $\sin(\theta)$, where θ is an inclination angle of the unit vector $\mathbf{n}$ relative to some reference axis, $\mathbf{x}$. The components of N_{ij}, therefore, may be written as follows [84]:

$$N_{11} = \frac{1}{N} \sum_{c=1}^{N} \sin^2(\theta)^{(c)} \tag{2-10}$$

$$N_{12} = \frac{1}{N} \sum_{c=1}^{N} \sin(\theta)^{(c)} \cos(\theta)^{(c)} \tag{2-11}$$

$$N_{22} = \frac{1}{N} \sum_{c=1}^{N} \cos^2(\theta)^{(c)}. \tag{2-12}$$

These components can be converted to two principal values N_1 and N_2 by:

$$[N_1, N_2] = \frac{1}{2}(N_{11} + N_{22}) \pm \left[\frac{1}{4}(N_{11} - N_{22})^2 + N_{12}^2 \right]^{1/2}. \tag{2-13}$$

The corresponding principal directions θ_1 and θ_2 can be estimated as

$$[\theta_1, \theta_2] = \theta_o \pm \frac{1}{2} \arctan \frac{2N_{12}}{N_{22} - N_{11}}, \tag{2-14}$$

where θ_o is the angle of the principal axis. A graphical representation of the anisotropy of a granular packing may then be obtained by plotting the corresponding approximated

distribution $E(\theta)$ – obtained from the expansion in Eqn. 2-6 – on a rose diagram (i.e., Figure 2.1) by the expression [87]

$$E(\theta) \;=\; \frac{1}{2\pi}\left[1 + (1 - F_{11})\cos(2\theta) + F_{12}\sin(2\theta)\right]. \tag{2-15}$$

Although researchers have indicated the importance of the structure of the bed [31, 89, 90], incorporating its effects into the evaluation of effective properties, have proved to be a formidable task. The complexity of the problem is such that most of the approaches to date favor the evaluation of isolated effects [91]. Heat transfer in fixed beds is a typical example. Heat conduction in this systems has usually been studied and evaluated separately of convective effects, the contributions are then added to account for the global process [30, 92, 93, 94].

Studies which incorporate the structure of the bed into the estimation of the effective properties are sparse. Cheng, Yu and Zulli [31] recently applied the concept of the so-called Voronoi tessellation in an effort to incorporate the structure of the bed into the estimation of effective thermal conductivity of packed beds. This technique has been previously used by some other investigators (see for example Sahimi and Tsotsis [27] and the references therein). In Cheng's study the effective thermal conductivity and the heat flux of a packed bed of mono-sized spheres, in the presence of a stagnant fluid was determined. The results indicated that the packing structure plays a vital role in the quantification of effective properties.

In this same line of reasoning, Zhuang [95] developed a quasi-static model to prove electric conductance in granular media. Once again, a strong correlation between the effective electrical conductivity, the stress and the fabric tensor was found in this study. Despite this fact, few correlations for the effective properties of granular materials explicitly include the fabric. A notable exception is the correlation proposed by Jagota and Hui [96]. For packings

Isotropic

(a)

Anisotropic

(b)
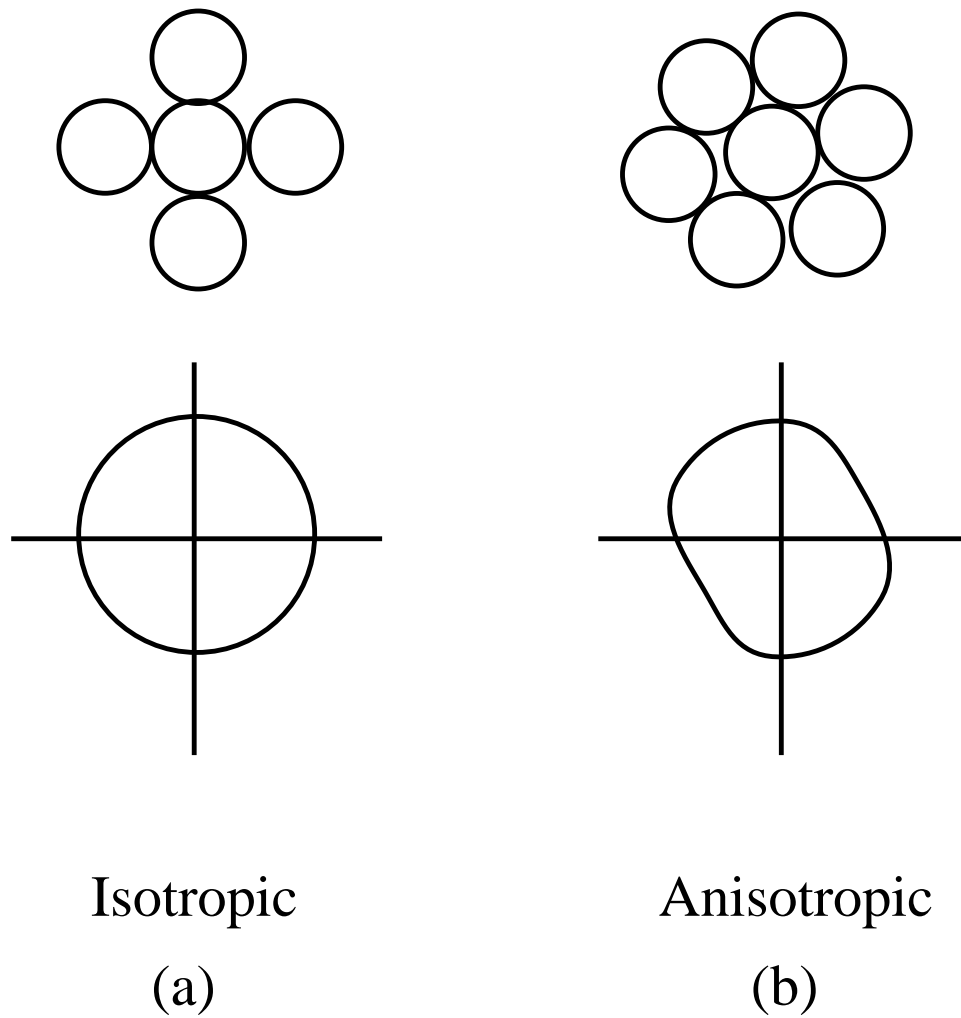
Figure 2.1   Evolution of the contact distribution of a 2D granular media. (a) Isotropic case, (b) Anisotropic case. Elementary microstructural information is contained in a scalar property such as the void fraction, while material anisotropy requires fabric tensors of higher rank.

made of equal spheres, these authors – using a volume-average approach in the same line of reasoning used by Batchelor and O'Brien [37] – proposed the following anisotropic upper bound to characterize the effective conductivity tensor, K_{ij}, of a packed bed:

$$K_{ij} = \frac{3\bar{Z}k_s(1-\epsilon)}{\pi} \left(\frac{a}{r}\right) F_{ij}, \tag{2-16}$$

where $\bar{Z}$ is the average coordination number, ϵ is the void fraction, and F_{ij} is the fabric tensor as discussed in the previous section. While the granular fabric is considered to be one important factor in the estimation of effective properties, the direct measurement of fabric in real granular media is difficult and tedious (e.g. Kuo *et al.* [97], Kanatani [98]) so that, in practice, expressions like Equation 2-16 are difficult to evaluate experimentally. TPD (see Section 3.2)– which incorporates both mechanical and thermal modeling components– offers a unique platform for testing this type of correlation, since both the fabric tensor and the effective conductivity are easily available from the simulated data. Comparison between TPD results and Jagota and Hui's [96] expression (Eqn. 2-16) can be found in Chapter 4.

2.3 Heat transfer in particulate systems

Many industrial processes involve particulate materials undergoing heat transfer. Knowledge of the thermal properties of the system is therefore essential to the proper design and operation of such processes. In general three related phenomena, conduction, radiation and convection, account for the heat transport in any medium. The conduction contribution, is usually the most significant in particulate materials [99]. This contribution depends on the conductivity of the solid material, the characteristics of the interparticle contacts (the contact conductance) and the structure of the particle packing. The contribution by radiation depends on temperature and it becomes significant at high temperatures ($> 1000\,K$).

Convection and conduction through the pores can be neglected when the thermal conductivity of the fluid filling the void spaces is low and for low to moderate temperatures. A description of the several mechanisms found to contribute to the overall process of heat transfer follows.

2.3.1 Heat transfer mechanisms

In describing heat transfer in static packed beds the following mechanisms, independent of the fluid flow are recognized [92, 100]:

1. Thermal conduction through the stagnant fluid

2. Thermal conduction through the solid

3. Thermal conduction through the contact area between two particles

4. Radiant heat transfer between surface of particles

5. Radiant heat transfer between neighboring voids

   If the fluid flow is included then the following mechanisms need to be considered

6. Thermal conduction through the fluid film near the contact surface of the two particles

7. Heat transfer by convection solid-fluid-solid

Based on these mechanisms a variety of correlations and techniques have been developed to address the heat conduction in granular media. Yet, no unique solution to this problem has been found. As indicated in Section 2.2, previous investigations have shown that only by taking the actual bed structure into account and by looking at the local(micro-scale) phenomena in packed beds, will it be possible to tell how the effective transport coefficients should be correlated [10, 31, 101]. However, the complexity of the problem is such that developing an exact representation from first principles has not been feasible.

Heat transfer in granular media under flow conditions occurs by the same mechanisms as in a static packed bed namely, conduction (e.g., particle-particle contact, particle-wall contact), convection (e.g., gas-particle), as well as radiation [102, 103]; however, due to the movement of particles within the granular bed, an advective component for energy transport is superimposed which in some cases might dominate the overall heat transfer. In granular flows of polidisperse particles (e.g., differences in size or density), it is well known that the motion of the granular material may cause segregation within the bed which tends to counteract advective transport of energy, thus promoting temperature gradients in the bed [102]. Therefore, particle size distribution and particle properties – if mixtures of particles are used – will also play a very important role.

2.3.2 Thermal Contact Conductance

Contact conductance refers to the ability of two touching materials to transmit heat across their mutual interface. The most basic problem in contact conductance is that of heat transport between two smooth particles in elastic contact – where it is assumed that the radius of curvature of the spheres is much larger than that of the contact spot. The main heat transfer mechanism under evacuated conditions is conduction through the contact surface of the packed particles. This problem is well understood, and approximate analytical solutions have been proposed independently by Yovanovich [104], Holm [105], and Batchelor and O'Brien [37]. A slightly more accurate, completely rigorous, numerical solution is attributed to Chan and Tien [106]. All of these models predict that the conductance, $H_c = hA$ (where h is a heat transfer coefficient and A is the contact area), through a smooth, elastic contact varies with imposed normal force as $H_c \propto F_n^{1/3}$.

The thermal contact conductance for linear elastic spheres in contact can be expressed by:

$$\frac{H_c}{k_s} = 2 \left[\frac{3 F_n r^*}{4 E^*} \right]^{\frac{1}{3}} \tag{2-17}$$

where E^* is the effective Young's modulus for the two particles, and r^* is the geometric mean of the particle radii and are given by

$$\frac{1}{E^*} = \frac{1 - \nu_1^2}{E_1} + \frac{1 - \nu_2^2}{E_2} \tag{2-18}$$

$$\frac{1}{r^*} = \frac{1}{r_i} + \frac{1}{r_j} \tag{2-19}$$

respectively. In this expression, r_i is the particle radii, E_i is the Young's modulus and ν_i is the Poisson ratio. Chan and Tien [106] extended the analysis of two single spheres to that of the entire bed and provided both exact and approximate solutions for solid, hollow and coated spheres involving different void fractions. The conductance of the bed was defined as

$$k_{eff} = \frac{N_a}{N_t} \cdot \frac{1}{R_{ij}} \tag{2-20}$$

where R_{ij} is the constriction resistance of a single particle. The first subscript denotes the type of sphere (solid, hollow or coated), and the second subscript refers to the packing pattern(simple cubic, body-centered cubic, face-centered cubic). N_t and N_a are the number of particles per unit length and per unit area, respectively. The expression for the effective

thermal conductivity of a packed bed of solid spheres, as related to the compressive force, was developed as

$$k_{eff} = S_p k_s \left(\frac{1 - \nu^2}{E} P_a \right)^{1/3} \tag{2-21}$$

where S_p is a constant depending on the packing pattern. The relation between the normal force F_n and the apparent pressure P_a is given as

$$F_n = S_f \frac{P_a}{N_a} \tag{2-22}$$

The constant S_p is given by

$$S_p = \frac{1.56}{S_r S_j} \left(\frac{N_a}{N_t} \right) \left(\frac{0.75 S_f r_o}{N_a} \right)^{1/3} \tag{2-23}$$

where a is the contact radius, S_r is a constant based on the value of the ratio a/r_o and the constants S_j, S_f, N_t, N_a are parameters for the different packing patterns. The values of these parameters are provided by the authors. In a recent publication, Duncan et al. [107] conducted an experimental investigation to evaluate the effect of mechanical load on the thermal conductivity of random packed beds of different materials under different atmospheres and compared their results with those predicted from Chan and Tien correlation. This study showed that that Chan and Tien's correlation yielded accurate results for packed beds of materials with low thermal conductivities in the elastic deformation region. However, the accuracy of the model appears to decrease significantly as the thermal conductivity increases or when the load is such that the material is in the plastic deformation region.

More sophisticated models have attempted to relax the assumptions of smoothness and/or elasticity. These models generally allow for more realistic contact (elasto-plastic [108], for example) with varying degrees of roughness [109, 110]. Some investigators also

Table 2.1 Summary of load exponents for contact conductance models.

References	Load exponent (x)	Remarks
Cooper *et al.* **(1968)**	0.985	Theo.
Yovanovich (1969)	0.950	Theo.
Mikic *et al.* **(1970)**	0.98	Theo.
Greenwood *et al.* **(1966)**	0.95-1.4	Theo.
Zhuang *et al.* **(1995)**	2.4	Exp.
Majunmdar and Tien (1991)	0.5-1.0	Theo.

allow for the inclusion of oxide films [111]. In general, these more realistic models predict that the conductance goes as $H_c \propto F_n^x$, where x is *greater* than 1/3 (reported as high as 1.4 in one case [111] and experimentally measured at 2.4 in Ref. [10]). Experimental data for validating these models is available, but is relatively sparse [10, 112, 113].

In general, the non-dimensional contact conductance in vacuum and the load have been related, in the case of elastic particles with rough surfaces, as:

$$\frac{H_c \sigma}{k_s m} = C_1 \left[\frac{P_a}{H} \right]^x = C_1 \left[\frac{F_n}{H A_a} \right]^x . \tag{2-24}$$

In Equation 2-24, σ is the roughness, m is the slope of the asperities, H is the Vickers microhardness and A_a is the apparent contact area. The load exponent x in Eq. 2-24 is listed in Table 2.1, for several empirical and theoretical studies. Note that several authors have used an equation similar in form to Eqn. 2-24 to describe the case of smooth and/or rough, *plastic* particles. Much of the work on this area has been reviewed by Lambert and Fletcher [114]; Shridar and Yovanovich [115].

2.4   Heat transfer in granular flows

Granular materials subjected to shearing are encountered in many practical applications of material processing. Furthermore, many of these applications also involve heat transfer

whereby solids come into contact with cooling or heating surfaces and heat is exchanged between the surface and the particles during the duration of the contact. The magnitude of the heat exchanged depends on the thermophysical properties of the particles and the walls, the interstitial fluid, the shape of the particles and the contact time [116] among other variables.

In addition to heat transfer within the bulk material, the flow behavior is also important to other transport processes such as mixing (or segregation). When the shearing force is small, only minor shifting of the particles occurs, the particles experience multiple lasting contacts which lead to force networks or "stress chains" that may involve many particles; as the shearing increases, significant dilation of the structure takes place and deformation of the bulk material occurs along localized slipping planes [117], particle contacts disappear and new ones are formed, and the structure of the stress chains has a random transient character[118]. At the microscopic scale, the mixing of granular materials and therefore the heat transfer is accomplished by the motion of particles relative to one another. Thus, the mixing in granular materials – which is essential for heat redistribution – is flow-induced [119]. Macroscopically, mixing is induced both by the random motion of the particles and advection.

While a fundamental understanding of the mechanisms of granular mixing is beginning to emerge, the role of mixing and microstructure in relation to heat transfer under conditions of flow is still not clear. Experimental studies of granular flows involving heat transfer are scarce and so far restricted to bulk measurements. Experimental data concerning the variation of the effective conductivity with solid fraction and shear rate in a Couette flow device were reported by Wang and Campbell [120]. In this study the effective thermal conductivity and the effective viscosity of a particulate system under conditions of simple shear were measured. Both viscosity and conductivity were found to increase with

shear rate. Experimental studies of granular gravity flows down a vertical channel were reported by Natarajan and Hunt [121], Sullivan and Sabersky [122]. Heat transfer to granular materials flowing along a chute was studied by Spelt *et al.* [123]. The results in this study indicate that contrary to the usual observations in the companion cases of continuous phases, increasing the flow velocity does not necessarily yield higher heat transfer. This authors noted that a maximum is observed in the heat transfer coefficient at the wall as a function of the flow velocity. They conclude that the effects of density change on the heat transfer mechanisms near heated walls is most likely not a simple function of velocity and depth of the material, although these two variables are considered to play a very important role.

Heat transfer to vibrated vessels was reported by Muchowski [124], Wunschmann and Schlünder [125]. These studies indicate that small vibrations have a positive effect on the heat transfer coefficients – an enhancing effect is observed – but the trend does not continue at large vibrational accelerations. No conclusive explanation was given for this behavior. Few detailed experimental heat transfer studies in rotating drums have been reported. Ito *et al.* [126] carried out batch experiments on transient heat transfer in a rotating drum heated from the wall. They found that the heat transfer resistance at the wall plays an important role and it needs to be considered when correlating data on heat transfer coefficients at the wall. Wess *et al.* [127] and Lehmberg *et al.* [128] conducted experimental as well as a theoretical analysis of the heat transfer in industrial scale horizontal drum reactors. An experimental and computational study for rotary kilns including heat transfer within the bed was reported by Boateng and Barr [102].

The studies of Wang and Campbell [120], Ito *et al.* [126] and Lehmberg *et al.* [128] are the most relevant to the present work since they measured effective conductivities for

slow granular flows as a function of several variables in a simple shear flow and a rotating tumbler. The information in these publications will be used for comparison in Chapter 5.

These studies, which mostly deal with slow flows and high solid fractions (the object of the present work), show that the effect of the change in void fraction close to the wall was small and therefore, the value of the contact resistance at the wall remained reasonably constant [121]. In contrast, at high flow rates, due to the shearing-induced dilation of the particles close to the wall, there is a progressive increase in the thermal resistance at the wall. This factor coupled with the decrease in the void fraction in this region, according to Natarajan and Hunt [121], is responsible for the progressive decrease in the heat transfer observed in experiments as the shearing rate increases. This observation may as well explain the maximum experimentally observed by Spelt *et.al* [123].

Studies at the other side of the spectrum namely – rapid flows– where contact times are short and the fractions of solids is relatively low indicate that the heat transfer may actually increase with increasing shearing rate, leading to an enhancement of the thermal mixing [120, 121, 129].

In order to reconcile the theoretical results with experimental observations a gas film and/or a contact resistance at the wall have been introduce to compensate for the increased in voidage in the proximity of the wall [130]. So far there is no conclusive evidence of either a stagnant film or time-dependent contact resistance and both concepts remain as empirical parameters which allow reconciliation of experiments with theory.

2.4.1   Heat transfer by contact

Heat transfer between heated surfaces and particles in motion, takes place primarily by the contact conductance. This process constitutes one of the mechanisms of heat transfer

in particulate systems (see Section 2.3.1). Many authors have addressed this specific problem [76, 116, 131]. Molerus [76] has shown through the evaluation of data published in the literature that the contact resistance between particles in contact and between the heated surfaces and the particles is the factor that primarily determines the heat transfer between a heated wall and particles in a moving bed.

Sun and Chen [131] on the other hand, using analytical and numerical solutions for the problem of heat transfer between two colliding spheres, concluded that the contribution of heat transfer due to solid contact is negligible. According to Sun and Chen's analysis, the energy exchange during contact increases with particle mass, radius and velocity and decreases as the Young modulus increases. The correlation by Sun and Chen [131] for particle to surface heat transfer h, considering particles with the same properties, is expressed by

$$h = 0.41 C \dot{N} \rho c_p A_c \sqrt{\alpha t_c}, \tag{2-25}$$

where C is a correction factor which is an exponential function of the ratio $\alpha t_c / r_p^2$, $\dot{N}$ is the number flux of particles, ρc_p the heat capacity per unit volume, A_c the area of contact between particles or between particles and surface, t_c is the contact time and α the thermal conductivity of the material.

For heat transfer to moving particles at short and intermediate contact times (e.g. $t > 0.1$ sec), Schlünder [116] found that a relation for the heat transfer coefficient of the form

$$h = 2 \sqrt{\frac{(\rho c_p k)_e}{\pi t_c}}, \tag{2-26}$$

describes the experimental observations. However if the contact time is very small, the measured data no longer agree with Equation 2-26. Experimental observations indicate

that the measured points tend toward a finite, constant limiting value at very small contact times. From these observations Schlünder concluded that the mechanism of heat transfer at medium and long contact times is different to that at very short contact times which are presumably better described by Eqn. 2-25.

Although, this heat transfer mechanism may be considered negliglibe for dilute systems under rapid flow ($t_c \rightarrow 0$), it cannot be ignored in systems under slow flow conditions and with high densities, where lasting contacts between particles are predominant. In fact, as will be shown latter, this is the dominant heat transfer mechanism in dense slow flowing systems.

2.4.2 Kinetic theory

Kinetic theories exploit the analogy between the fluctuating nature of rapid granular motion and the random molecular motion within a dense gas [132]. The particles in a real granular flow are inelastic and have some finite roughness. Hence, when particles interact with one another, a significant amount of energy is dissipated. The need to account for this dissipation of energy is the primary difference between granular flows and molecular motion[118]. In kinetic theories, the grains are assumed to interact with their neighbors through energy dissipating binary collisions. The effects of enduring contacts as well as the effects of friction are ignored. By considering a statistical description of the particle collisions, it is possible then to define mean fields such as density, velocity and granular temperature and to derive conservation equations corresponding to each property. Constitutive relations are then obtained through appropriate statistical averaging. In the rapid granular flow regime, the principal transport mechanisms are kinetic transport by particle fluctuations and collisional transport due to particle interactions.

For many authors working on developing theories for the flow of granular materials, the rapid granular motions of the particles are analogous to the random molecular motion within

a dense gas. Therefore a quantity commonly referred to as the "granular temperature" has been introduced to characterize the particle motion. The granular temperature is therefore a byproduct of the local flow field and its magnitude depends on both flow and particle properties [119]. The granular temperature Υ is associated with the mean-square particle velocity fluctuations by

$$\Upsilon = \frac{< (u_i - < u >)^2 + (v_i - < v >)^2 + (w_i - < w >)^2 >}{3}, \qquad (2\text{-}27)$$

where u, v_i, w_i are the instantaneous particle velocities of each individual particle in each direction, $< u >, < v >, < w >$ are the mean velocities and the angle brackets $< . >$ designate an ensemble average.

The granular temperature which is a measure of the kinetic energy associated with the translational velocity fluctuations of the granular particles has an obvious analogy with the definition of temperature in a gas at the molecular level. The kinetic theories developed for granular flows can be considered as perturbations of the case of perfectly elastic spheres in which the dissipation of energy should be "small" in some sense for this analysis to be valid [118]. This corresponds to small values of the so-called Savage-Jeffrey parameter S defined as

$$S = d_p \frac{du/dy}{\sqrt{\Upsilon}}, \qquad (2\text{-}28)$$

where du/dy is the shear rate, d_p is the particle diameter. In the case of the shear flow of a gas the value of S is small (i.e. $S \to 0$). In granular flows, due to the energy dissipation the values of S are of order unity. This raises the question of validity of the granular flow kinetic theories. However, comparisons with experimental measurements and numerical simulations have shown good agreement for cases of low dissipation and for particle concentrations

ranging from small to moderate. In physical terms, S is primarily a function of the coefficient of restitution, e and the solid fraction ν. Expressions relating S and e may be established by balancing the shear work and the energy dissipation. An extensive study and comparison of this relations has been provided by Lun *et al.* [133].

Analytical solutions of heat conduction problems in granular flows are scarce, and there are few comparisons of theoretical predictions based on kinetic theory analysis to experimental results. Hsiau and Hunt [134] used kinetic theory arguments to investigate the heat transport process in granular flows. This study showed that associated with the heat transfer process, there is an enhancement of the thermal conductivity due to the mixing of the particles. An equation for the thermal conductivity was found that is directly proportional to the square root of the granular temperature and varies inversely with the solid fraction. Natarajan and Hunt [129] applied the results of Hsiau and Hunt [134] to examine the heat transfer to granular flows from heated walls, in a vertical chute flow.

The kinetic theory analysis as presented by Hsiau and Hunt [134] is based on dense-gas theory and therefore is appropriate for rapid granular flows, where particle interactions are characterized by short contact times, high shear rates and low to moderate solid fractions. Consequently, these solutions have a limited range of application. Although these solutions may not be appropriate for dense and slow granular flows, the ideas and arguments put forward can help to advance the development of transport relations for dense granular flows.

2.4.3 Granular flow in simple shear cells

Shear cell flows have been aptly explored both experimentally and computationally by Campbell and coworkers [119, 120, 135, 136, 137]. Wang and Campbell [120] experimentally found that the bulk shear motion improves the internal transport of both heat and momentum and that both transport coefficients (i.e. apparent thermal conductivity and viscosity)

increase linearly with the imposed shearing rate. According to these authors this indicates that similar internal mechanisms drive both transport processes. Momentum is transported both by particle collisions and by random motion of the particles. However, since heat is a slow process, little heat is conducted during short contact times. Therefore, at large particle concentrations, Wang and Cambell found that there is almost no shear-induced enhancement on the effective thermal conductivity due to the limited mobility of the particles. Recent computational studies in granular shear flows also include those reported by Karion and Hunt [138], Louge [139], Schöllmann [140] and Lun [141]. Simple shear flows of particles has also been extensively explored using kinetic theory analyses [118, 132, 133, 142, 143].

Significant boundary effects on the dynamics of granular flows have been observed both in experimental and numerical results. In particular, Lun [141] conducted a detailed computational study on the effects of bumpy walls on stress and energy dissipation. The results indicate that different wall-particle packing patterns with the same solid fraction of particles at the wall cause variations in stresses and slip velocity. The wall particle concentration and distribution directly influence the collision angle and the collision frequencies thus changing the effectiveness of the bumpy wall to transfer energy and momentum to the particles in the flow field.

A striking feature on both experiments and simulations of granular media under shear is the level of local fluctuations that occur at the walls. Experimental observations by Miller *et al.* [144] and Howell and Behringer [23] on continuously sheared granular materials indicate that localized time-dependent stress present very large variations around the mean and that these variations can occur over a broad range of time scales. These observations have also been confirmed by computational experiments [138, 145, 146]. Computational studies by Antony [147] on the evolution of contact normal force distribution at small shearing rates indicate that the probability distribution of contact forces is shear-state dependent

and it seems to have a certain periodicity with the shear rate. These results indicate that during slow shearing the contact force distribution is sensitive to the shear history. This fluctuating behavior at the boundaries have been related with a so-called "stick-slip" motion which many researchers believe appears to be shear-induced and is the result of the formation and collapse of stress chains.

2.4.4 Granular flow in a rotating cylinder

In a slowly rotating container avalanches move material from the upper part of the surface to the lower, and mixing occurs only during the avalanche (Figure 2.2). In the context of heat transfer, therefore, the mixing process serves to equalize the temperature within the drum. Several studies have dealt with mixing in rotating containers [14, 148, 149, 150, 151]. These investigations have demonstrated that the movement of solids in a rotating cylinder, such as rotary kilns, rotary coolers or dryers, can be resolved into two components, i.e. flow in the axial direction caused by the inclination of the cylinder and flow in the radial direction imparted by rotation [117].

Depending on the properties of the material, the rotation rate and the degree of filling of the drum, various types of bed motion may result in the radial plane of a rotating cylinder (see Figure 2.3 [152]). Six modes of bed movement have been identified [103, 153, 154]. With increasing rotation rate, these include sliding, slumping, rolling, cascading, catarating and centrifuging. In practice, industrial-scale drums are often operated in the rolling or slumping regime. This work therefore will consider flows in rotating cylinders operated in or near the rolling regime. The rolling regime is characterized by a uniform flow of a particle layer on the surface (cascading region), while the majority of the bed (solid–body rotation region) is transported upwards by solid body rotation with the rotational speed of the wall. The bed surface is almost flat and the dynamic angle of repose depends on rotational speed and filling level [153].
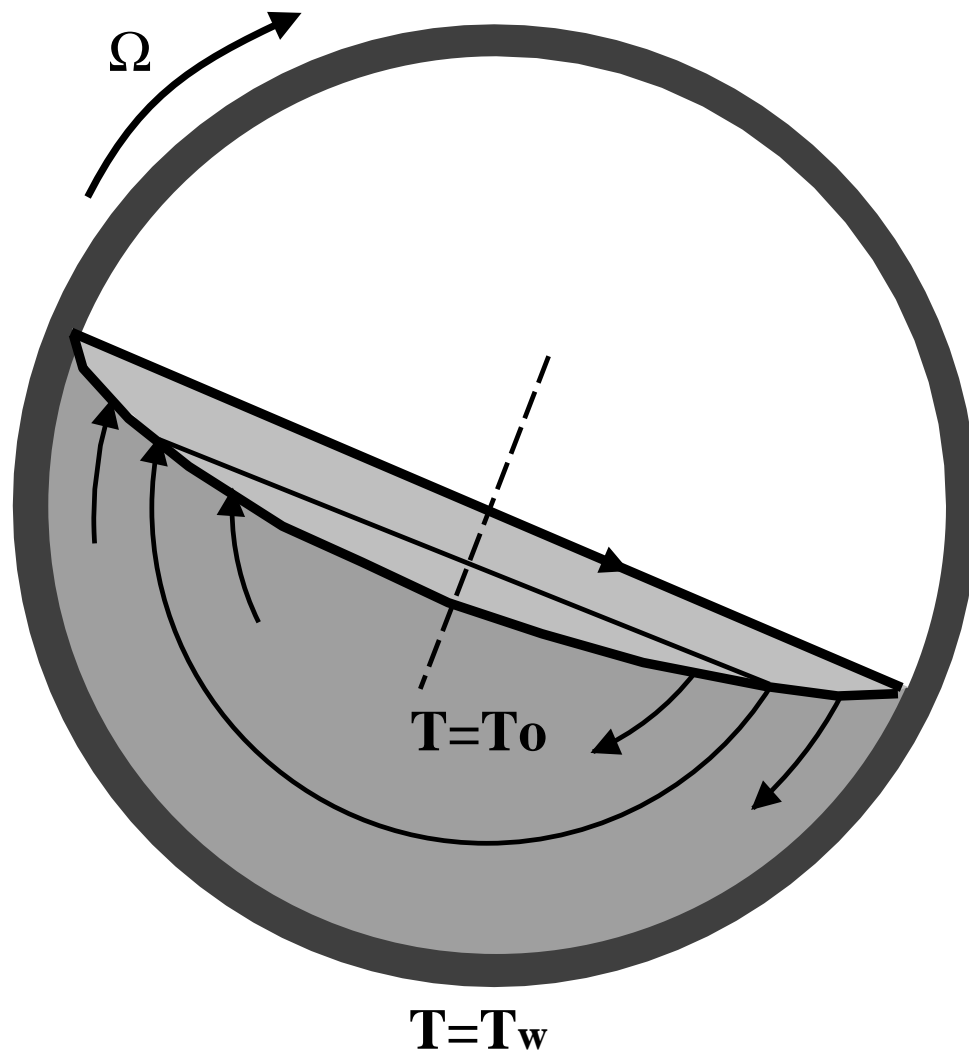
Figure 2.2 Schematic of the flow in a rotating cylinder with heat transfer at the wall. Lighter gray area: cascading layer; dark gray section: solid–body rotation region
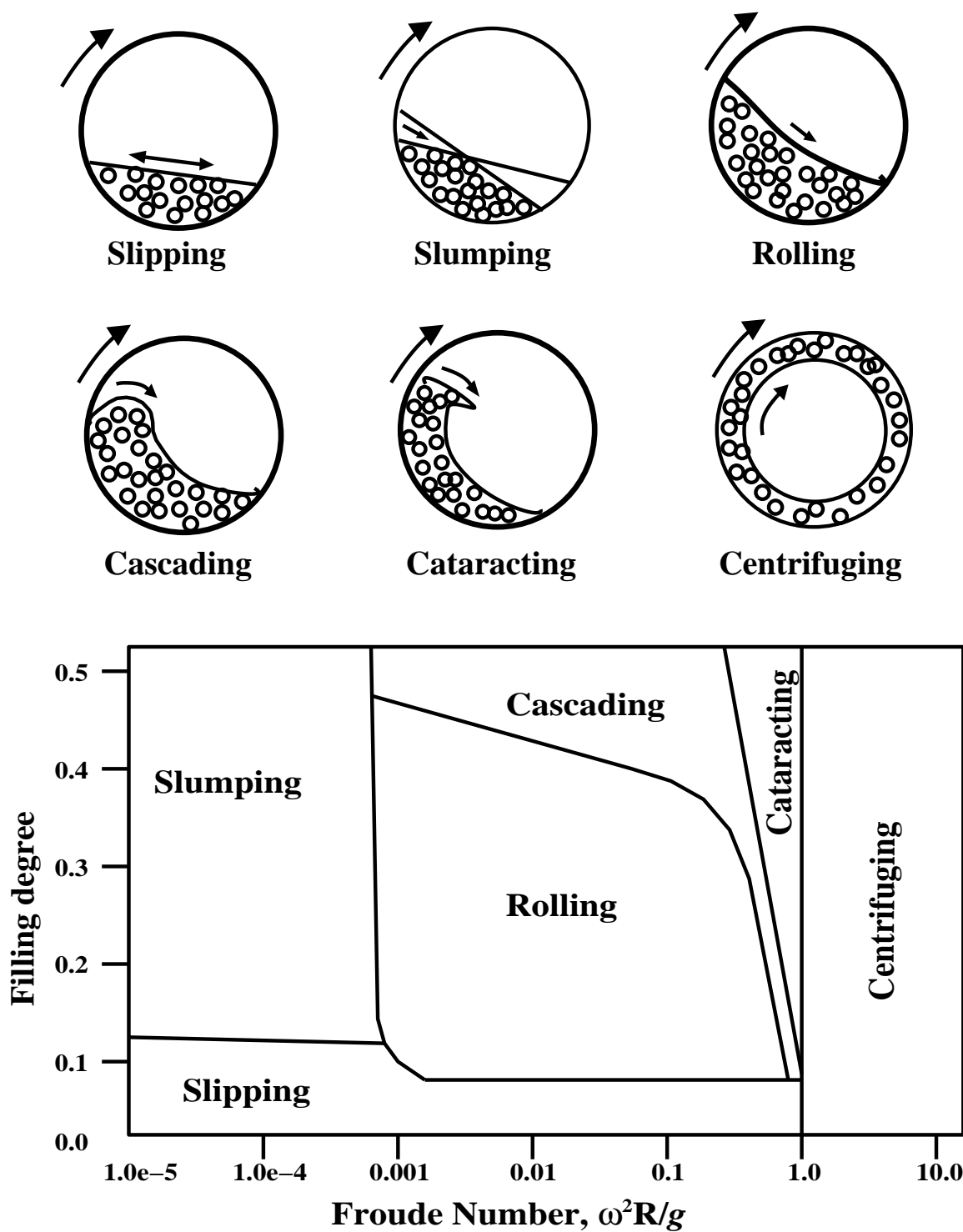
Figure 2.3 Tumbler flow behavior diagram. Depending on the rheological properties of the material, the rotation rate and the degree of filling of the drum, the various types of bed motion that may result are illustrated.

It has been well documented [117, 154, 155, 156, 157] that axial mixing in a tumbler can be well described by a simple diffusive relation. On the other hand, radial mixing, while much faster than axial mixing, is considerably more complex – depending strongly on both drum filling and rotation rate. Moreover, segregation, when present, is much more pronounced in the radial direction than in the axial direction. It is expected, therefore, that radial mixing/segregation will have a much stronger influence on the heat transfer process than does axial mixing/segregation. Despite its complexity, radial mixing/segregation has been extensively studied [158] and can be generalized in the following way: convective mixing occurs when circulation times vary as a function of radial position; diffusive mixing – which causes particles to move across streamlines – is due to collisions within the shearing, surface layer.

Theoretical [159], computational and experimental [148, 160] estimates of the diffusion coefficient D are available for nearly elastic spheres in simple shear flows. The self-diffusion coefficient obtained by Savage [159] for spherical particles in a shear flow using PD simulations is given by

$$D = 0.025 d_p^2 \left(\frac{du}{dy} \right) \tag{2-29}$$

for a solid fraction $\nu = 0.5$ and a coefficient of restitution for the particles $e = 0.6$ [158]. From kinetic theory the self-diffusion coefficient is given by [159]

$$D = \frac{d_p \sqrt{\pi \Upsilon}}{8(1 + e)\nu g(\nu)}. \tag{2-30}$$

By replacing $\Upsilon^{1/2}$ in Equation 2-30 in terms of S and du/dy from Equation 2-28 an expression similar to that in Equation 2-29 can be obtained which is given by

$$D = \frac{d_p^2 \sqrt{\pi}(du/dy)}{8(1+e)\nu g(\nu)S}.$$

(2-31)

where $g(\nu)$ is the radial distribution function at contact.

Diffusional effects in granular mixing are scale dependent. For a rotating drum the Péclet number – the ratio of the characteristic advection time ($<u>/2\ell$) to the diffusion time (δ_o^2/D) is

$$Pe = \frac{\Omega \delta_o(\ell)}{D}.$$

(2-32)

where δ_o is the middle layer thickness and ℓ the half-width length of the top plane of the tumbler. Experimental work by Khakhar $et.$ al [148, 149] and McCarthy [158] indicate that at a constant acceleration, $2\ell\Omega^2$, the middle layer thickness,δ_o, scales with system size 2ℓ roughly as $\delta_o = c2\ell$ so that $Pe = [c^3/f(v)][2\ell/d_p]^2$. Thus diffusion decreases with increasing system size, and would play a minimal role in large-scale systems.

Although theories exist that allow the prediction of the flow in the active layer to the best of our knowledge no works have addressed the problem of heat transfer in this layer. Detailed experimental studies of flow in a rotating drum are scarce. The most notable seems to be that of Nakagawa et $al.$ [161] in which concentration profiles and velocity field were obtained using magnetic resonance imaging techniques. Based on their results, the following conclusions were drawn:

1. The thickness δ of the flowing layer increases monotonically with rotation rate but with an ever decreasing rate. It reaches a maximum at the midpoint, and the value

at the midpoint increases with rotational speed achieving a saturation value at high rotations rates.

2. The mass flux along the free surface is not linearly proportional to the rotation rate.

3. Velocity, concentration and mass fluxes are not symmetric around the center with the asymmetry depending on the rotation rate. The peaks move from the upper half to the lower half as the rotation rate is increased.

While rotating drums are encountered in numerous process applications, attempts at modeling the heat transfer phenomena in such devices are rare although a considerable amount of experimental and theoretical work has been carried out(see Ding *et. al* [103] and the references therein). Boetang and Barr [102] developed a multi-phase continuum model to examine heat transfer in rotary kilns and compared their results with experimental measurements. It was found that for a drum in the rolling regime with uniform particle size and fixed filling level, the velocity field resulting from the rotation of the drum enhances the effective conductivity of the bed and promotes temperature uniformity within the bed –the effective conductivity and the self-diffusion coefficient were determined using Eq. 2-30. According to Boetang and Barr, due to the strong diffusion effects caused by the granular flow behavior (increased granular temperature), the bed tends to isothermal conditions at higher rotation rates. Significant temperature non-uniformities were observed for segregating beds. Use of discrete modeling techniques to describe heat transfer phenomena in rotating tumblers has not been reported.

3.0   DISCRETE MODELING

Discrete modeling of granular materials has recently gained widespread acceptance as a research tool in studying the mechanical behavior of granular materials – often replacing/complementing experimental studies of granular flows [162, 163, 164, 165, 166, 167, 168, 169]. The predominant method of discrete simulation is still fashioned after Cundall and Strack's [170] pioneering work, which we call Particle Dynamics (PD). Relatively recently, investigators have expanded this model to include fluid drag effects [171] and complex force schemes such as van der Waals forces [22], interstitial liquid effects [172], and even solid-bridge formation (sintering) [173]. Extensions of Particle Dynamics to heat transport for collision-dominated flows have been developed by Hunt [9], and Li and Mason [174]; however, neither of these approaches are applicable to slowly flowing or static granular beds. In this Section, we present background relevant to discrete simulation and outline the theory and implementation of the Thermal Particle Dynamics technique.

3.1   Particle Dynamics (PD)

Particle Dynamics captures the macroscopic mechanical behavior of a particulate system via calculation of the trajectories of each of the individual particles within the mass. The time evolution of these trajectories, which are obtained via explicit solution of Newton's equations of motion for every particle, then determines the global flow of the granular material [170]. The forces on the particles – aside from gravity – typically are determined from contact mechanics considerations [175]. In their simplest form, these relations include normal (Hertzian [176]) repulsion and some approximation of tangential friction (due to Mindlin [177]). A thorough description of possible interaction laws can be found in Ref. [178]; therefore they will not be reviewed here.

PD is a numerical scheme that is capable of dealing with particles of any shape, as long as a suitable contact mechanics model and contact detection algorithm is available [3]. The method is based on the most basic mechanism of the constitutive phenomena in a granular assemble, that is, particle-to-particle interactions at contact points. To determine the translational and rotational motion of the particles in the assembly the classical Newtonian mechanics is used. The equations that describe the particle motion, therefore, are:

Linear motion

$$m_i \frac{d\mathbf{v}_i}{dt} = -m_i \mathbf{g} + \sum_{j=1} \mathbf{F}_c, \tag{3-1}$$

Angular motion

$$I_i \frac{d\boldsymbol{\omega}_i}{dt} = \sum_{j=1} |\mathbf{F}_t| \times r. \tag{3-2}$$

where $\mathbf{F}_c = \mathbf{F}_n + \mathbf{F}_t$, $\mathbf{F}_c$, is the total contact force, with $\mathbf{F}_n$, $\mathbf{F}_t$ corresponding to the normal and tangential force, respectively. The particle to particle interaction is established by allowing the assumed soft particles to overlap at the contact point (Figure 3.1). This overlap serves as a parameter in contact mechanics models used to determine the resultant contact force $\mathbf{F}_c$. Cundall and Strack [170] first formulated their PD method approximately accounting for the full contact mechanics through the use of a spring, a dash-pot and a slider configuration, as shown in Figure 3.2.

The key feature of a Discrete Element Simulation (here taken to be synonymous with Particle Dynamics) is that many simultaneous two-body interactions may be used to model a many-body system [170] and Equation 3-1 may be used to evaluate their next position. This idea works because the time-step is chosen to be sufficiently small such that any disturbance (in this case a displacement-induced stress on a particle) does not propagate further than that particle's immediate neighbors within one time-step. Generally, this criterion is met by choosing a time-step which is smaller than r/λ, where r is the particle radius and

λ represents the relevant disturbance wave speed (for example, dilational, distortional or Rayleigh waves [179]).

Under these conditions, the method becomes explicit, and therefore at any time increment the resultant forces on any particle are determined exclusively by its interaction with the closest neighbors in contact. With the accelerations known, the velocities and displacements may be obtained by numerical integration using a finite differences scheme.

3.2   Thermal Particle Dynamics (TPD)

The TPD simulation technique is based upon a traditional Particle Dynamics (PD) technique (often referred to as the Discrete or Distinct Element Method [170]) so that every particle is tracked individually to determine trajectories, velocities, forces and temperatures. This allows the determination of both mechanical and transport properties of granular systems under static and/or dynamic conditions. Again, the particle trajectories are obtained via explicit solution of Newton's equations of motion for every particle [170] and the forces on the particles are determined from contact mechanics considerations [175].

The key feature of TPD is that by incorporating contact conductance theories many simultaneous two-body interactions may be used to model heat transfer in a system composed of many particles. In analogy with PD, this description requires that the time-step be chosen such that any disturbance (in this case a change in a particle's temperature) does not propagate further than that particle's immediate neighbors within one time-step. While for this work we are considering particles in lasting contact, this criterion is also satisfied in the majority of collision-dominated flows, although the amount of heat transferred between colliding particles under these conditions can be small [131].
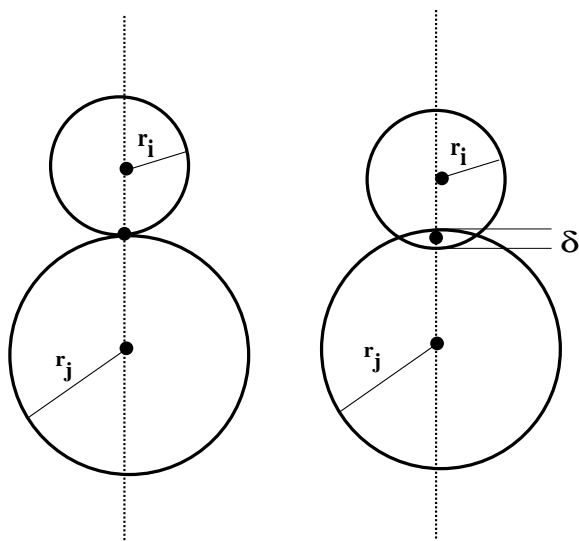
Figure 3.1   Contact point between two particles, showing definition of the overlap(δ)
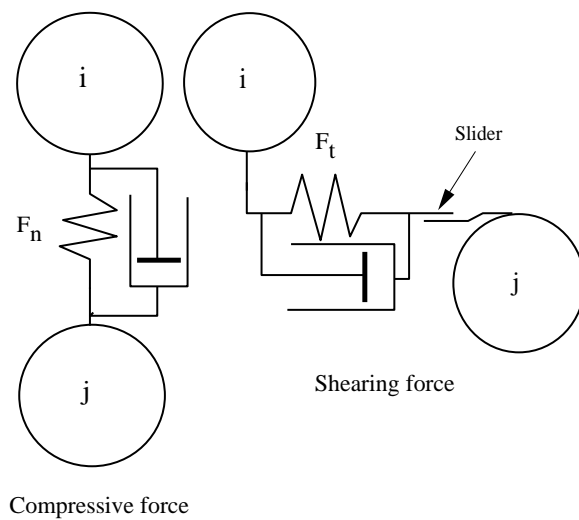
Figure 3.2   Models of contact force. Schematic illustration of the forces – *e.g.*, compressive and shearing – acting on particle i from contacting particle j.

3.2.1   General method

In much the same way that contact mechanics for a two-body interaction is well under-stood [175] – allowing PD simulations to reflect particle mechanical properties accurately – contact conductance models are also well established [114, 115, 180]. It is appealing, there-fore, to make a direct analogy with Particle Dynamics's use of contact mechanics in the context of heat transfer. Here, the disturbance is not a displacement-induced stress, instead it is a temperature change.

Incorporating the concept of contact conductance into a PD model – in order to formu-late the TPD method – can be accomplished as follows [181, 182]. Consider two particles (i and j) which are in contact and whose temperature "far" from the contact points are given as T_i and T_j, respectively (see Figure 3.3). The contact conductance theories in section 2.3.2 dictate H_c (Eqn. 2-17), whereby

$$Q_{ij} = H_c(T_j - T_i), \tag{3-3}$$

denotes the amount of heat which is transported across their mutual boundary per unit time. According to Equation 3-3 the solid-solid interface is assumed to be isothermal. In other words, there is no resistance to heat transfer across the contact plane. This assumption will hold true for our perfectly smooth elastic spheres and it is approximately true for particles with very low degrees of roughness. For very rough or oxide-coated particles this assumption will be invalid and a different contact mechanics/conductance pair is needed.

If only pair-wise contacts exist (all contacts are decoupled), the evolution of the tem-perature of particle i (in some average sense) may be given as

$$\frac{dT_i}{dt} = \frac{Q_i}{\rho_i c_i V_i}, \tag{3-4}$$
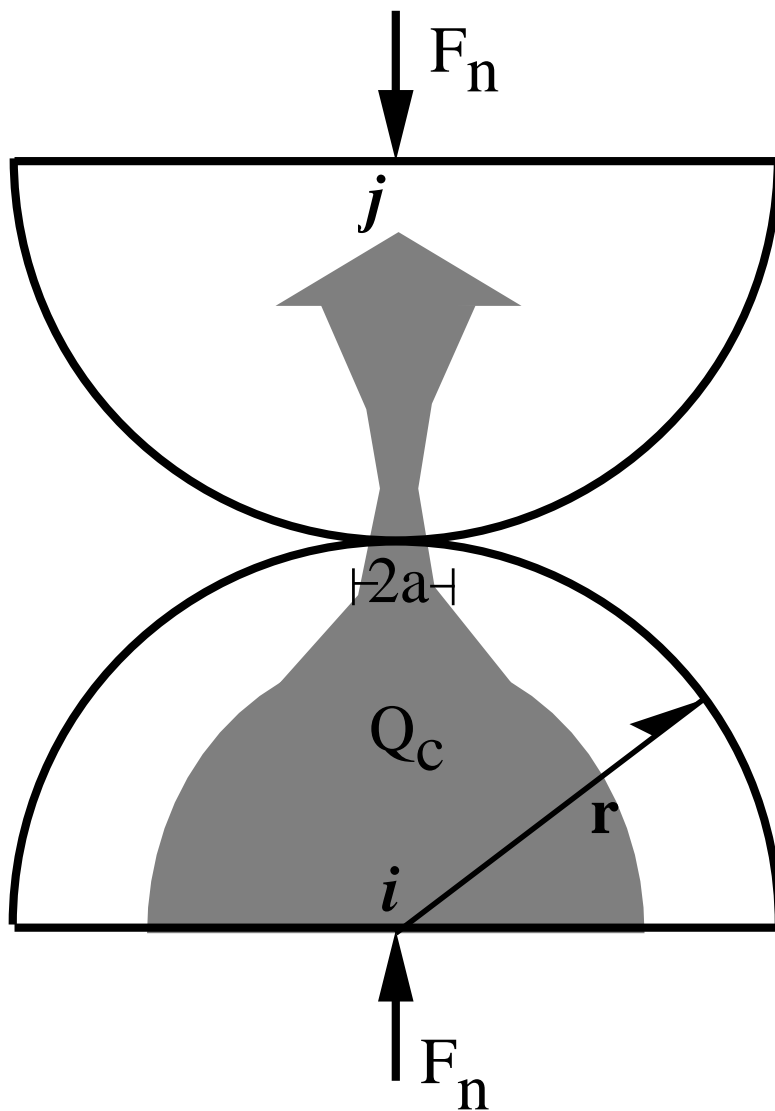
Figure 3.3 Heat conduction between to smooth-elastic spheres. For particles under vacuum the total resistance to heat transfer is determined by the radius of the contact a. The heat flux occurs almost entirely in the particle material, and is proportional to a when $\frac{k_s a}{k_f r} \gg 1$. The heat flux is unidirectional from i to j.

where Q_i is the total amount of heat transported to particle i from its neighbor (particle j), and $\rho_i c_i V_i$ is the particle's "thermal capacity".

Scale-up from this equation to multi-body contacts (for use in TPD Simulations) is straight-forward, but requires two caveats. The first is that each i-j particle contact "sees" the same temperature for particle i such that the temperature does not vary significantly from one contact point to another and each heat interaction may be calculated from Eqn. 3-3. Under these conditions it is reasonable to assume that the total heat transfer between particle i and all (N) of its neighbors, j, can be expressed as

$$Q_i = \sum_{j=1}^{N} Q_{ij}. \tag{3-5}$$

While this approximation is not strictly correct – incorporating a contact "capacitance" is possible to make this formally true [28] – it is conceptually simple and is found to be accurate over the time-scales examined here.

In order to justify this assertion, we must assume that the resistance to heat transfer inside a particle is significantly smaller than the resistance between interacting particles so that, for two elastic spheres in contact (see Eqn. 2-17)

$$Bi = \frac{H_c}{k_s A/r} = \frac{H_c}{k_s \pi r} = \frac{2}{\pi}\left(\frac{a}{r}\right) \ll 1, \tag{3-6}$$

where Bi is known as the Biot number, and A is the cross sectional area of the particle. It is important to note that this first of our two validity criteria does not directly depend on material properties and, in fact, the condition that the contact radius a is small relative to the particle radius r is often required by the contact mechanics models in use. Our second requirement is that the temperature of each particle changes slowly enough that thermal disturbances do not propagate further than its immediate neighbors during one time-step

(in direct analogy to the quasi-static condition of PD). Mathematically, this quasi-steady temperature criterion can be shown to be met by choosing a time-step which satisfies

$$\frac{dT_i}{(T_j - T_i)} = \frac{H_c dt}{\rho_i c_i V_i} \ll 1, \tag{3-7}$$

where dT_i is the change in the temperature of particle i during the time-step, and dt is the time step. Expanding this expression in terms of the contact conductance of smooth elastic spheres (see Eqn. 2-17) yields

$$\frac{2k_s a dt}{\rho_i c_i V_i} \ll 1, \tag{3-8}$$

which can be satisfied by choosing a sufficiently small time-step, dt. As before, it should be noted that the condition of small dt for TPD is often orders of magnitude less restrictive than the analogous time-step restriction in PD, such that these methods may be combined with little additional computational overhead (over a traditional PD technique).

In practice, Equation 3-4 is combined with Equation 3-5 and integrated to give T_i at the current time $t + \Delta t$ as

$$T_i^{t+\Delta t} \;=\; T_i^t + \sum_{j=1}^{N} \Delta T_{ij}^{t+\Delta t} \quad = \; T_i^t + \sum_{k=1}^{N} (T_j^t - T_i^t)(1 - e^{\left[-\frac{H_c}{\rho_i c_i V_i}\right]\Delta t}). \tag{3-9}$$

Figure 3.4 depicts a flowchart for the TPD model.

3.2.2 Stagnant Interstitial Fluids

The extension of TPD to include the effect of stagnant interstitial fluids (assumed to be explicitly applicable for small Rayleigh numbers; i.e., $Ra \ll 1.0$) is straightforward provided the following assumptions are met:

- The phases are assumed to be inert and thermally stable
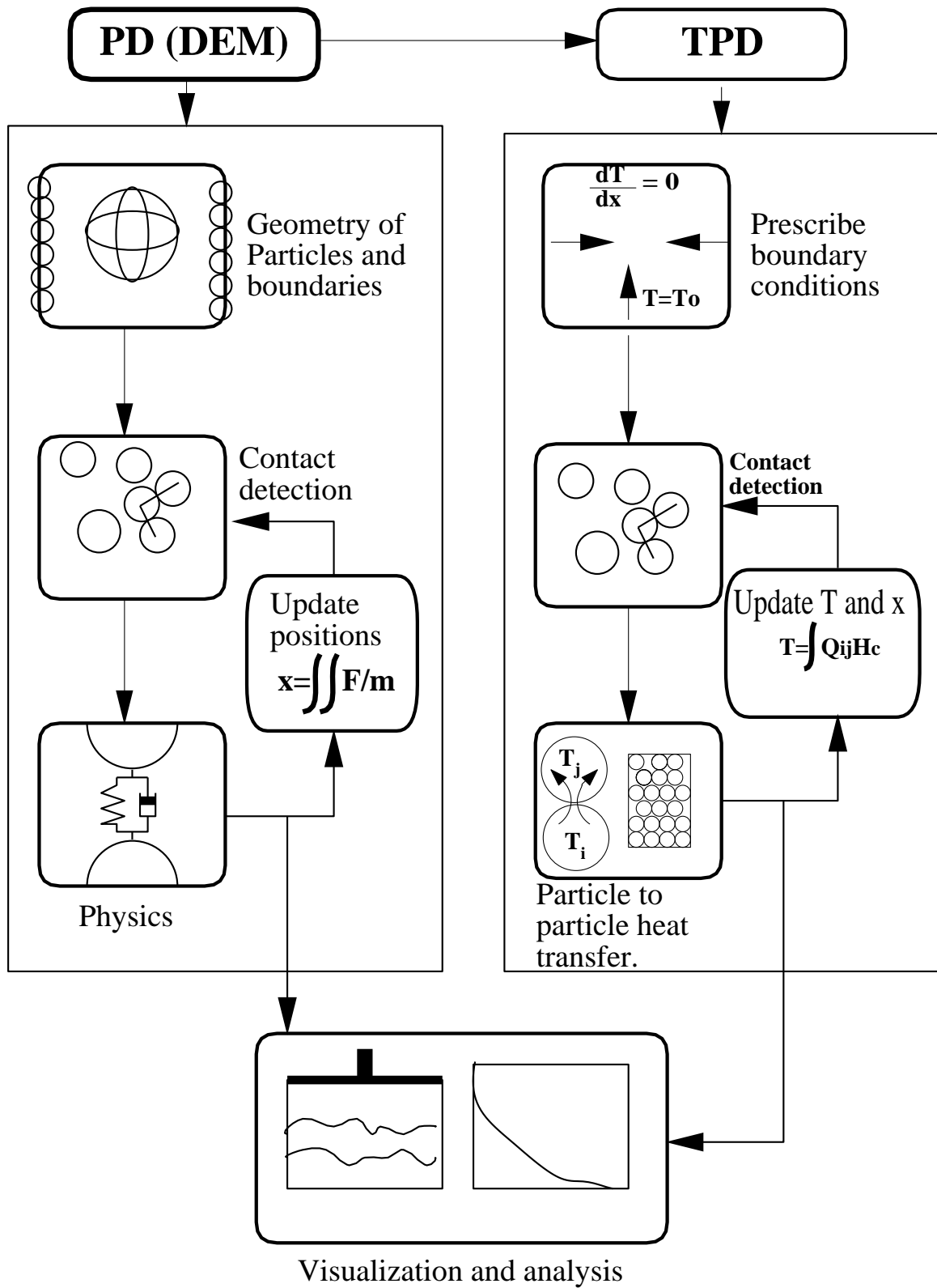
Figure 3.4   Thermal Particle Dynamics Flowchart.

- solid particles are non-porous

- the gas is insoluble in the liquid

- adsorption of the gas on the solid surface is negligible

- temperatures are continuous across all interfaces (this assumption can be easily relaxed by introducing an interfacial resistance)

With these simplifications it is possible to assume that the total thermal conduction may be obtained from summing the contributions of each of the three mechanisms (all acting in parallel) considered here; (1) through the area of contact between particles,(2) through the gas phase, (3) and through the liquid phase. Therefore, the total contact conductance can be expressed as

$$H_t = H_c + H_g + H_l. \tag{3-10}$$

The contributions of the fluid phases to the total conductance can be determined from the geometry of the system by taking

$$H_f = k_f \left[\frac{A_f}{\ell_f} \right], \tag{3-11}$$

where A_f is the area of contact – perpendicular to the heat flow – for the fluid phase and ℓ_f is a characteristic averaged length over which the flux applies. The problem then reduces to determining the areas of contact A_f and the respective averaged lengths ℓ_f in each of the cases considered. Once the total conductance is determined; H_c in Equation 3-9 is replaced by H_t and the method of solution continues as described in 3.2.1.

Masamune and Smith [183], Kunii and Smith [184], Okazaki [185] and Yovanovich [104] have used similar reasoning to develop correlations for the effective conductivity of packed beds.

3.2.2.1 Interstitial Gas.

From the geometry of the system (see Fig. 3.5), H_g is calculated as follows. For a unit cell (two spheres in contact), the area exposed to the gas can be estimated as half of the particle's surface area minus the area of solid-solid contact and is given by

$$A_g = 2\pi r^2 \left[1 - \frac{1}{2} \left(\frac{a}{r} \right)^2 \right].$$

(3-12)

The averaged length ℓ_g over which the heat flux applies can be determined as

$$\ell_g = \frac{r^2 \left[1 - \frac{\pi}{4} \right]}{r - a}.$$

(3-13)

The conductance can then be expressed as

$$H_g = k_g^* \left[\frac{A_g}{\ell_g} \right] = k_g^* \left[\frac{2\pi \left[1 - \frac{1}{2} \left(\frac{a}{r} \right)^2 \right] (r - a)}{1 - \frac{\pi}{4}} \right],$$

(3-14)

where k_g^* is the gas conductivity appropriate for use over finite lengths (not necessarily large with respect to the mean free path of the gas molecules). This finite-length conductivity, k_g^*, has been related to the conductivity in an infinite gaseous medium, k_g, as a function of the interstitial gas pressure by Kennard [186]. Kennard's expression is developed for heat flow in the gas space between two parallel plates separated by a fixed distance [186], l, to yield

$$k_g^* = \frac{k_g}{\left[1 + \left(\frac{M}{l} \right) \right]}.$$

(3-15)
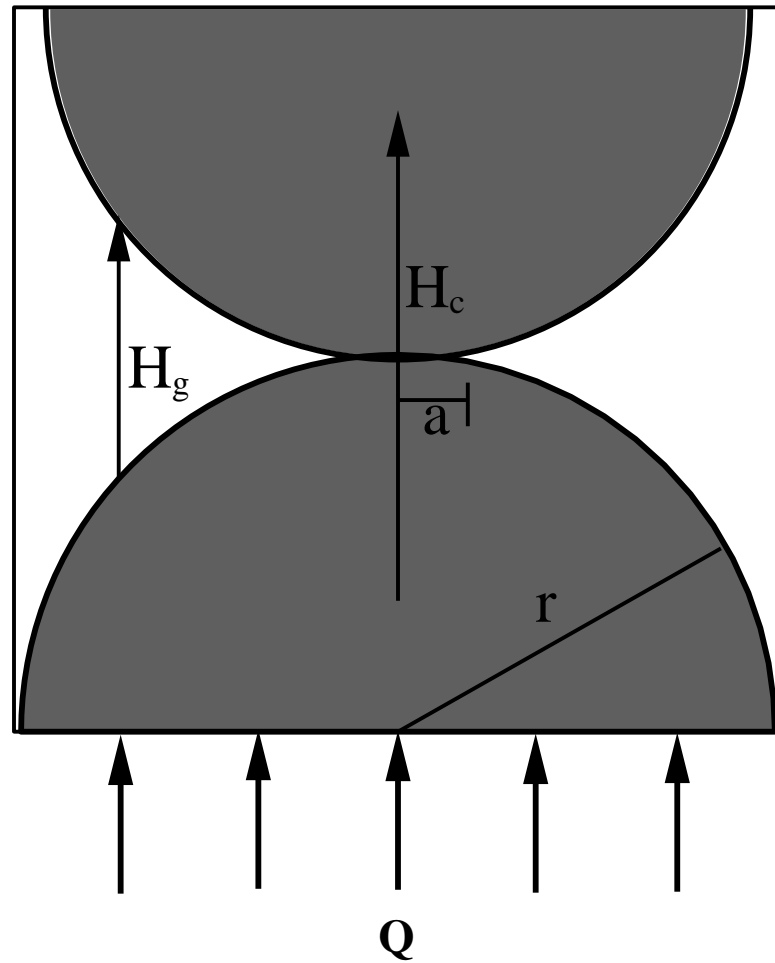
Figure 3.5 Heat transfer model for particles in contact with a stagnant gas. For particles in point contact, it is assumed that the particles are surrounded by a stagnant gas. Heat transfer is unidirectional during contact.

Following the approach of Masamune and Smith [183], we will use this expression for the conductivity between sphere surfaces by simply replacing l with our averaged length, ℓ_g (see Equation 3-13). The quantity M represents a length commonly referred to as the *temperature jump distance* [186] which can be estimated as

$$M = \left[\frac{2 - ac_1}{ac_1} + \frac{2 - ac_2}{ac_2} \right] \frac{\gamma}{\gamma + 1} \frac{1}{Pr} \Lambda, \qquad (3\text{-}16)$$

where ac_1 and ac_2 are the thermal accommodation coefficients of the two surfaces and γ, Pr and Λ are the ratio of the specific heats, the Prandtl number, and the molecular mean free path, respectively. The mean free path Λ of the gas molecules is given by

$$\Lambda = \frac{k_B T}{\sqrt{2} \pi d_g^2 P}, \qquad (3\text{-}17)$$

where P is the gas pressure, T is the temperature, d_g the diameter of the gas molecules and k_B is the Boltzmann constant [186]. It is important to note that the relations in Equations 3-15– 3-17 introduce one empirical parameter, namely the accommodation coefficient ac. In keeping with the spirit of the TPD simulations, we do not use this constant as a freely adjustable parameter, instead we take it from results previously reported in the literature [30, 186].

3.2.2.2 Interstitial Liquid.

Figure 3.6 shows a unit cell for two particles in contact with a liquid bridge between them. Heat transfer is assumed to occur in one direction.

From the geometry of the system (see Fig. 3.6) the area for the liquid A_l, the gas A_g and the characteristic lengths ℓ_g and ℓ_l are determined as follows. If the filling angle ϕ for all particles in contact is approximately constant and fixed, and the particles are under a
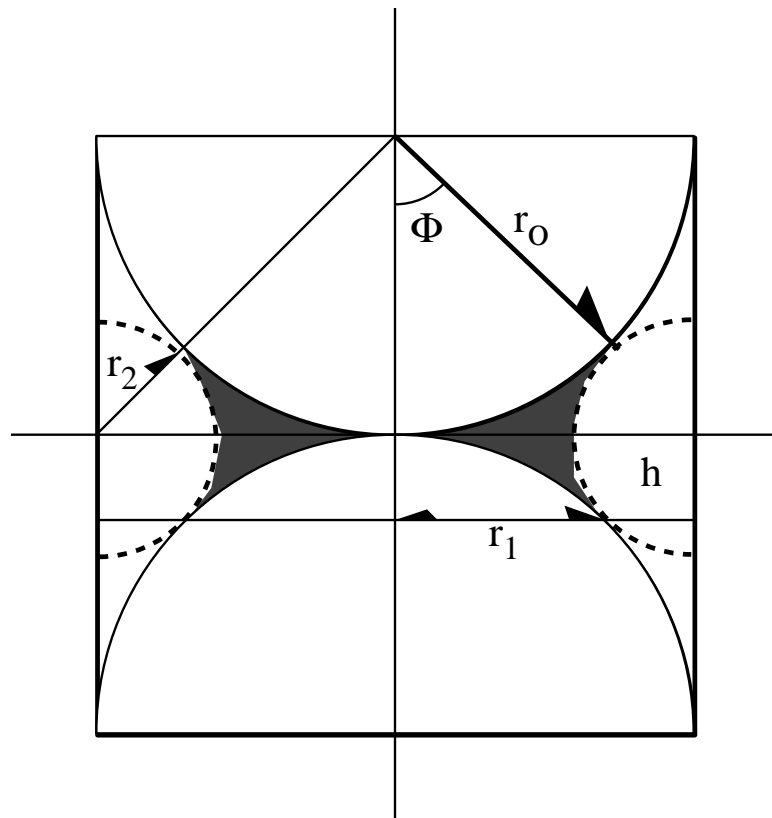
Figure 3.6 Heat transfer model for particles in contact with a stagnant liquid. For two uniform spherical particles in point contact, the degree of saturation is assumed to be determined by a liquid bridge in the pendular regime with a fixed filling angle ϕ. Heat transfer is presumed unidirectional.

normal force (see Figure 3.3), the interfacial surface area in contact with the liquid (modified from Rose [187]) is expressed as

$$A_l = 4\pi r^2 \left[\left(\frac{\pi}{2} - \phi \right) \tan \phi - (1 - \cos \phi) \right] \left[\frac{1 - \cos \phi}{\cos \phi} \right] - \pi a^2. \tag{3-18}$$

The characteristic length ℓ_l for the heat flux through the liquid phase can be determined as

$$\ell_l = \frac{r_{cap} * r - \left[\frac{r^2(\phi)}{2} + \frac{r_{cap}\sqrt{r^2 - r_{cap}^2}}{2} \right]}{r_{cap} - a}, \tag{3-19}$$

where r_{cap} is given as

$$r_{cap} = \sqrt{r^2(1 - \cos \phi)(1 + \cos \phi)}. \tag{3-20}$$

By a similar geometrical analysis, the surface area in contact with the gas, A_g, is the surface area of the particle minus the area for the liquid A_l and that of the solid-solid contact spot, so that

$$A_g = 2\pi r^2 - A_l - \pi a^2. \tag{3-21}$$

The characteristic length ℓ_g for the heat flux through the gas phase can be determined as

$$\ell_g = \frac{r^2 \left[1 - \frac{\pi}{4} \right] - r_{cap} * r - \left[\frac{r^2(\phi)}{2} + \frac{r_{cap}\sqrt{r^2 - r_{cap}^2}}{2} \right]}{r - r_{cap}}. \tag{3-22}$$

3.2.3   Heat conduction in granular flows

Since TPD is built on the framework of a traditional PD method, it uses the same computational procedures and introduces no additional restrictions on the applicability of the technique (see Section 3.2); TPD in granular *flows*, therefore, can be implemented in much the same way as is done for a static bed.

3.2.4   Limitations

As presented in this work, the TPD method considers conduction through a bed of identical, elastic, smooth particles in the presence of stagnant interstitial fluids; however, this method is eminently extensible. Differing contact mechanics, and therefore contact conductance, can be easily included as can the effects of variations in particle mechanical and thermal properties.

The main factors affecting the computational complexity of this model include: the contact mechanics model used, the number of particles and the thermal properties of the phases involved. Under flow conditions, regardless of the contact model used, the time-step chosen must be small enough such that the collisions between particles are properly resolved in order to approximate realistic interactions. Since the time-step requirement for TPD is orders of magnitude less restrictive than the analogous time-step requirement for PD, the global time-step for this method is dictated by the requirements of PD. As mentioned previously, this criterion is met by choosing a time-step which is smaller than r/λ, where r is the particle radius and λ represents the relevant disturbance wave speed (for example, dilational, distortional or Rayleigh waves [179]). In general, the relevant wave speed

$$\lambda \propto \sqrt{\frac{E}{\rho}}, \tag{3-23}$$

which, for the materials considered here, yields a time-step of approximately $10^{-7}s$.

Another consideration is the number of particles. While under flow conditions, periodic boundaries can be used to approximate large systems and therefore a relatively small number of particles can be used to simulate the system; a relatively large number of particles is required for static problems. Clearly, the necessity of a large number of particles coupled with small time-steps, makes for a very computationally intensive simulation. This situation can be exacerbated in applications where multiple particle sizes or complex particle shapes are required. This problem however can be partially overcome by the used of more effective contact detection algorithms [188].

4.0   STATIC PARTICLE BEDS

The emphasis in this work is on the development of a simulation technique to predict the effective thermal conductivity from first principles thus, we primarily treat particle beds composed of well characterized materials such as steel and glass in the presence of common gases and liquids. Unless otherwise stated, the solid properties used in this study are those of SS-304 and soda-lime glass.

In the following sections, we begin with a description of the results obtained for static systems of particles under vacuum conditions, including the effects of external load, geometry of the boundaries and aspect ratio, then focus on issues related to the presence of stagnant interstitial fluids and conclude with some generic remarks and implications of these observations [181, 189, 190].

4.1   General procedure

For the 2-D experiments, the simulation consists of a mono-disperse system of perfectly smooth spheres forming a two-dimensional pseudo-regular packed bed (one particle deep), compressed by a wall of known weight. All material properties are taken directly from the literature and consist solely of the thermophysical properties of the solids considered and the physico-chemical properties of the fluids. The bottom and top walls are kept at high and low temperature, respectively. Both the left and right walls are insulated. No effect of gravity is considered (i.e., the bed is assumed to be horizontal). It should be noted that there are no freely adjustable parameters in our simulation, however some of the correlations used in the estimation of fluid properties involved empirical parameters as described in Section 3.2.2 [191, 192, 193, 194].

A typical initial condition for the 2-D simulations is obtained by perturbing a hexagonal lattice (by removing random particles from the lattice) and allowing the bed to resettle under an imposed load using a tradition isothermal PD simulation (particle mechanics only). The 3-D beds tend not to form perfect crystalline structures and so no such measures are need for those simulations. The thermal conductivity for the various beds (2-D and 3-D) pressed at different loads with or without the presence of a fluid are determined using the steady state values of the heat flows. This procedure mimics the most commonly used experimental techniques for the determination of effective thermal conductivity [74]. For two-dimensional (rectangular) beds, the effective conductivity is determined from

$$k_{eff} = -\frac{Q}{\left(\frac{W \times d_p}{H}\right) \Delta T}. \tag{4-1}$$

For the three dimensional case a bed is created which mimics the well known co-axial cylinder method. The heat source here is represented by a core of radius R_1 comprised of particles which are maintained at a (high) constant temperature. The concentric cylindrical shell of radius R_2 that serves as heat sink is kept at a constant and lower temperature. The heat flow at equilibrium is then used to determine the effective conductivity of the bed as follows.

$$k_{eff} = -\frac{Q \ln(R_2/R_1)}{2\pi H \Delta T}. \tag{4-2}$$

Table 4.1 provides typical parameters used in the numerical experiments.

Table 4.1 Typical set of parameters used in the simulations of static beds. The physical properties are those of SS-304.

Parameter	Value
Density	7500 kg/m^3
Poisson ratio	0.29
Young's Modulus	193 GPa
Particle radius	3.175×10^{-3} m
Thermal Diffusivity	$3.95 \times 10^{-6}\ m^2/s$
Thermal conductivity	15.0 W/m^oK
Applied load	1.5 - 165 Kg
Number of particles	15548
Length	0.45 m
Height	0.31 m
Friction coefficient	0.29
Damping coefficient	1.0×10^{-3}

4.2   Vacuum systems

4.2.1   Experimental

The experiments are carried out using a heated, Hele-Shaw-like device (see Figure 4.1). This device allows a mono-layer of cylindrical particles to be uni-axially loaded, where two walls (as well as the front and back plates) are insulated, while the other two are heated and/or cooled. Temperature profiles within the bed were obtained using liquid-crystal thermography, a technique based on the principle of selective reflection [195, 196].

Since color is a subjective entity, in this technique the human factor is removed by capturing images of the color reflected by the thermographic liquid crystal and calibrating the liquid crystal through image analysis [196, 197, 198] . RGB images are captured by a color digital camera (Qimaging), the digitized images are read by an image processing software (Khoral Research), and converted into the HSI (Hue, Saturation and Intensity) space for analysis. This allows the use of only one component of the HSI space –the hue–, to describe the color reflected from the liquid crystals. A calibration is then performed by heating the

Top view

Heating medium out

Heating medium in

Vacuum lines

Springs

Cross section

Mirror

C.C.D camera

Plexiglass plate

Air gap

Liquid Crystal Sheet

Loading device

Heater/Cooler

S.S. cylinders

Insulating foam
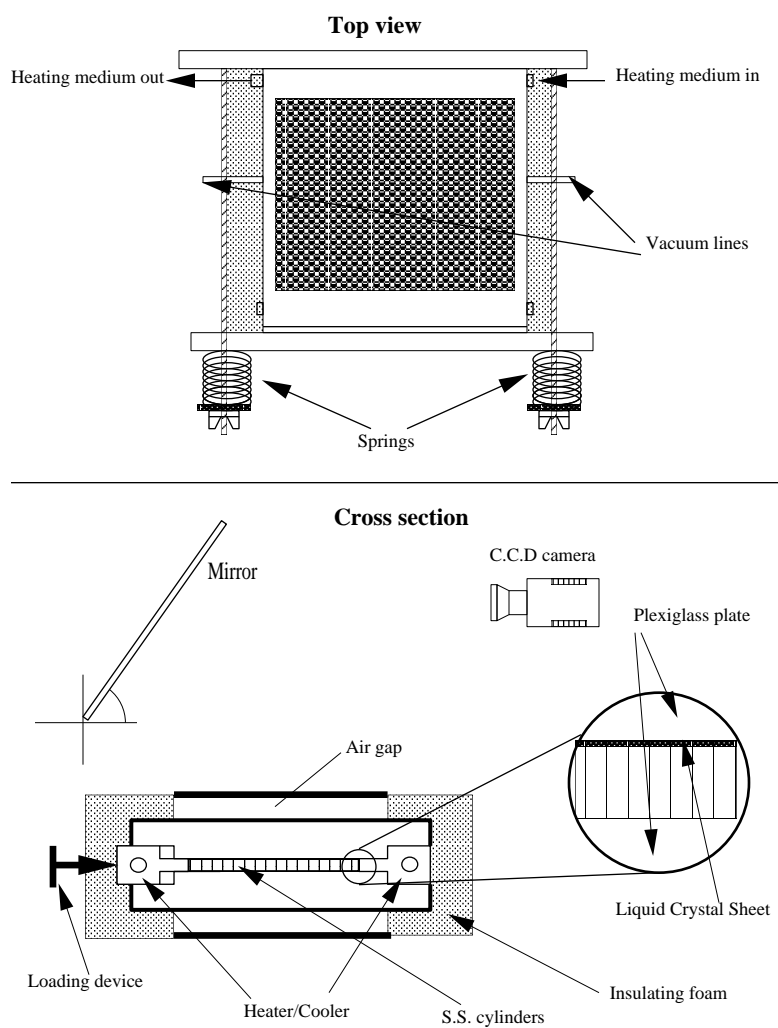
Figure 4.1 A schematic diagram of the static-bed experimental apparatus. A mono-layer of cylindrical particles are placed between the front and back plates (see Side View). A uni-axial load is imposed by compressing the bed – fins transmit the force to the individual particles. Three walls are insulated while the other is heated.

liquid crystal sheet at different constant temperatures, where for each temperature images are captured and hue values are measured. A curve fitting procedure is then performed through the collected points. A detailed description of the technique is given by Dabiri and Gharib [196]. With appropriate control of the thermochromic liquid crystal sheets, illumination and photographic recording, Dabiri and Gharib [196] have demonstrated that the temperature resolution ranges from a minimum of 0.01^o C at the lower temperature of the band to a maximum of 0.12^o C at the upper bound of the temperature band.

4.2.1.1 Procedure.

The liquid crystal used in the experiments is Hallcrest liquid crystal sheets with a temperature range from 25 to 30 ^oC, as specified by the manufacturer. In a typical experiment the liquid crystal sheet is placed between the two walls that contain the particle bed (see Figure 4.1), the device is sealed, loaded with a specified force by means of compressive springs and, finally, a vacuum is applied to extract the air from the particle bed. Unless specified otherwise, a total pressure in the range 27.0-50.0 kPa was used in all the experiments. The Rayleigh Number for our porous bed may be defined [199] as

$$Ra = \frac{Kg\beta l \Delta T}{\alpha_f \nu},$$ (4-3)

where K is the bed permeability, g is the acceleration of gravity, β, α_f, and ν are the thermal expansion coefficient, thermal diffusivity and kinematic viscosity of the fluid, respectively, and l is the gap spacing parallel to the gravity vector. Under the conditions examined in our experiments, this value ranges from $Ra = 2.0 \times 10^{-4}$ to $Ra = 7.0 \times 10^{-4}$ so that convective effects may be ignored (however, static conduction through the gas phase may still be important). Once the experimental device has been prepared, following the procedure described above, hot water at constant temperature is pumped through the heating device

in the experimental apparatus. The response of the liquid crystal sheet is followed in time by capturing images with a CCD camera. The RGB digitized images are saved for further analysis.

4.2.1.2 Image processing and calibration.

The processing of the RGB images involves first transforming the image from the RGB color space into HSI color space. The transformation used for calculating the HSI values follows the procedure described by Peterson *et al.* [200]. The HSI representation of the RGB color space is obtained through the transformation

$$\mathbf{H} = \quad cos^{-1} \left| \frac{0.5[(R-G)+(R-B)]}{[(R-G)^2+(R-B)(G-B)]^{1/2}} \right| \tag{4-4}$$

$$\mathbf{S} = \quad 1 - \frac{3}{(R+G+B)} min(R,G,B) \tag{4-5}$$

$$\mathbf{I} = \quad \frac{(R+G+B)}{3} \tag{4-6}$$

where the R, G, B values come from the digitized image. Equation 4-4 gives a value of hue in the range 0 to 180 degrees. When the ratio B/I $\geq$ G/I then H was set to H=360-H. $min(R,G,B)$ corresponds to the minimum of the three values of R, G, and B [201].

In order to calibrate the response of the liquid crystal sheet, a piece of sheet (6" x 12") of the one used in the experiment is heated to different constant temperatures, where for each temperature, images are captured and average hue values are determined. The hue averages are then correlated against their corresponding temperature.

4.2.2   TPD vs experiments

As a test of the TPD model of Section 3.2, consider an initially isothermal rectangular bed of particles under a uni-axial load (see Figure 4.2). Following the procedure described in Section 4.1, if three side walls are insulated and the bottom wall is subject to a step change in temperature, the transient thermal response of the "slab" of particulate material can then be evaluated. For a homogeneous system – or one for which a suitable effective medium assumption (EMA) may be made – this experiment represents an essentially one-dimensional heat transfer problem (see Figure 4.1) that can be described by the equation

$$\frac{\partial <T>}{\partial t} = \alpha_{eff}\frac{\partial^2 <T>}{\partial x^2} \tag{4-7}$$

where $\alpha_{eff} = \frac{k_{eff}}{<\rho C_P>}$ is the effective thermal conductivity of the bed, which in this work is obtained from the component of the anisotropic conductivity tensor that is parallel to the direction of heating. Due to changes in granular packing near a wall, it is common to denote a constant temperature boundary in granular materials as a "convective" boundary condition [71] to account for the imperfect contact between the bulk bed and the wall. In this case, we can obtain the temperature field analytically from Equation 4-7 – for times small enough that conductive effects do not reach the far wall – using

$$t = 0 \qquad T = T_o \qquad x \geqslant 0 \tag{4-7a}$$

$$x = 0 \qquad -k\frac{\partial T}{\partial x} = h_w(T|_{x=L} - T_w) \qquad t > 0 \tag{4-7b}$$

$$x \to \infty \qquad T = T_o \qquad t > 0. \tag{4-7c}$$

This yields the solution

$$\Theta = \quad erfc\left[\frac{\eta}{2\sqrt{\tau}}\right] - erfc\left[\frac{\eta}{2\sqrt{\tau}} + Bi_{bed}\sqrt{\tau}\right] e^{(Bi_{bed}\eta + Bi_{bed}^2\tau)} \qquad (4\text{-}8)$$

where Θ is the dimensionless temperature given by $\Theta = (<T> -T_o)/(T_w - T_o)$,$\eta = x/L$, $\tau = \alpha t/L^2$, and the Biot number of the bed $Bi_{bed} = h_w L/k$. In what follows, the effective thermal conductivity from both TPD and experiments is obtained by fitting the width-averaged data using Equation 4-8. In a (roughly) hexagonally packed system (like the one used in our experiments), the local void fraction is approximately constant so that effective properties may naively be expected to be essentially independent of space. In this case, the temperature front should propagate uniformly (across the width) through the bed.

Figure 4.3 shows a series of snapshots (essentially a contour plot, color-coded by temperature) of a TPD simulation, an experiment, and the corresponding one-dimensional, scalar EMA solution of this exercise (Eq. 4-8). The experiments are carried out as described in Section 4.2.1.1.

One can see in the case of both the TPD simulation and the experiment that the temperature front is, in fact, not uniform across the width of the container – a result which would be impossible in a one-dimensional, scalar EMA description. The presence of stress chains provides a simple explanation of this result. As the conductivity of each particle-particle junction is dependent on the imposed load, one would intuit that the conductivity along stress chains would be elevated. Therefore, even in a seemingly uniform bed, the temperature front will be jagged, with the vertical position of the front at a particular point along the container's width oscillating as stress chains converge and diverge along the bed height. However, for the particle beds examined here, a quantitative comparison of the width-averaged temperature as a function of bed height (see Figure 4.4) shows good agreement between both TPD simulation and the EMA model(Eq. 2-1) – using the effective
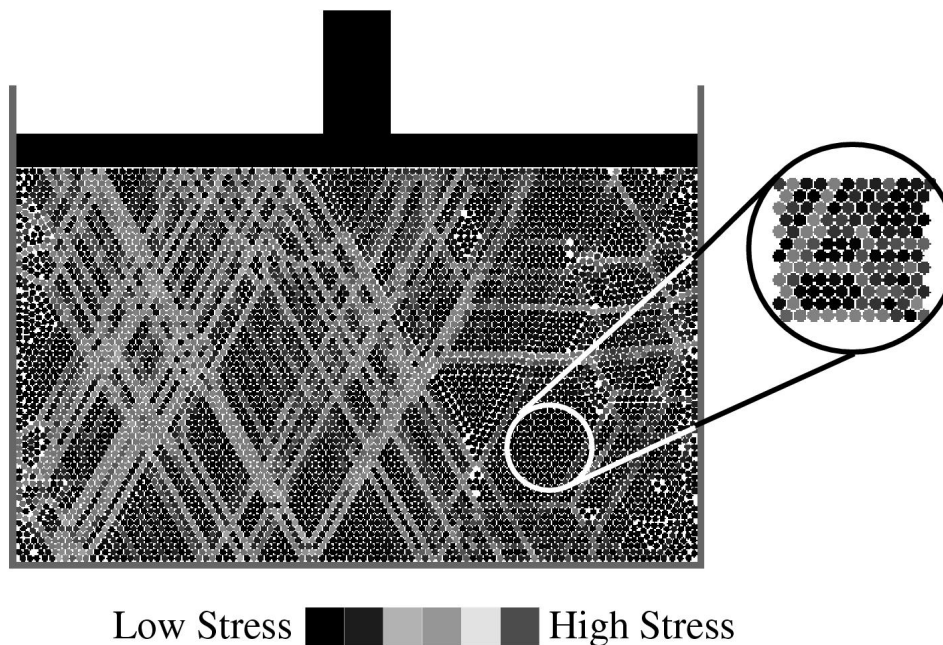
Figure 4.2 Stress chains in a particle bed under loading. In all but a perfect lattice, forces follow preferred paths in a granular material – "stress chains". As the contact conductance (H) is proportional to the normal force (F_n) between the particles ($H \propto F_n^{1/3}$ for smooth, elastic particles; $H \propto F_n^{1.0}$ for rough contacts), stress inhomogeneities can be expected to play an important role in granular heat conduction. (Note that inhomogeneities are evident even in the (rescaled) blown up region.)

| TPD Model | Experiment | EMA Model |

75 min

25 min

3 min
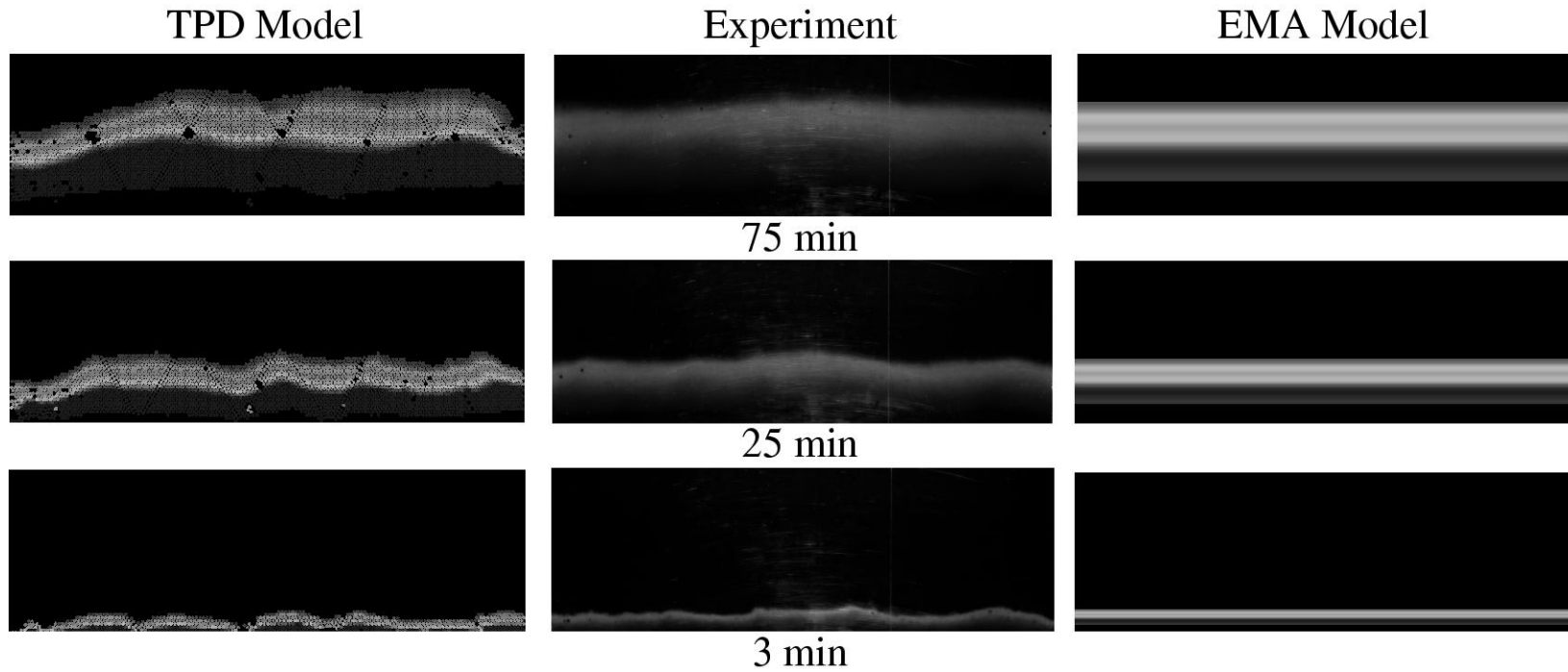
Figure 4.3 Thermal maps of a two-dimensional particle bed. The temperature front in a transiently heated granular bed does not propagate uniformly, as may be expected using an effective medium approximation. Instead, the front oscillates as stress chains converge and diverge along the bed height. This figure shows snapshots of a TPD simulation, an experiment, and a one-dimensional EMA simulation of a heated particle bed at three different times.

thermal diffusivity as a fitting parameter – and our experiments. This suggests that macro-scale quantities may still be captured using an averaging technique (provided the distance between stress chains remains small compared to our averaging length).

Perhaps a more striking result is seen when one examines both the stress distribution and the heat transfer together. Consider the granular bed shown in Figure 4.2. By simple measures of the local structure of the bed (void fraction, for example) the bed is approximately uniform; however, stress chains distribute the confining load non-uniformly. Superimposing the stress-field onto a temperature contour obtained from TPD (see Figure 4.5(a)), shows that the propagation of heat is also non-uniform. The temperature front on the left-hand side has advanced considerably relative to that of the right-hand side. Following our simple arguments above, this is certainly due, in part, to the high density of stress chains on the left. Additionally, however, the essentially *horizontal* stress chains on the right seem to act as barriers to heat transfer! These chains effectively channel heat along their length until the lateral temperature gradient is so small as to prohibit further re-direction. As further evidence of this, Figure 4.5(b) shows a vector field of the heat flow through the bed. It is clear that along the stress chains heat conductivity is large and heat flow is rapid (large, red arrows), and that heat flow beyond the horizontal stress chains on the right of Figure 4.5(b) is severely hampered. Moreover, one can see that there are regions within the bed, perhaps isolated from their neighbors by similarly *insulating* stress chains, that receive little or no heat flow (open circles).

4.2.3   Effect of external load

In order to examine the effective thermal conductivity as a function of external load several simulations and experiments are performed. Data of the effective conductivity at vacuum conditions provide a measure of the solid conductivity in the packed bed. These vacuum results are shown in Figure 4.6.
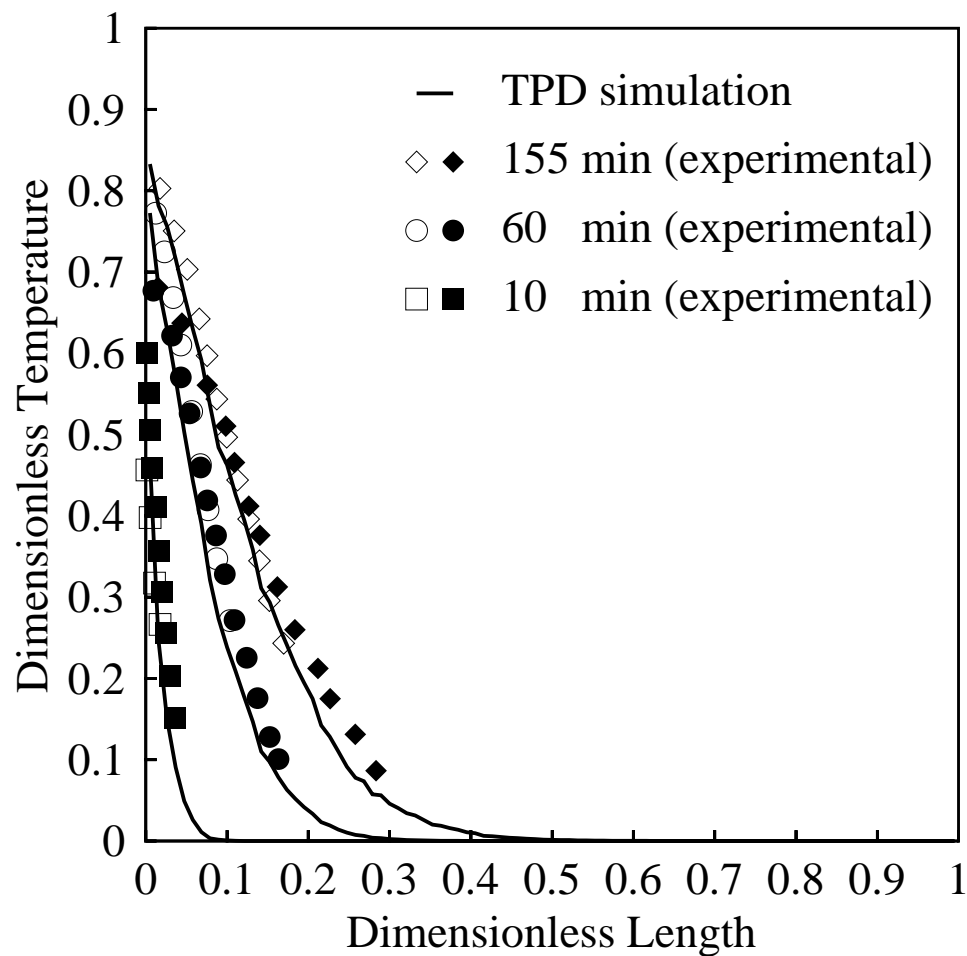
Figure 4.4 Quantitative comparison of TPD and experiment. Shown is the width-averaged temperature of the particle bed from Figure 4.3 for both the TPD simulation (lines) and the experiment (symbols). Note that the agreement is quite good without requiring any adjustable parameters. However, a consistent under-estimation is observed which may be due to the small by finite conductivity of the gas still present during the experiments.
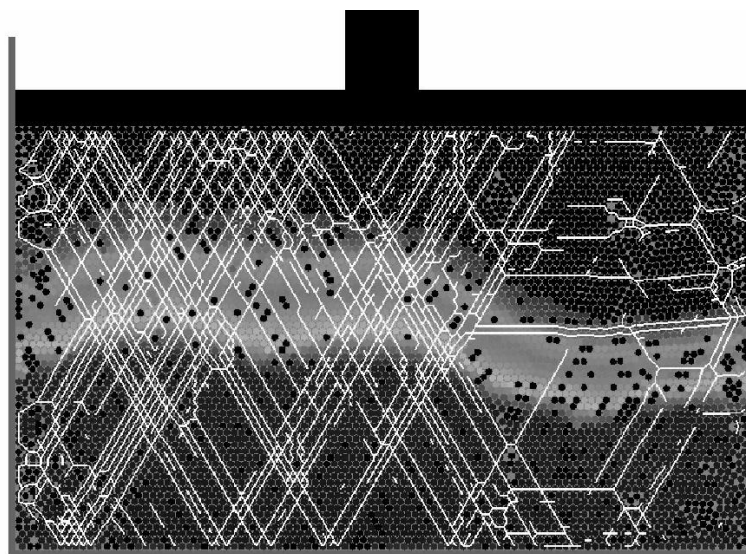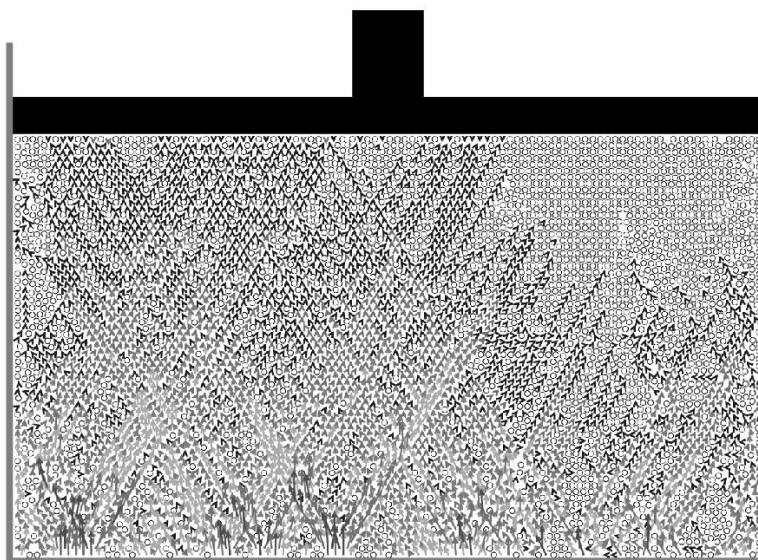
Figure 4.5 The effect of stress chains on heat transfer. (a) Here the temperature field (color-coded) is superposed over a plot of the stress field within the material. The white lines denote particle contacts which experience larger-than-average stress. Note that the temperature front on the left-hand size has propagated further than the right-hand side. (b) Examining the heat flow in the particle bed provides hints to the origin of these non-uniformities. Heat flow along stress chains is significantly enhanced (large, red arrows). Additionally, however, the *horizontal* stress chains on the right seem to act as barriers to heat transfer. Similar effects may explain the isolated regions of very low heat transfer (open circles) which are effectively insulated from the rest of the bed.
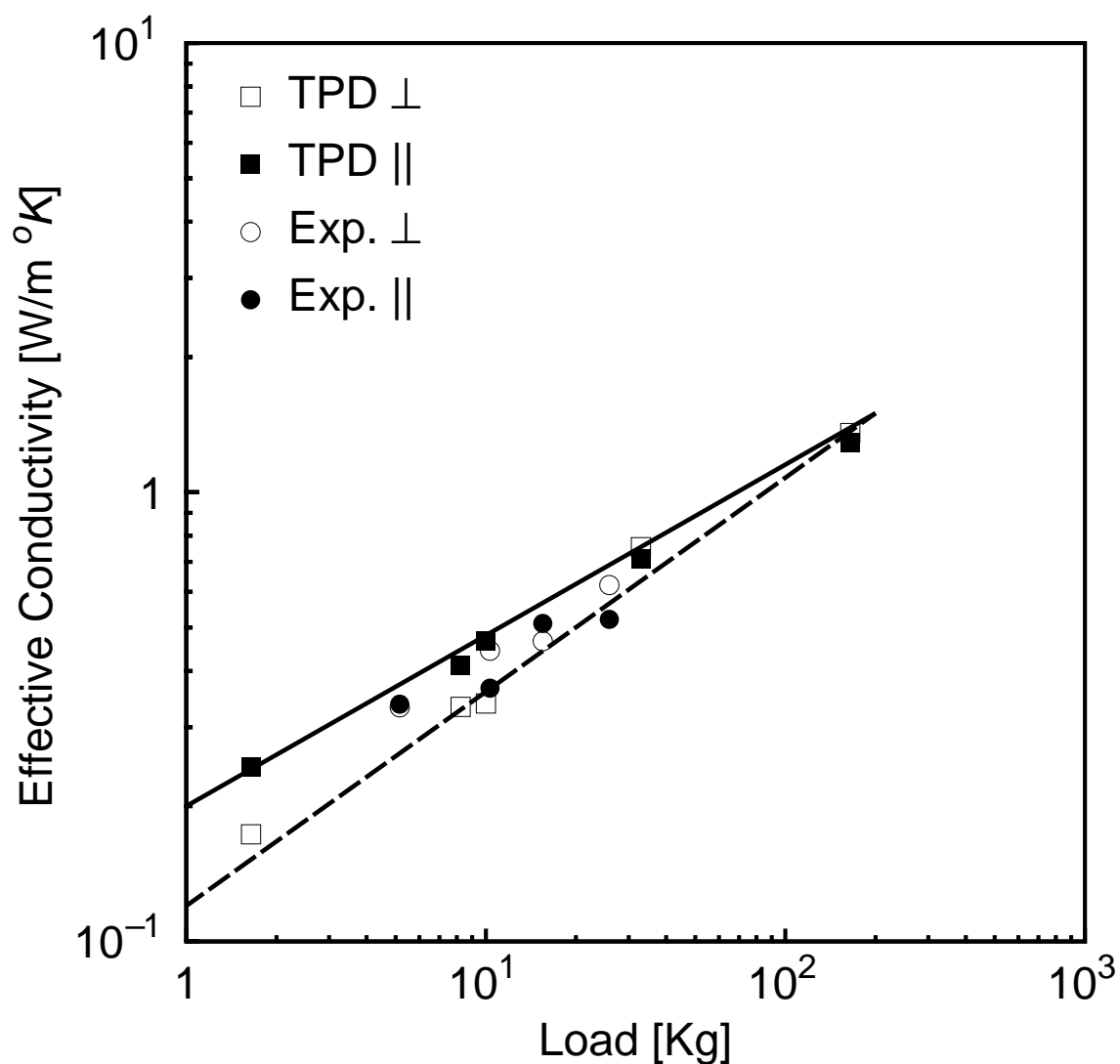
Figure 4.6 Thermal conductivity in a 2-D packed bed of aspect ratio $(W/H) = 1.5$ under vacuum conditions as a function of external load. The lines indicate curve fits of the TPD data. It is interesting to note that the slope for the solid line is 0.37, and for the dashed line the corrresponding value is 0.46 in close agreement with the theoretical value of $1/3$ which would be obtained for the Hertzian deformation of a single particle. A possible explanation of this result is that the distribution of contact forces is only a weak function of the overall contact force.

Figure 4.6 illustrates data for two different configurations, we will refer to this configuration as parallel ($\parallel$) and perpendicular ($\perp$). The *parallel case* involves raising the temperature of the bottom wall, while maintaining the top wall at the initial temperature of the bed (so that heat flows parallel to the direction of the imposed load). The second case, here called the *perpendicular case*, corresponds to the heat being supplied at the right wall (so that heat flows perpendicular to the direction of the imposed load). Two important observations can be made from Figure 4.6. First, the dependence of the effective conductivity on external load is surprisingly close to the 1/3 value that would be expected from the Hertzian deformation of *one* particle. The log-log slopes for the parallel and perpendicular cases are 0.36 and 0.46 respectively. This suggests that, as the total load is increased, the distribution of contact forces throughout the bed does not vary – in agreement with the findings of other authors[13, 23, 202]. Second, the anisotropy of the bed, as a result of the preferential orientation of the contacts in the direction of the load, decreases steadily with the increase in external load and eventually reaches a limiting value.

The effect of structural anisotropy on the effective thermal conductivity is evaluated by calculating the fabric tensor (see Sec. 2.2). The fabric tensor components are obtained from our simulations following the procedure described in Section 2.2. A typical plot of the evolution of the distribution of contact normals, $E(\mathbf{n})$, as a function of compressive load is shown in Figure 4.7 for the beds considered in the present study.

It can be observed that the degree of anisotropy decreases with the externally imposed load. This effect is due, in part, to small changes in the average coordination number at high compressions, but is primarily due to rearrangements of the stress distribution. As evidence of this assertion, it is instructive to examine the probability distribution of relative force *magnitudes* as seen in Figure 4.8. As the imposed load is increased, one can see that
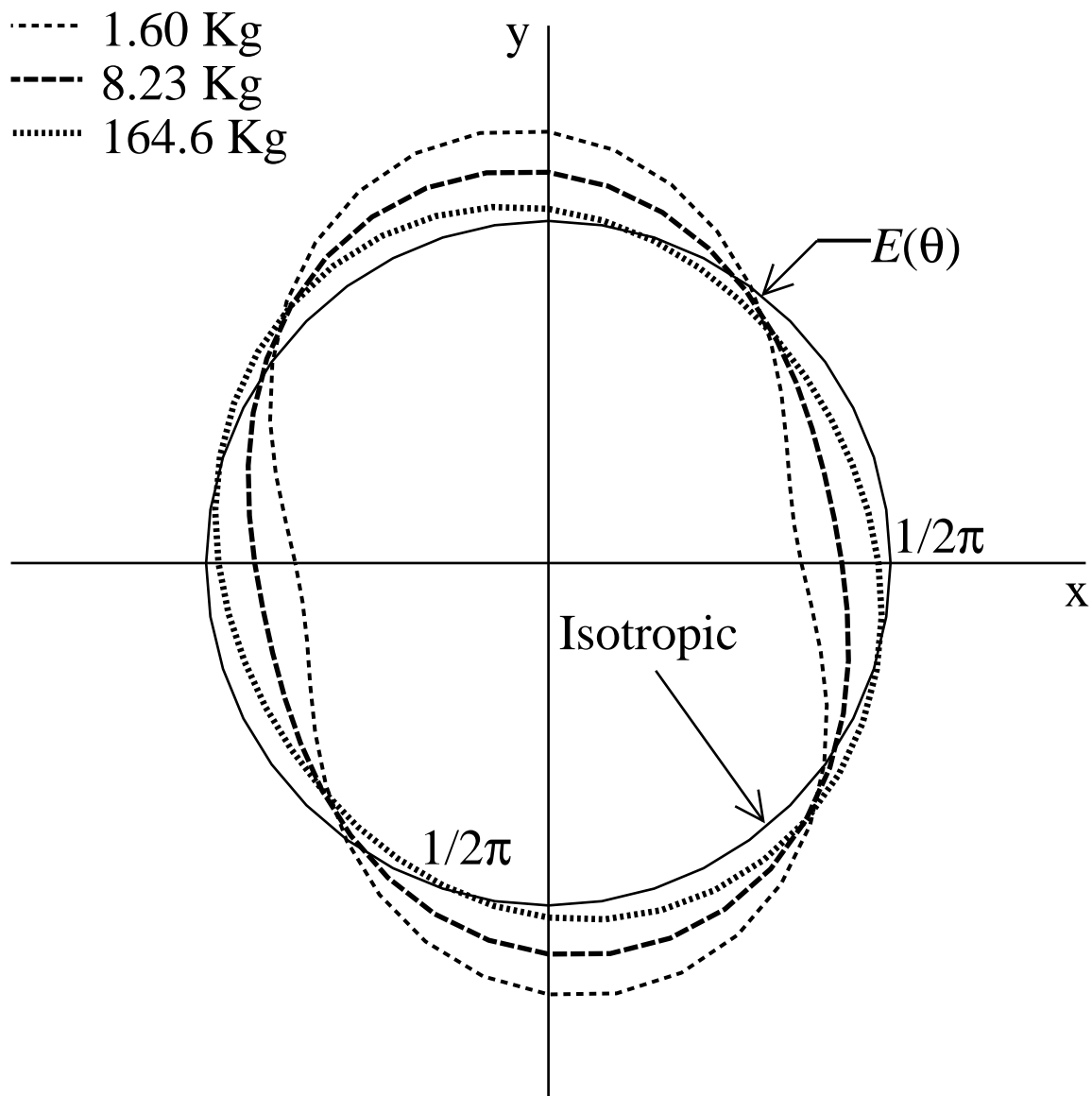
Figure 4.7 Evolution of the contact distribution anisotropy for a two dimensional bed of granular media under differing compressive loads. Description by a second rank tensor F_{ij}. The second rank tensor F_{ij} seems to be enough for the description of structural anisotropy for simple loading history. A four order rank tensor seems to be necessary in the case of more complex load history [203].
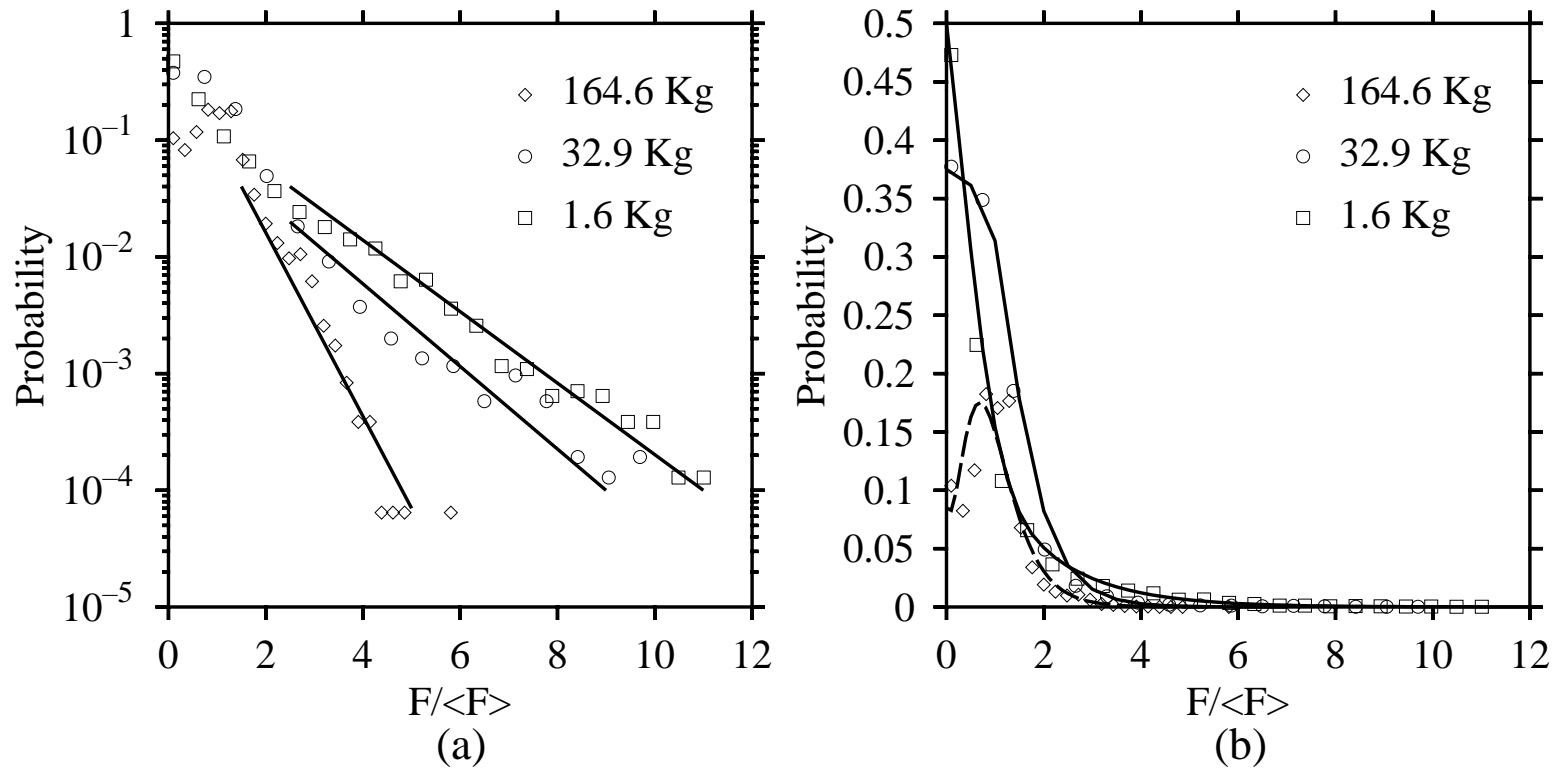
the width of the force distribution becomes smaller and the probability of finding a contact with the *average* force increases [204].

The stress map shown in Figure 4.9 illustrate how the contact force distribution changes as a function of the load. It is observed that the forces above the average, here represented by the dark lines, become more dense as the external load is increased from roughly 1.6 kgs to 165 kgs. The differences in the degree of ordering evident from Figure 4.9, is also clear in Figure 4.8 where the distribution of contact force has been plotted for the three loads depicted in Figure 4.9.

4.2.4   Effect of aspect ratio

The stress map shown in Figure 4.10 illustrate how the contact force distribution changes with aspect ratio W/H at constant load. The evolution of the distribution of contact normals $E(\mathbf{n})$, is used to visualize the effect of varying the aspect ratio as shown in Figure 4.11. Figure 4.10 and 4.11 indicate that for the conditions and parameters considered here, beds with aspect ratio below or close to one exhibit a similar degree of anisotropy. On the other hand, beds with aspect ratios above one exhibit a high degree of anisotropy. In general, a similar effect to that of changing the load is observed (see Section 4.2.3). The anisotropy of the bed changes significantly with relatively small changes in the aspect ratio. A rearrangement of the microstructure is evident.

The results of the predicted effective conductivity from TPD and continuum models (Equation 2-16) are shown in Figure 4.12. It is observed that, the conductivity in the parallel and perpendicular cases are different and that, as the aspect ratio increases, the differences between them seems to increase. This observation suggest that the microstructure of a granular bed can be altered by changing the bed geometry or the imposed load and, as in traditional materials processing, the effective properties can be *tuned* via these changes in microstructure.

Figure 4.8 The distribution contact force magnitudes as a function of external compressive load plotted on (a) a log scale to emphasize the width of the distribution, and (b) a linear scale to show the growth of the maxima at $F/ < F > = 1$.
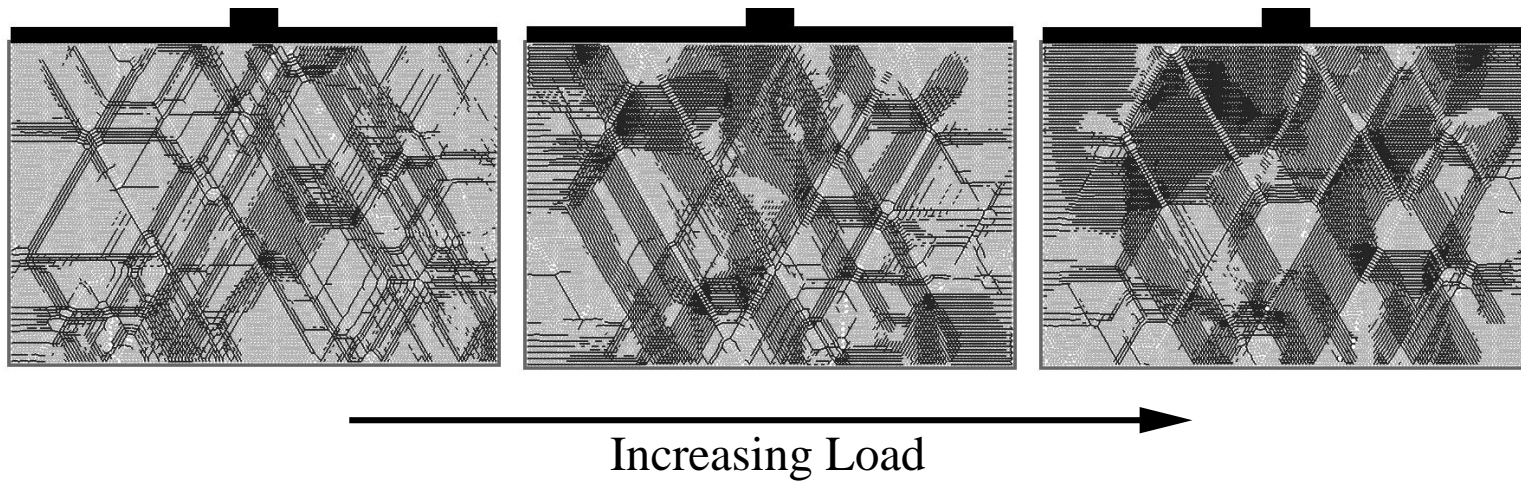
Figure 4.9 Stress maps as a function of external load. Dark lines represent forces above the average. As the imposed load is increased, the probability of finding contacts with the *average* force also increases. Note the higher density of dark lines.

W/H=4.8

W/H=2.0

W/H=1.0

W/H=0.22
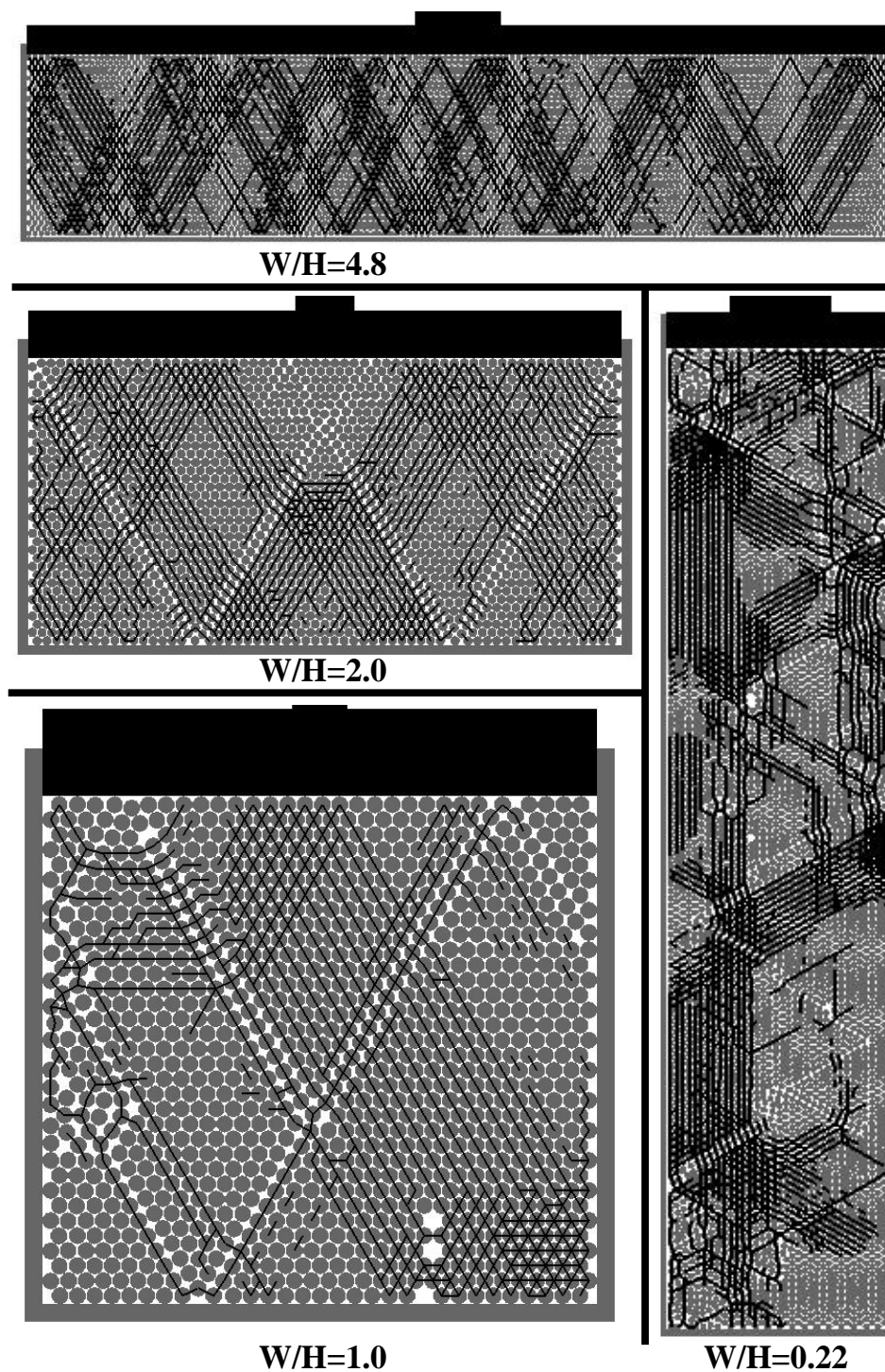
Figure 4.10 Stress maps as a function of aspect ratio. Dark lines represent forces above the average. The distribution of the contact forces changes significantly with relatively small changes in the aspect ratio. This suggests that the effective properties of the beds can be *tuned* via these changes in microstructure.
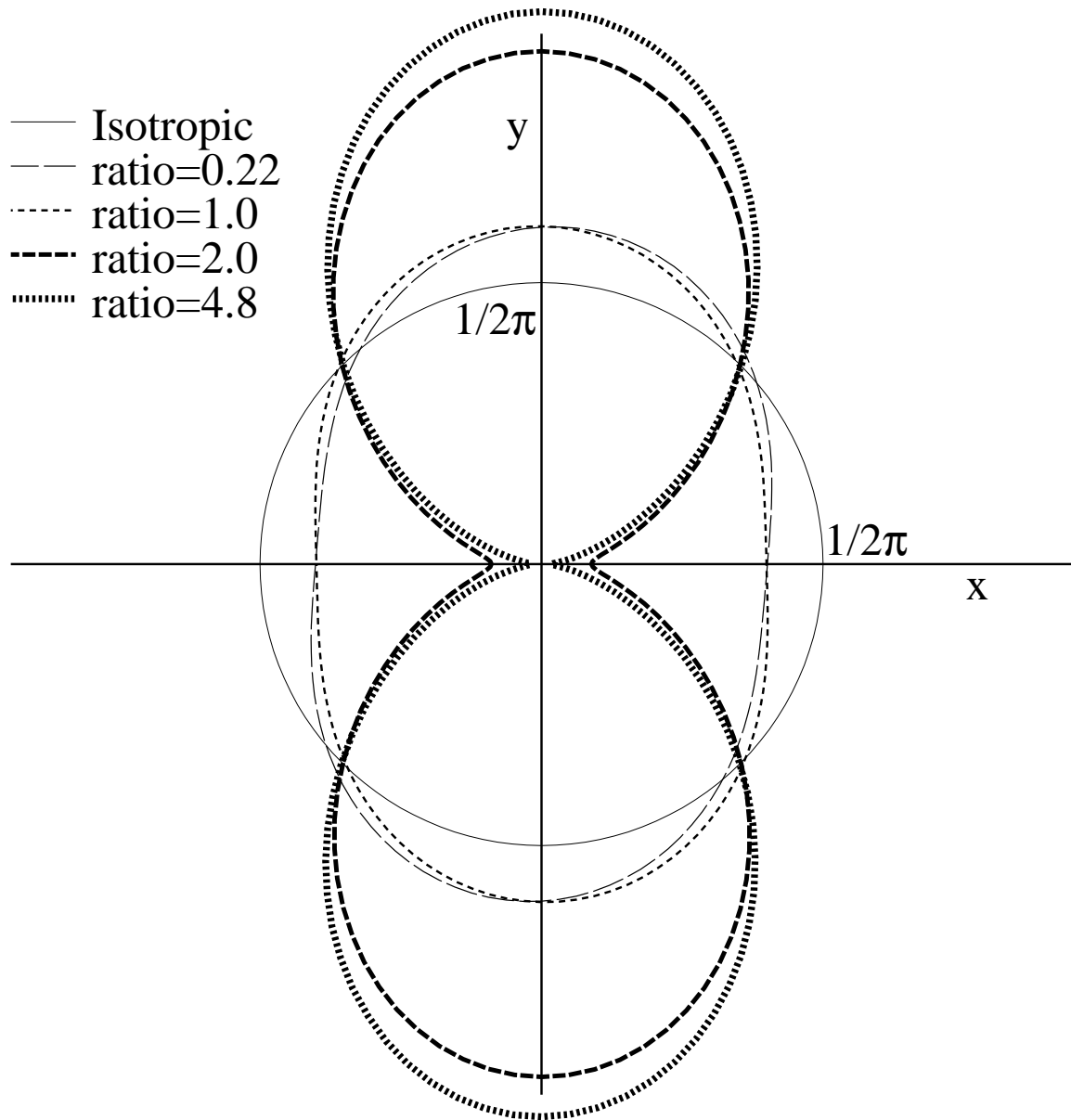
Figure 4.11 Evolution of the contact distribution anisotropy for a rectangular two dimensional bed of granular media with different aspect ratios.
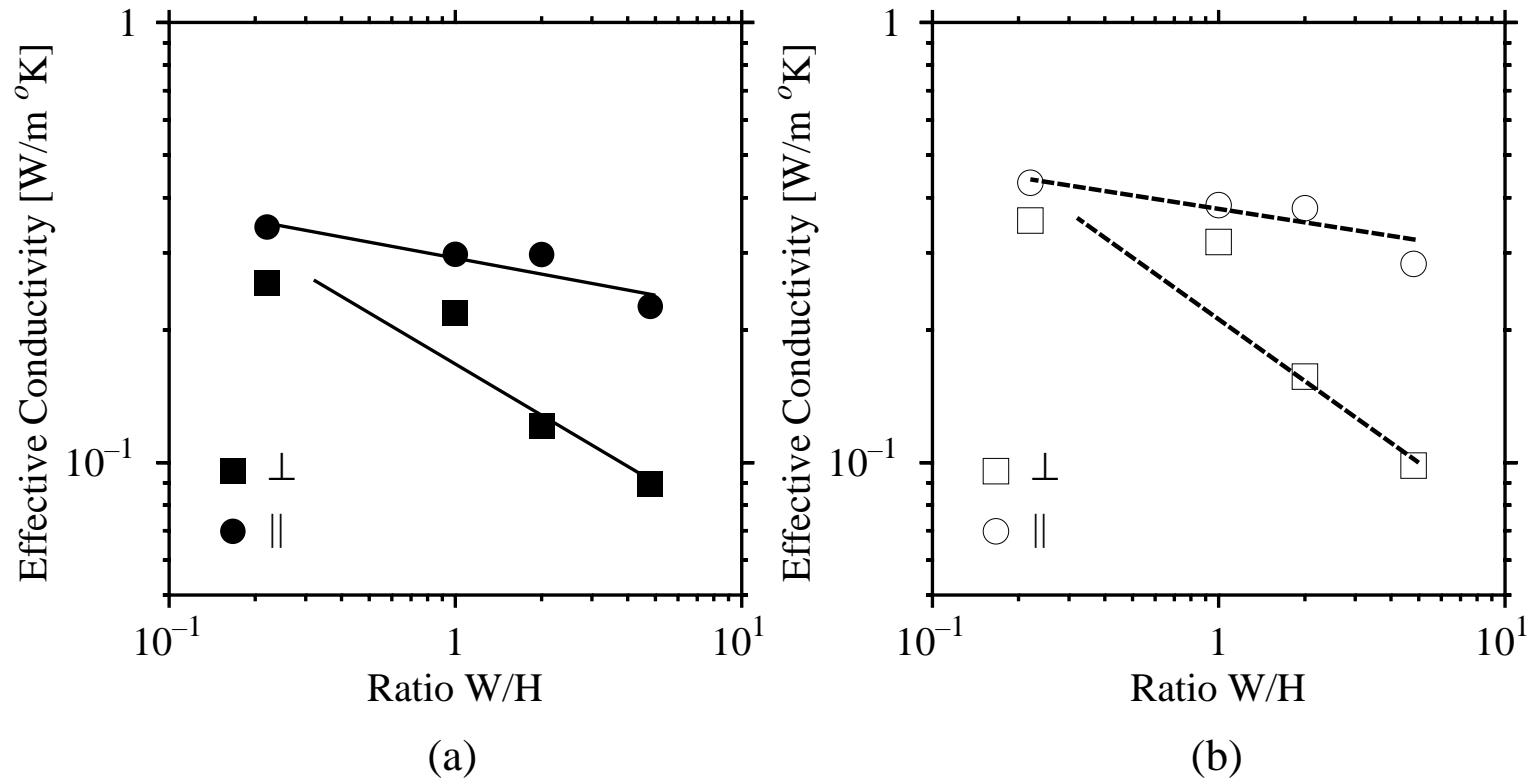
Figure 4.12 Effect of the aspect ratio on the effective conductivity (a) TPD model (b) continuum model based on the fabric tensor. Macroscale effective properties can be well reproduced using averaging techniques that take into account microstructural information other than void fraction.

4.2.5   Effect of the boundary geometry

The stress distribution inside granular media and its relation to microstructure remains a difficult problem to solve. For example, it is still unclear whether or when, a correct macroscopic description should include fluctuating aspects of the stress distribution, revealing the influence of boundary conditions, boundary geometries, material properties and/or the effects of long range stable structures in the bulk such as *stress chains* [205]. One might naively guess that the stress distribution at the interior of a two-dimensional packed bed under external stress (loading) might be influenced by the geometry of the boundaries retaining the particles as the walls take the load and redistribute it, causing large variations in the microstructural *fabric* of the bed. Experimental observations as well as numerical simulations can be used to determine the correct answer. The results of this exercise are the focus of this section.

Three somewhat ideal geometries have been used in this study, namely a rectangular box, a trapezoidal geometry (resembling the converging section of a hopper) and a semicircular boundary. In all cases the particles are close to hexagonally packed. The advantage of examining these ideal beds is twofold. First, due to the ordering of the packing, the experiments can be realized both numerically and experimentally. Second, the confined geometries allow a direct visualization of the stress distribution at the interior of the bed. Moreover, these results might have some relevance to real systems.

In a granular material under external load, the forces are redistributed via contacts between the grains. Because of interparticle friction, load may be transmitted off axis and may often be arranged in complex "networks" (*stress chains*, see Figure 4.2) [206]. Vertical stresses are transformed into "horizontal" stresses that eventually reach and push the vertical walls. This elementary observation is the idea behind the heuristic theory set forth by Janssen [207]. For this reason, it is expected that the shape and location

of the boundaries, as illustrated in Figure 4.13, may play a significant role in the bed microstructure and, hence, the thermal properties.

Although a consensus on the nature of the distribution of contact forces in granular media and a physical model to capture this same force distribution has not been achieved, numerical simulation results (Figure 4.13) as well as experimental observations (Figure 4.14) conducted in this work, reveal interesting features. Figure 4.13 shows the stress distribution in two-dimensional packed beds for three different bounding geometries. The stress field (here represented by the dark lines which denote particle contacts that experience stresses above the average) indicates that the geometry of the boundaries contributes significantly in the redistribution of the confining stress.

The images in Figure 4.14 demonstrate experimentally observed stress-chains visualized using a birefringence experiment. In birefringence experiments, polarized light is shown through photo-elastic particles. A camera with a cross polarized (90°) lens is then used to capture images. As the particles are stressed, they rotate the light so that stressed regions appear brighter than non-stressed regions. As expected, the lines of strongest stresses form a network which is more and more connected when the load is increased; however, even at high loads many grains remain excluded from the networks. The experimental photo-elastic study of Figure 4.14 qualitatively displays the same features observed in the simulations of Figure 4.13.

By simple measures of the local structure of the beds (void fraction for example), these beds are approximately uniform; however, stress chains distribute the confining load non-uniformly. It is clearly observed that the walls have a directing effect. To support this assertion, Figure 4.15 illustrates the evolution of the contact distribution anisotropy for the three geometries considered.
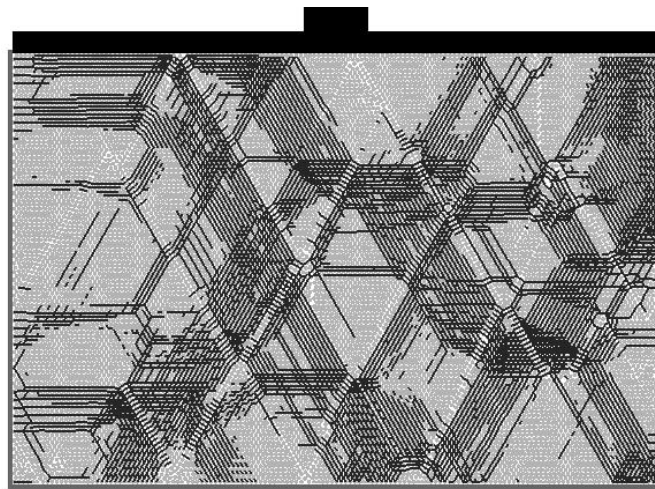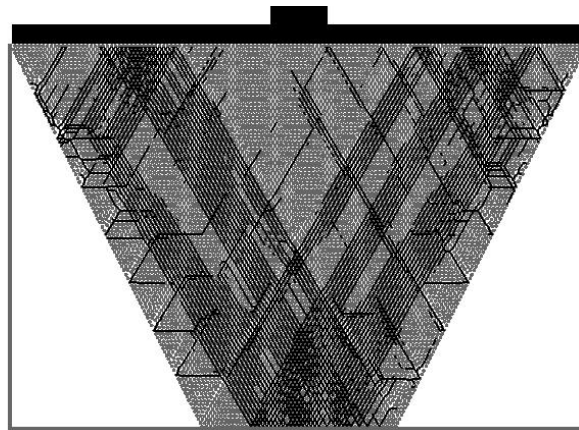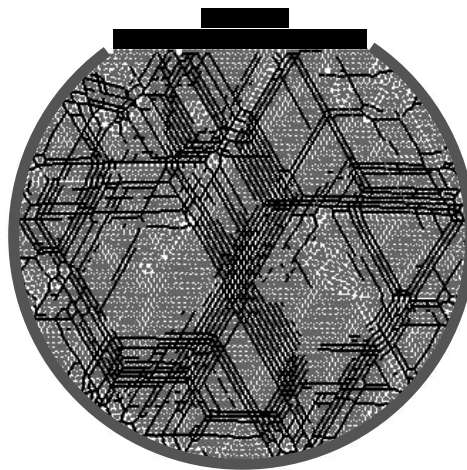
Figure 4.13 Stress distribution in two-dimensional packed bed geometries as calculated from TPD. (a) Rectangular. (b) Trapezoidal. (c) Circular. A constant external load of 10 Kg has been used in all three cases.
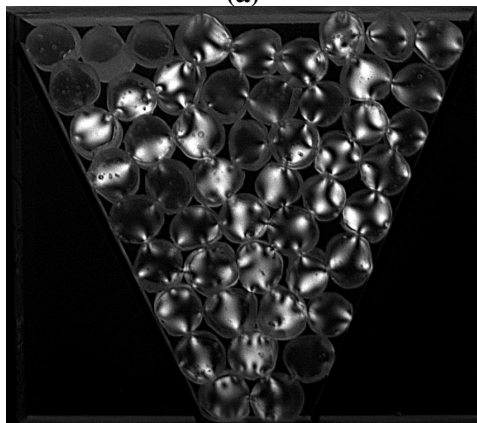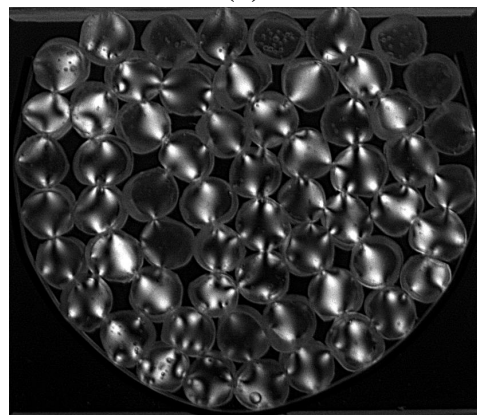
Figure 4.14 Experimental photo-elastic fringe patterns showing stress-chain formation within two-dimensional packed bed geometries. (a) Rectangular. (b) Trapezoidal. (c) Circular.
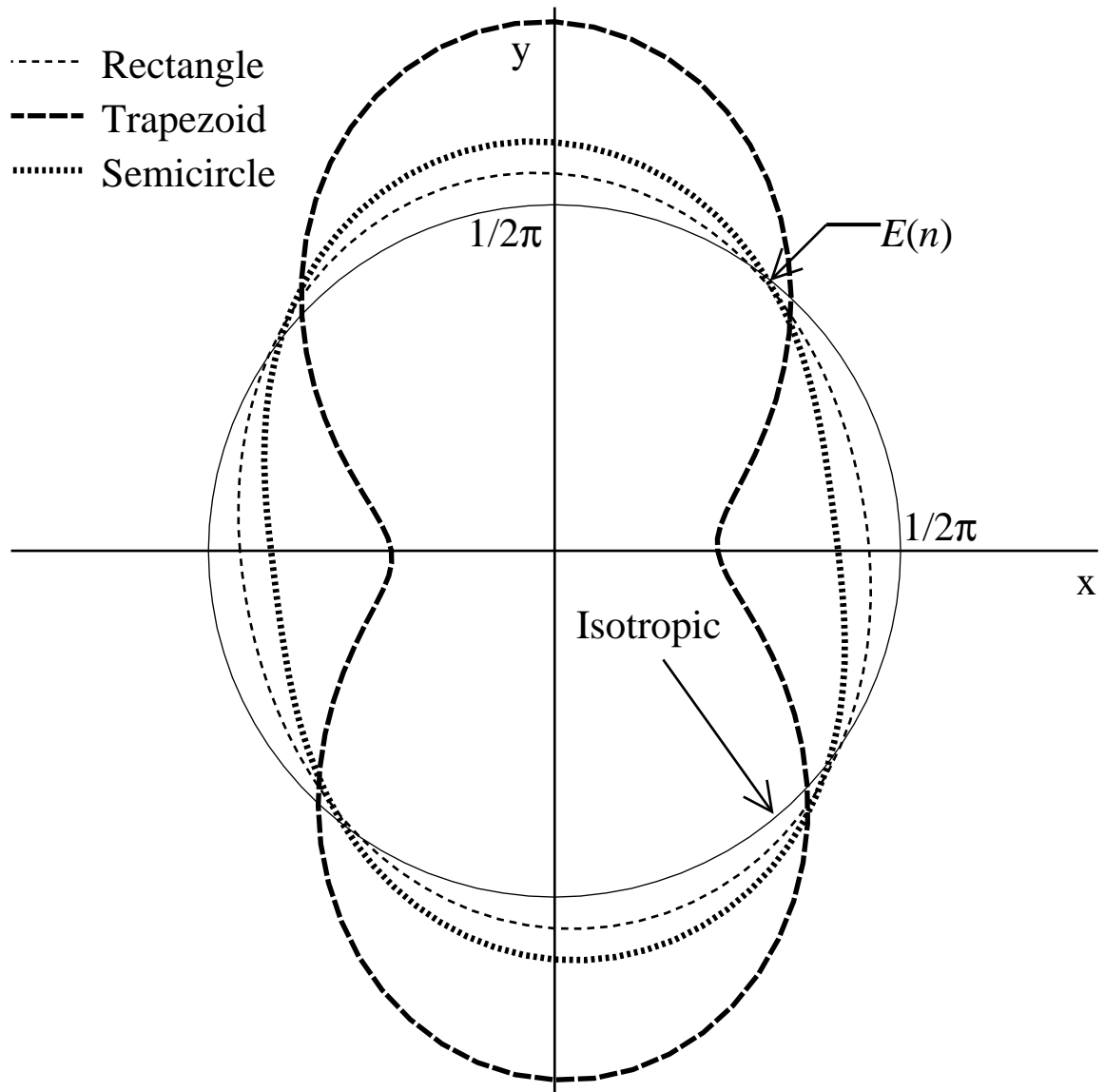
Figure 4.15 Evolution of the contact distribution anisotropy for a two dimensional bed of granular media as a function of the boundary geometry. Notice that the trapezoidal geometry induces significant structural anisotropy, while circular and rectangular geometries are less prone to preferential orientation.

Yet another way to investigate the microstructural effects caused by the geometry of the boundaries is to look at the contact force probability distribution. These distributions allow one to distinguish clearly the behavior induced by each of the bounding geometries. The probability distribution function of contact forces is plotted in Figure 4.16. A power law regime seems to describe the behavior of the distribution for forces above the average ($\frac{F}{<F>} > 1$), however, the slope (exponent) of the power law varies according to the geometry. For forces below the average a less obvious trend is observed. According with these observations, this orientational order (preference) has a great importance for the heat transfer problem in the three geometries considered.

Figures 4.17 - 4.18 illustrate the temperature field predicted using TPD for the circular and trapezoidal geometries, respectively. As the beds are heated from the boundaries, the temperature profiles at the interior of the bed are strongly influenced by the distribution of stress chains (see Figure 4.13). The effect of the bounding geometries is clearly visible in these figures. Experimental observations qualitatively support these observations, as described below.

The pseudo-two dimensional experiments are conducted using the same experimental set-up described in section 4.2.1. Inserts of the appropriate geometry are placed in between the plates in the experimental apparatus to provide the required bounding geometry. The experimental procedure is similar to that described in section 4.2.1.1.

A comparison of the predicted and experimental temperature profiles for the circular and trapezoidal geometries are shown in Figures 4.19 - 4.20. There is a reasonable agreement between the simulations and the experiments for the hopper geometry heated from the top (Figure 4.20). The semicircular geometry as well as the hopper geometry heated from the bottom show a qualitatively different behavior at the conditions considered: the profiles seem to be more flat in the experimental observations when compared with those of the
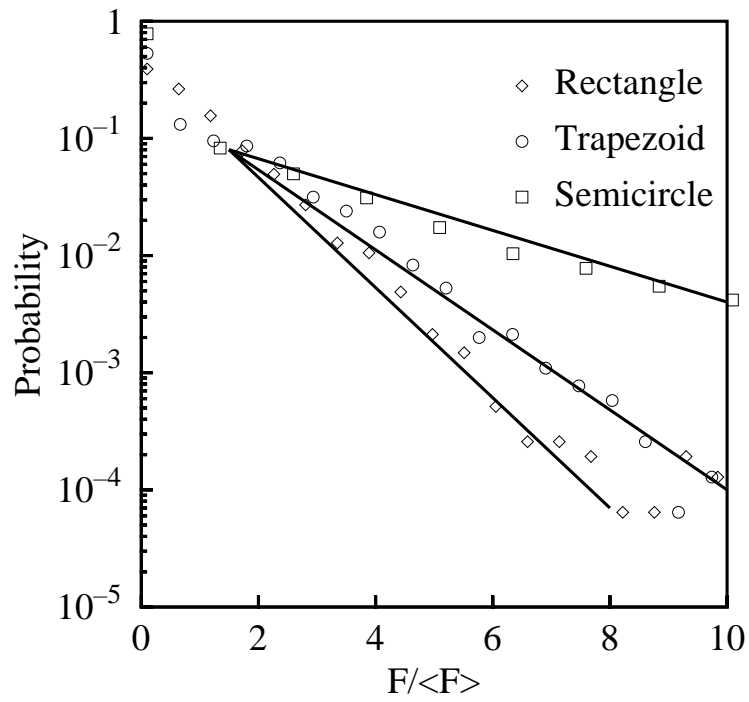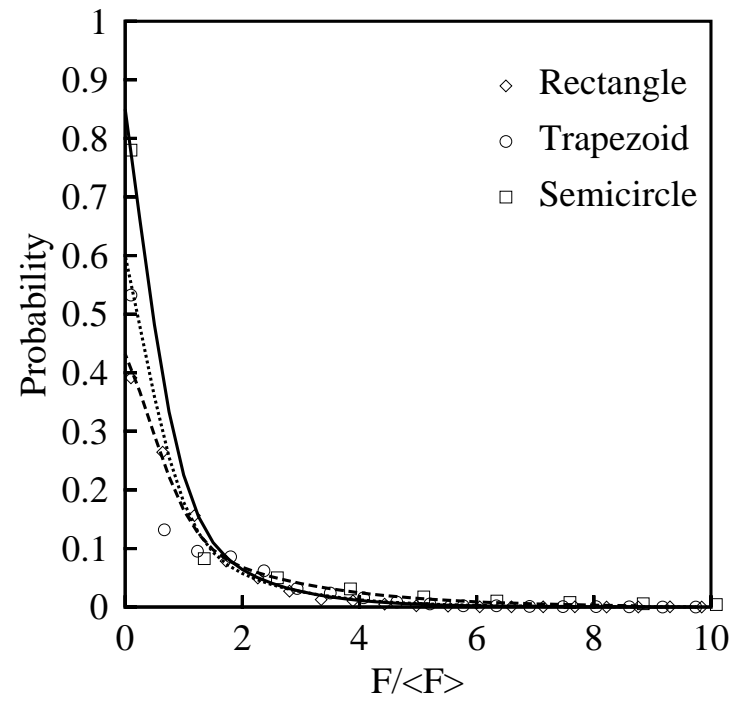
Figure 4.16 The distribution contact force magnitudes as a function of geometry (a) a log scale to emphasize the width of the distribution, and (b) a linear scale to show the intercept at $F/<F> \rightarrow 0$. The lines in (a) represent power law fits for values of $F/<F >> 1$. The lines in (b) represents curve fittings based on the correlation proposed by Mueth *et al.* [208].
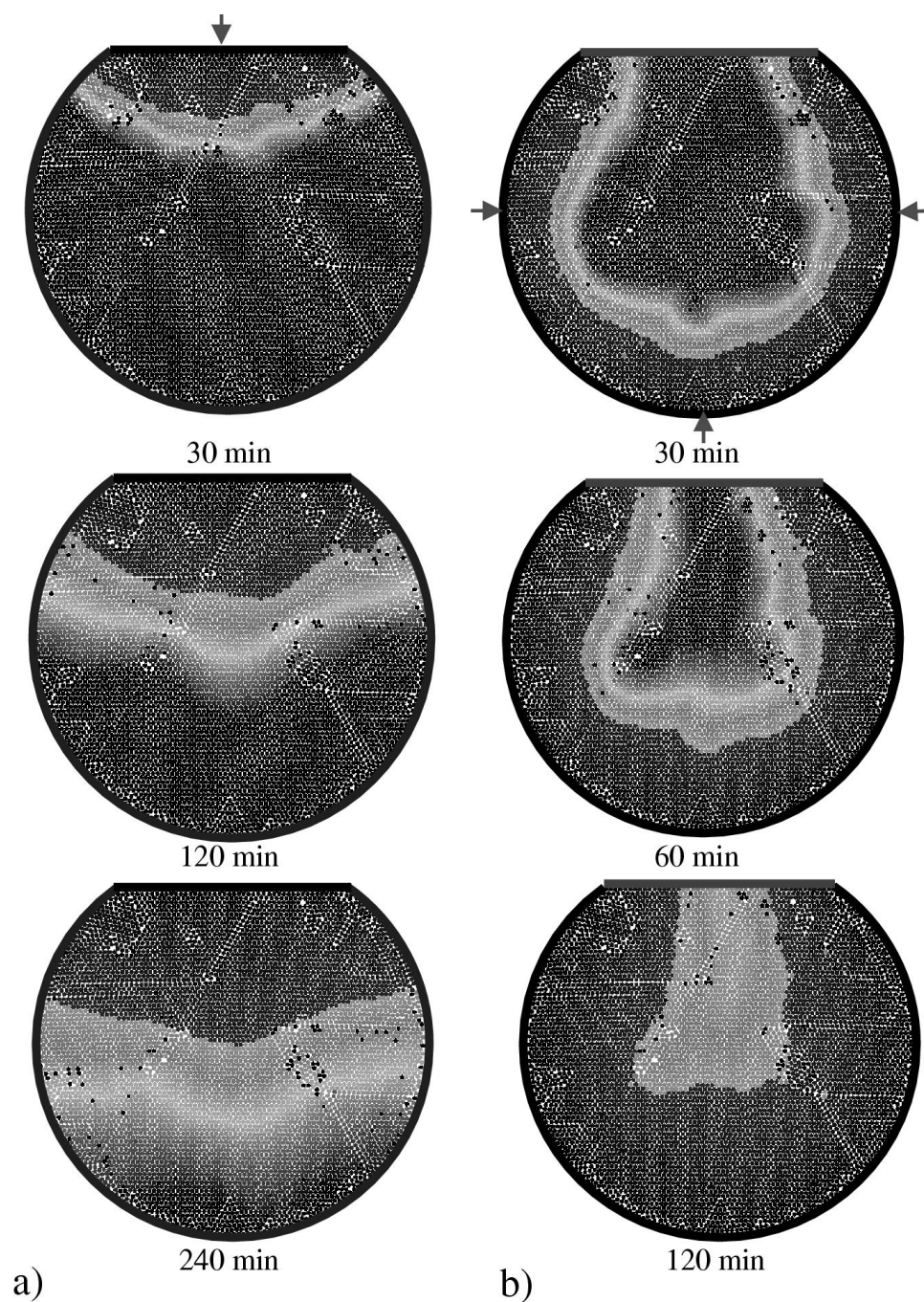
Figure 4.17 Temperature profiles in a circular geometry (a) Heating from the top. (b) Heating from the side walls. The arrows indicate the direction of the heat flow. Due to a higher surface area when heating from the side walls the time required for reaching an isothermal condition throughout the bed is substantially reduced.

30 min   30 min

60 min   120 min

120 min   180 min

a)   b)
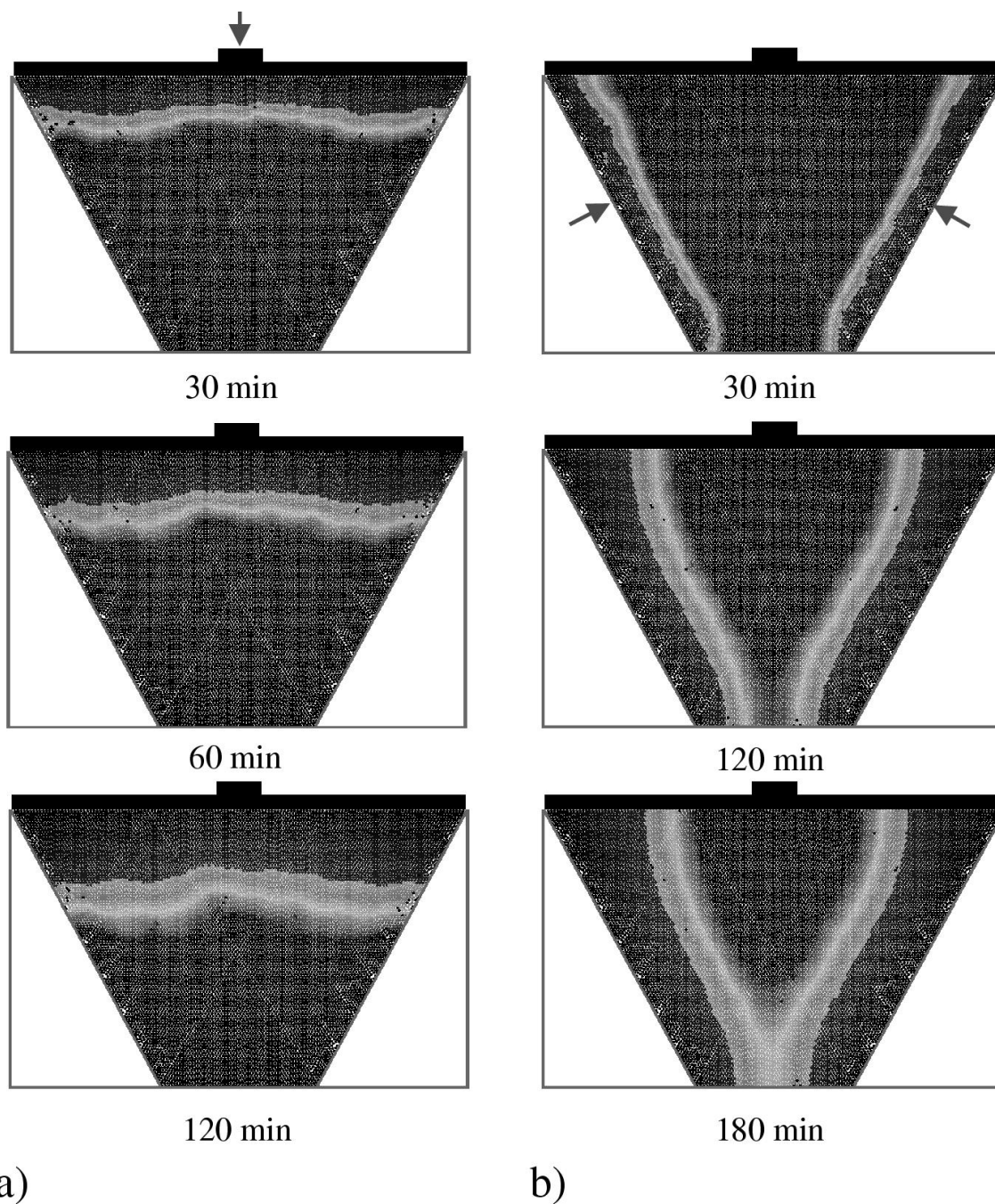
Figure 4.18 Temperature profiles in a hopper geometry (a) Heating from the top. (b) Heating from the side walls. The arrows indicate the direction of the heat flow.

simulations. This behavior could be a consequence of the shape of the particles (spheres in the simulation and cylinders in the experiments); however, the most probable cause for this discrepancy is the difference in the degree of friction at the walls of the container.

While the TPD simulations for the trapezoidal and circular geometries only roughly describe the experimental observations – for example, the advance of the front seems to be underpredicted, also the front of the profile is not as flat as in the experiments – the model does however, capture the essential behavior observed in these two geometries. A *structuring* effect on the heat flux as a result of the geometry of the boundaries is clearly visible.

4.3   Gas-Solid systems

The solids used in this part of the study are glass and SS-304 and the interstitial gases include air, CO_2 and helium. Beds ranging from 1000 to 10000 particles have been used in the simulations with all the relevant thermal and physical properties taken from the literature. The accommodation coefficient ac in Eq. 3-16, is a function of both the gas and the solid surface properties. Based on the experimental data available [30, 186], the following values for ac have been assumed: 0.95 for air, 1.0 for CO_2 and 0.3 for helium. Similar values have been used by Molerus [76], Masamune and Smith [209] and Zeng *et al.* [210].

4.3.1   Effect of gas pressure

Figure 4.22 illustrates the effect of the interstitial gas pressure on thermal conductivity for a 2-D bed of steel particles at a constant load. The sharp increase with pressure is due to a transition from free-molecule conduction (when the mean-free path is large with respect to the mean separation), for which k_g^* (Eq. 3-15) is directly proportional to the pressure, to a regime dominated by molecular collisions, in which k_g^* becomes independent of pressure and

Experiment	TPD Simulation

30 min

60 min

120 min
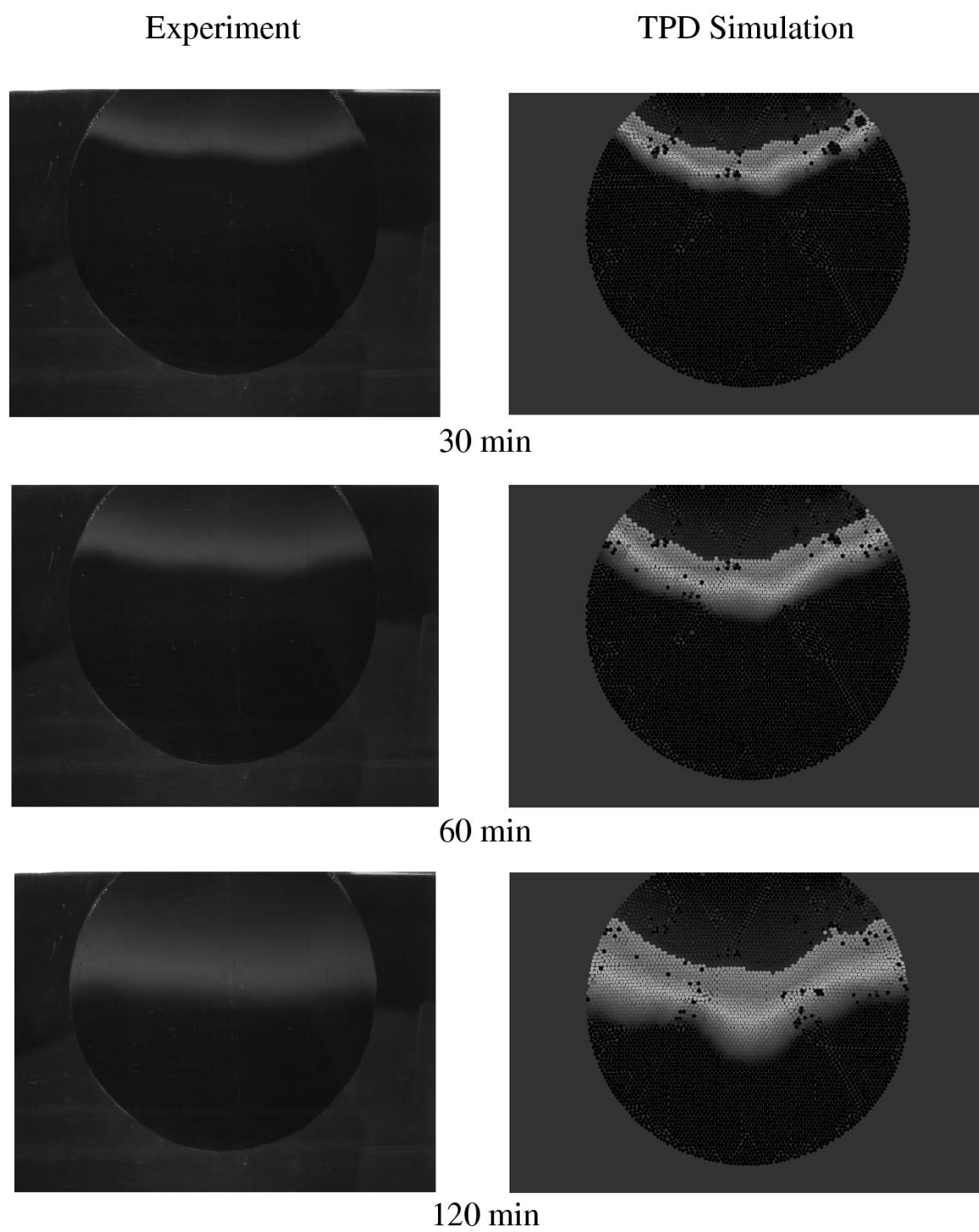
Figure 4.19 Temperature contours in a circular geometry. Experimental comparison.

Experiment TPD simulation

32 min

60 min

120 min
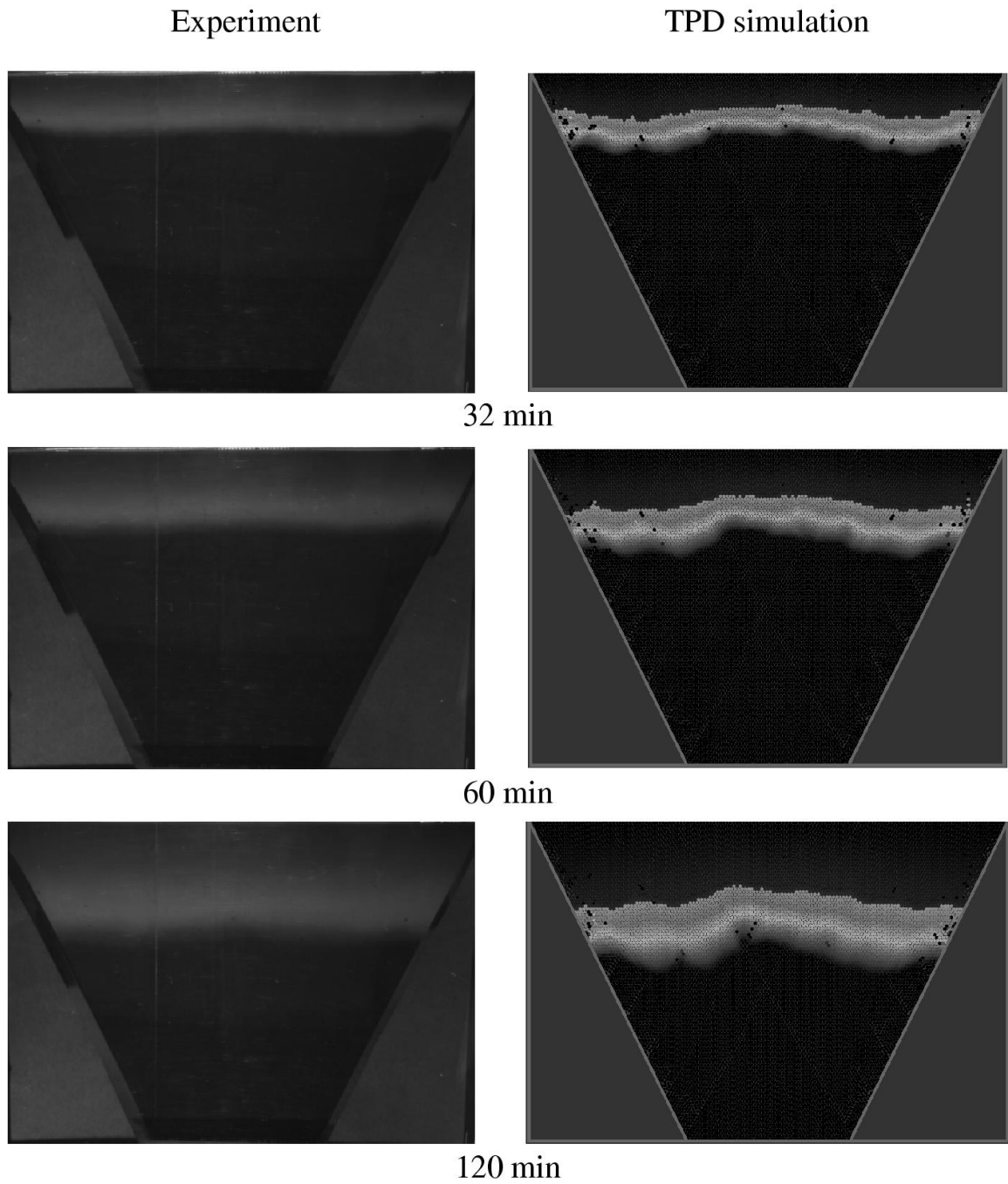
Figure 4.20 Temperature contours in a hopper geometry heated from the top. Experimental comparison.

Experiment   TPD simulation

120 min

60 min

30 min
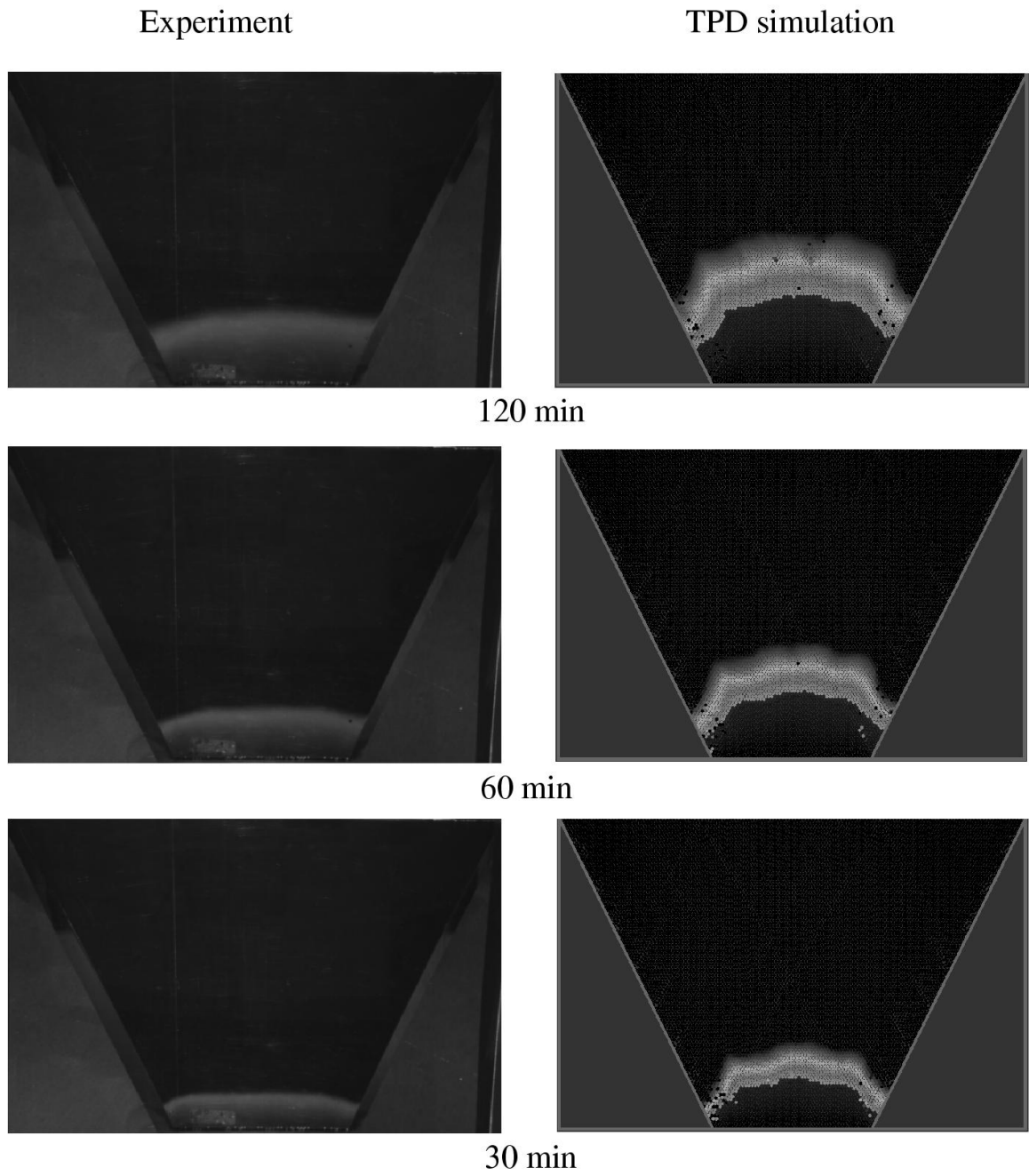
Figure 4.21   Temperature contours in a hopper geometry heated from the bottom. Experimental comparison.

$k_g^* \simeq k_g$ (and the mean-free path is small compared with the mean separation) [209, 211].
One should note that, under the conditions examined here (up to atmospheric pressure), the mean free path of Helium remains large compared to the mean particle separation. Experimental results qualitatively similar to those in Figure 4.22 have been reported by Masamune and Smith [183, 209] as well as Bauer and Schlünder [30].

Masamune and Smith [183] have proposed a semi-empirical correlation for calculating the effective conductivity of packed beds in the presence of gases that incorporates essentially the same mechanisms considered in our TPD simulations. Their equation is written as

$$k_{eff} = \alpha \epsilon k_g + \frac{(1 - \alpha \epsilon)(1 - \delta)}{\frac{\phi}{k_g^*} + \frac{1 - \phi}{k_g}} + (1 - \alpha \epsilon) \delta k_s. \qquad (4\text{-}9)$$

In this equation (Eq. 4-9) the terms on the right side represents the contribution of the (1) conduction in the void space (2) a series path involving the solid and gas phases and (3) conduction through the area of contact, respectively. The predictions based on this model are compared with those of a TPD simulation in Figure 4.22. In Eq. 4-9 δ is regarded as a specific parameter for each type of particle and is related by an empirical expression (Eq. 15 in their paper) to the contact area, whose value is obtained by extrapolating the conductivity to zero pressure (vacuum conductivity). Using the extrapolated value at zero pressure as determined from the TPD simulations in calculating the δ parameter in Masamune's model it is possible to obtain a good quantitative agreement between the correlation and the data predicted by TPD, as shown in Figure 4.22.

4.3.2 Effect of external load

The effect of air pressure on particle beds compressed at three different loads is shown in Figure 4.23. The results in Figure 4.23 show that the external loading affects primarily the conductivity of the solid phase – the value of the effective conductivity extrapolated at
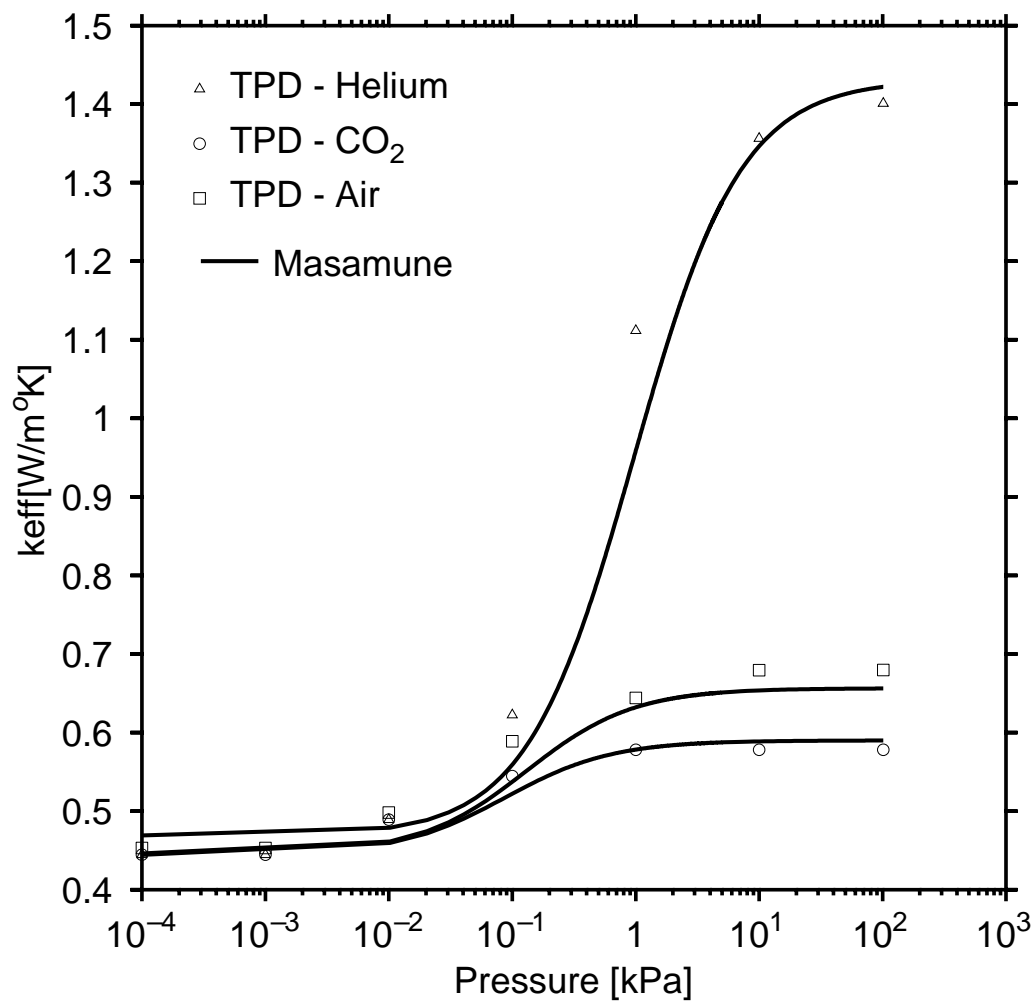
Figure 4.22 Predicted effective thermal conductivity in a 2-D packed bed as a function of pressure of the filling gas. Symbols indicate TPD simulations, the continuous line the predictions based on the correlation by Masamune and Smith [183].

zero pressure. All the profiles of effective conductivity reach a limiting value that is directly dependent on the effective conductivity at low values of pressure ("vacuum conditions"). Note however that as the load increases the effect of loading on the solid phase conductivity also seems to reach a saturation value – the separation of the curves at higher loads becomes smaller. A qualitative comparison with experimental data reported by Hadley [211] and Pratt [212] indicates that the shapes of the curves are similar.

4.4   Liquid-Gas-Solid systems

This set of numerical experiments are carried out with glass and SS-304 using water, glycerin and ethanol as interstitial fluids. All the physico-chemical properties of the fluids as a function of temperature are taken from the literature [191, 193].

4.4.1   Effect of Saturation

Figure 4.24 shows the variation of the effective thermal conductivity with fluid saturation. An increase of saturation degree up to about 10% results in a steep increase of the effective conductivity. Further increase of the saturation degree, however, gives rise to higher values, but at a rate of change which is much smaller. These observations can be easily understood considering the fact that the resistance experienced by the heat flux at the contact point is much higher than the one provided by the fluid; even a small liquid bridge can give rise to a steep increase in the effective conductivity. In contrast, at higher saturations, due to the curvature of the solid, an increase in the filling angle of the liquid bridge results in a small change in the cross section of the liquid bridge and little additional heat flow. Therefore, the increase of the effective conductivity becomes less pronounced at higher saturations. The predicted values in Figure 4.24 are in reasonable agreement with the experimental observations provided by Okasaki [185] and Büssing and Bart [213].
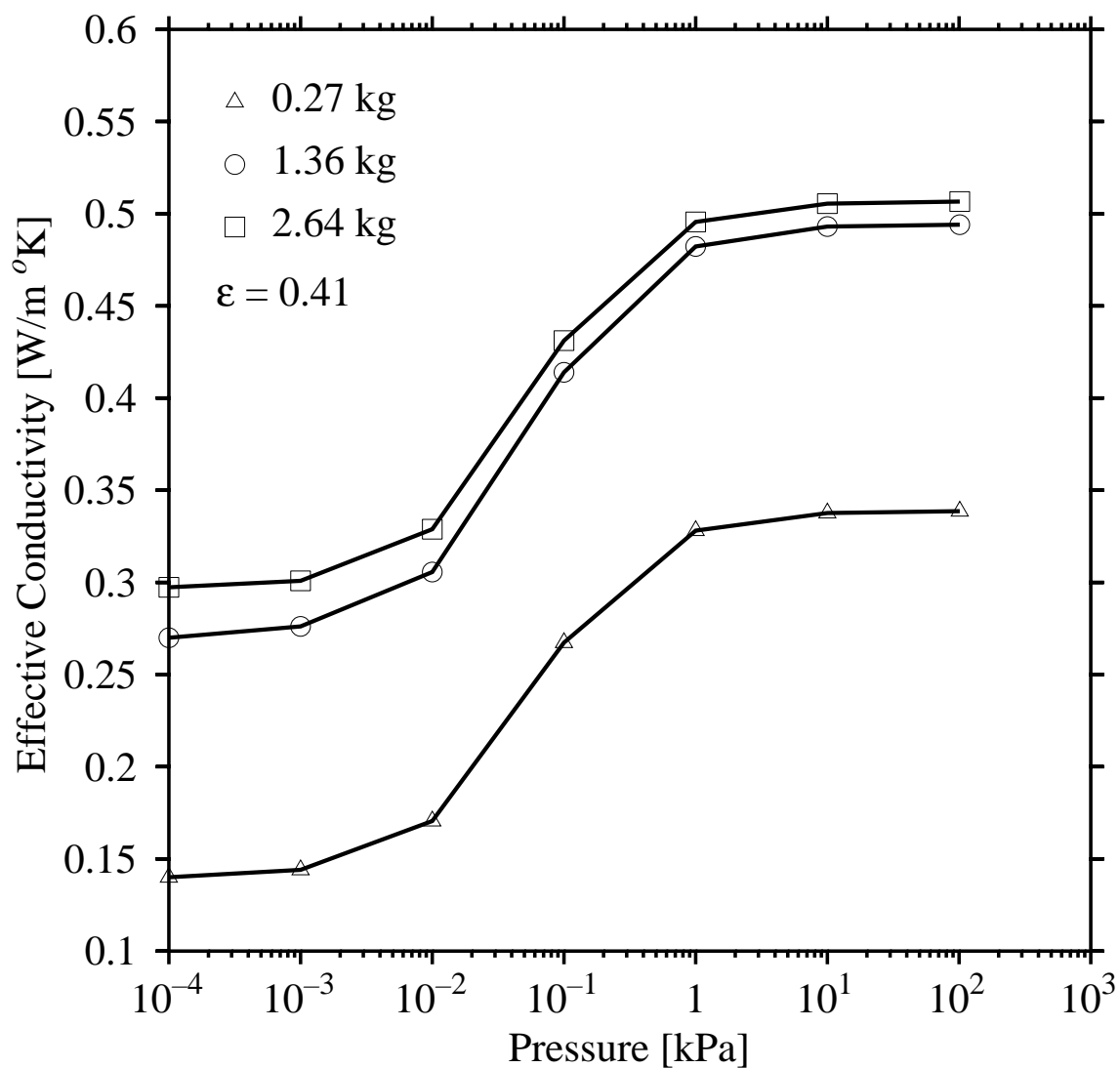
Figure 4.23 Thermal conductivity versus pressure of the filling gas in a 2-D packed bed. A plot of the predicted effective thermal conductivity versus air pressure at constant temperature, measured at three levels of external loading. Symbols indicate TPD simulations, the continuous line connects the points.
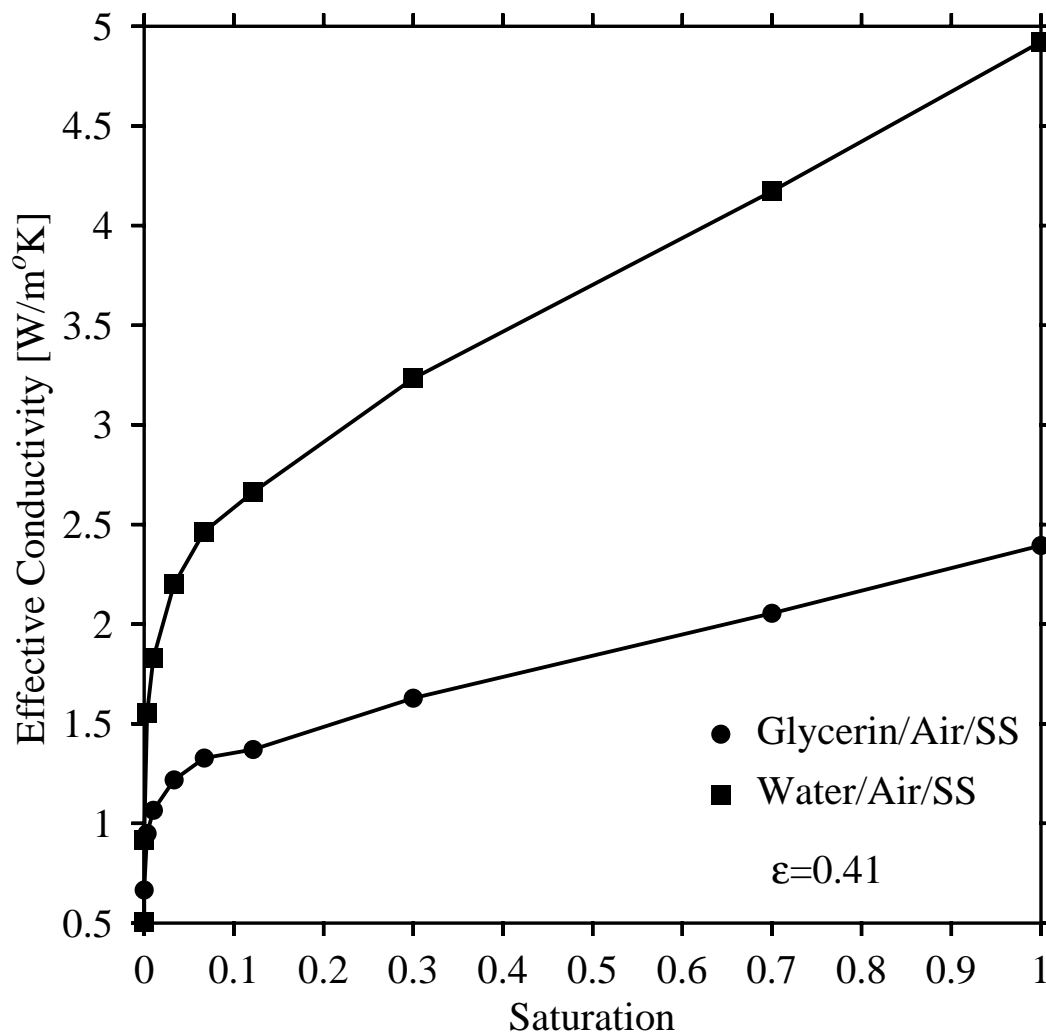
Figure 4.24   Thermal conductivity versus degree of saturation in a 2-D packed bed. A plot of the predicted effective thermal conductivity versus saturation at constant temperature, measured for water and glycerine. Note that in both cases even a small liquid bridge – low degree of saturation– can give rise to a steep increase in the effective conductivity, at higher levels of saturation due to the curvature of the particles the effect of the liquid bridge is less pronounced. Symbols indicate TPD simulations, the continuous line is drawn as a guide to the eye.

4.4.2 Effect of external load

Figure 4.25 illustrates the evolution of the effective thermal conductivity as a function of external load for a packed bed filled with spheres of SS-304 in the presence of air (at constant pressure) and water as the wetting fluid (at constant degree of saturation). As one might expect, the effect of an externally imposed load becomes less significant as the conductivity of the interstitial medium increases (i.e., from vacuum to gas to liquid).

Figure 4.26 illustrates the relative contributions of the different mechanisms of heat transfer considered in this study, namely contact conductance, conduction through the gas phase and conduction through the liquid between particles, as a function of the external load. Note that, at low load and high saturation, the contribution of the heat flow due to contact conductance, Q_c, represents a relatively small percentage of the total heat transferred, but that this value increases significantly with either an increase in the level of external loading imposed or a decrease in the bed saturation. Moreover, the case examined in this figure represents a water/air/ss-304 system where the ratio of solid conductivity to liquid conductivity is relatively large. The effect of varying this ratio is explored in Section 4.4.3.

Figure 4.26(b) shows that the contribution by contact conductance – in beds filled with only a stagnant gas – represents a significant fraction of the total heat when a moderate to high external load is imposed. Therefore, by changing the external load on a packed bed it is possible to alter the relative contributions of the different mechanisms involved and increase the effective conductivity (see Fig. 4.23).

4.4.3 A comparison of TPD results with correlations and experimental data

A comparison between TPD results, experimental values collected from various literature sources and a typical correlation proposed by Hadley [211] is presented in Figure 4.27.
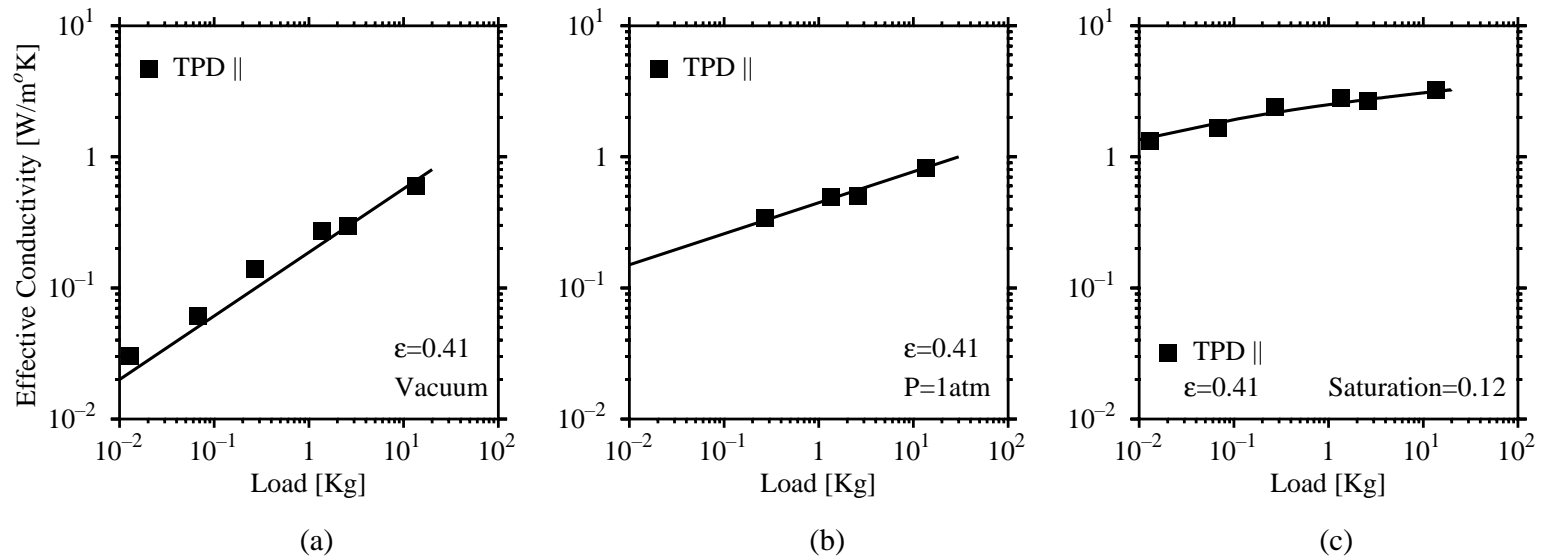
Figure 4.25 Thermal conductivity in a 2-D packed bed as a function of load (a) under vacuum, and in the presence of (b) gas (c) liquid plus gas. Symbols indicate TPD simulations, the continuous lines are drawn as a guide to the eye. As one might intuit, the effect of external loading becomes less significant as the conductivity of the fluid increases – i.e., from vacuum to gas to liquid.
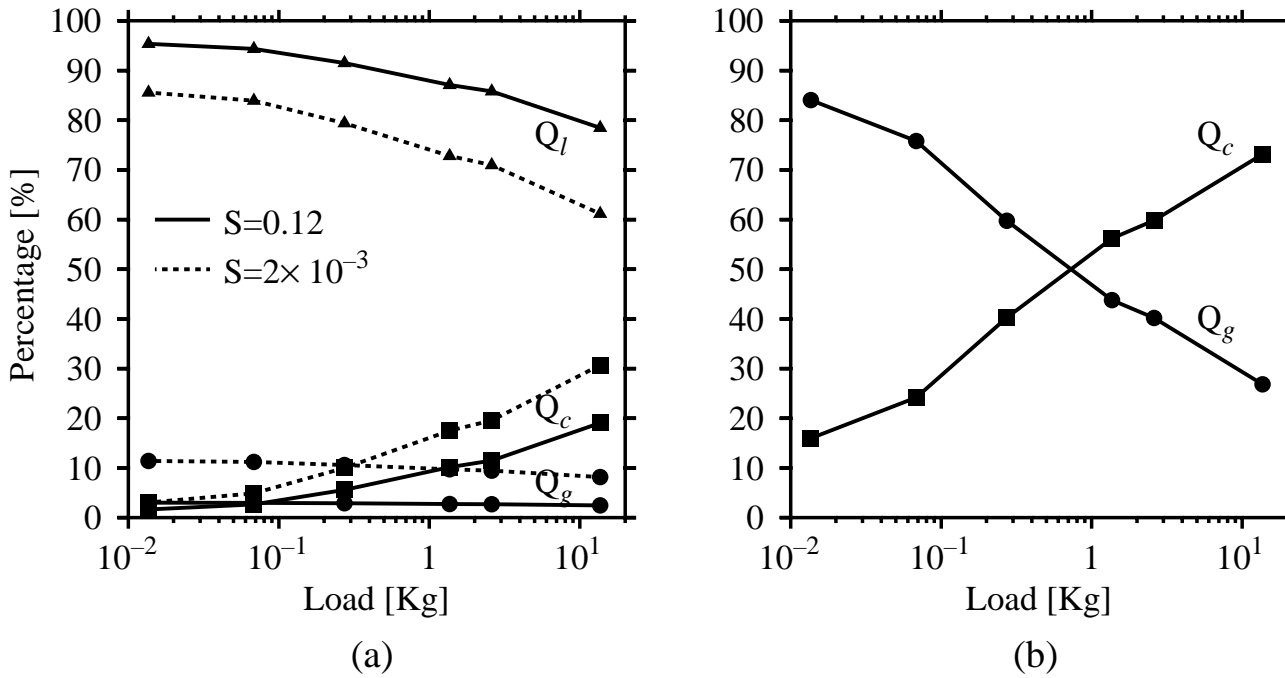
Figure 4.26 Relative contributions of the heat transfer mechanisms in a 2-D packed bed to the overall heat transfer (a) unsaturated bed (b) stagnant gas only. As expected, the contribution due to contact conductance becomes progressively more important with increased loading, for systems filled with a stagnant gas. The overall heat transfer process is dominated by the contribution of the liquid phase for systems in which liquid is present even in a small amount($S \rightarrow 0$)
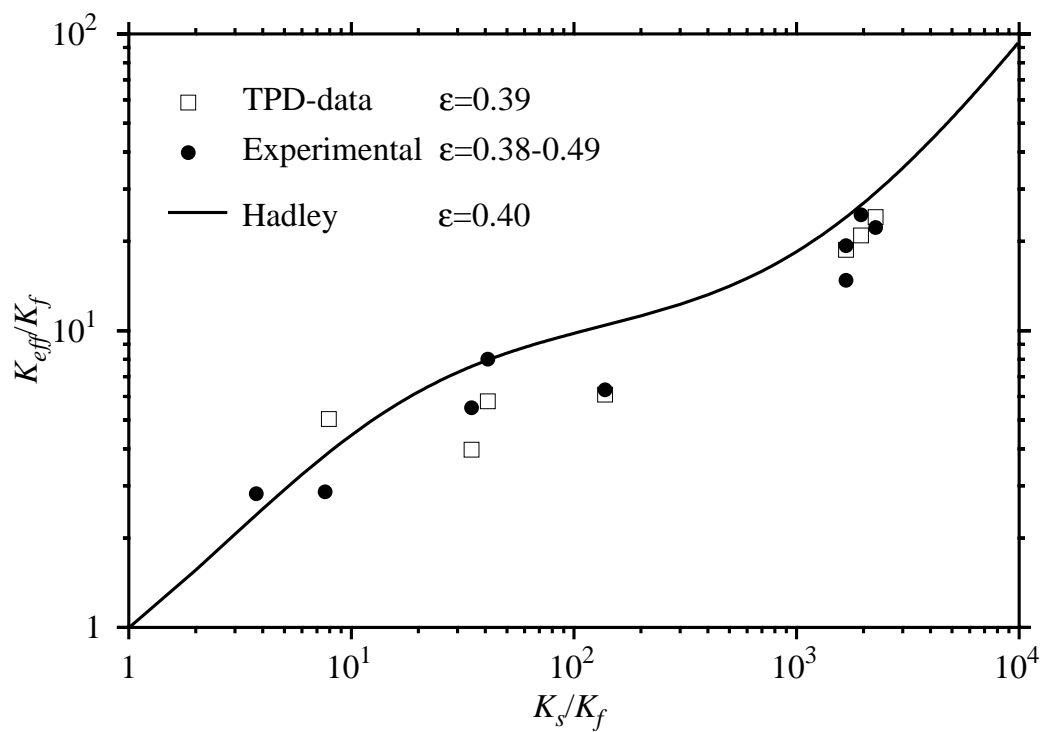
Figure 4.27 Comparison between model predictions and experimental values of the effective conductivity. ($\bullet$) measurements by Crane and Vachon [214], Prasad *et al.* [215] and Nozad *et al.* [216]. Solid line based on the correlation proposed by Hadley [211]

The values predicted by TPD agree reasonably well both with experimental observations and with the semi-empirical correlation of Hadley. This suggests that the proposed method correctly reflects the effects of the mechanisms considered. It is worth mentioning that none of the experimental studies used for comparison explicitly report the load imposed on the samples used in their experimental measurements. The TPD simulated data used for comparison in Figure 4.27 are based on predictions from a three-dimensional packed bed with an external load of 10 kg. We expect that this discrepancy may introduce some under or over-prediction since, as illustrated in Figure 4.25, the effect of the external load on the effective thermal conductivity may be significant. In general, the values predicted from TPD seem to deviate more from the experimental observations as the ratio k_s/k_f gets smaller. This behavior is not surprising since the model is built on the assumption that $k_s/k_f \gg 1$ (so that heat transfer between non-contacting particles may be ignored) and the heat storage capacity of the fluid is ignored.

However, it is important to note the wide range of conductivities over which the model has been successfully applied, as well as the variety of fluids that have been used, suggesting that the present model can be used – within its limitations – to predict the results for a variety of measurements. The experimental data collected by Crane and Vachon [214], Prasad et al. [215] and Nozad et al. [216] has been used for comparison. Whenever possible the data used in the simulation corresponds closely with the data provided by the authors. For the diameter of the particles, a value of 3 mm was assumed when this variable was not specified.

5.0   GRANULAR FLOWS

TPD offers the unique opportunity to computationally probe mechanical dynamics coupled with heat transfer processes. For collision dominated flows the contribution due to contacts between particles may be negligible [121, 131], however in slow granular flows with lasting contacts – the object of this study – the contribution due to contact conductance may be significant. As in the case of the static applications of chapter 4, the first step toward building an understanding of the heat transfer mechanisms in three dimensional sheared flows is to examine ideal flows with identical particles. In this chapter, we examine two prototypical flows namely, a simple Couette cell and the flow in a rotating drum, both under vacuum conditions.

5.1   Shear cells

A better understanding of the basic mechanisms governing transport in granular flows is of critical importance to a wide variety of industrial, geophysical, and scientific applications. Experimental and computational studies using annular shear cells have provide valuable information about the flow characteristics due to shear rates, boundary conditions, material properties and solids concentrations [141]. Shear cell flows have been aptly explored both experimentally and computationally by Campbell and coworkers [119, 120, 135, 136, 137], where computer simulations have shown to be a powerful tool to investigate granular flows. Recent computational studies in granular shear flows also include those reported by Campbell [119], Karion and Hunt [138], Louge [139], Schöllmann [140] and Lun [141].

For the numerical experiments in a simple shear cell, we use a mono-disperse system of perfectly smooth spheres bounded by two parallel bumpy walls separated by a distance H. Two monolayers of whole spheres are used to simulate the top and bottom bumpy

walls, with particle size identical to that of the particles within the flow. The coordinate system and the setup used in the simulation are illustrated in Figure 5.1. The bottom wall is fixed and the top wall moves with a known velocity U. All the open boundaries of the domain are bounded by periodic boundaries, therefore a particle leaving through one of the boundaries reenters the cell at the same relative location through the opposite boundary and with the same velocity. This procedure greatly enhances the computational efficiency of the simulation by limiting the number of particles to those initially considered inside the control volume. Figure 5.2 illustrates two typical set-ups of periodic boundaries used in the present study.

Before a heat transfer experiment is carried out, an initial condition is created by letting the particles settle under the weight of the top wall, thus creating a random distribution of the particles inside the domain. From this initial configuration, starting with a velocity profile with small random fluctuations about the continuum-fluid solution $U(y) = U[y/H]$, a simulation is carried until a statistical steady state is reached, a similar approach has been previously used by Campbell and Brennen [137]. To impose a shear rate (U/H), the top wall is set in motion with velocity U, in the positive x direction. Once the cell has reached steady state, the heat transfer process is turned on by setting the bottom wall at high temperature (T=T$_1$) and the top wall at lower temperature (T=T$_o$). The simulation is then run long enough for the cell to reach thermal steady state. Attainment of the steady state is determined by following some instantaneously observable parameter. In TPD simulations, steady state is reached when the balance of heat coming in and out of the system achieves a nearly constant value. The time required to achieved steady state is a function of parameters such as void fraction, number of particles and flow configuration.

Once the system reaches steady state, ensemble averages are used to estimate the effective conductivity for the cell. All of the simulations are performed on a cell containing
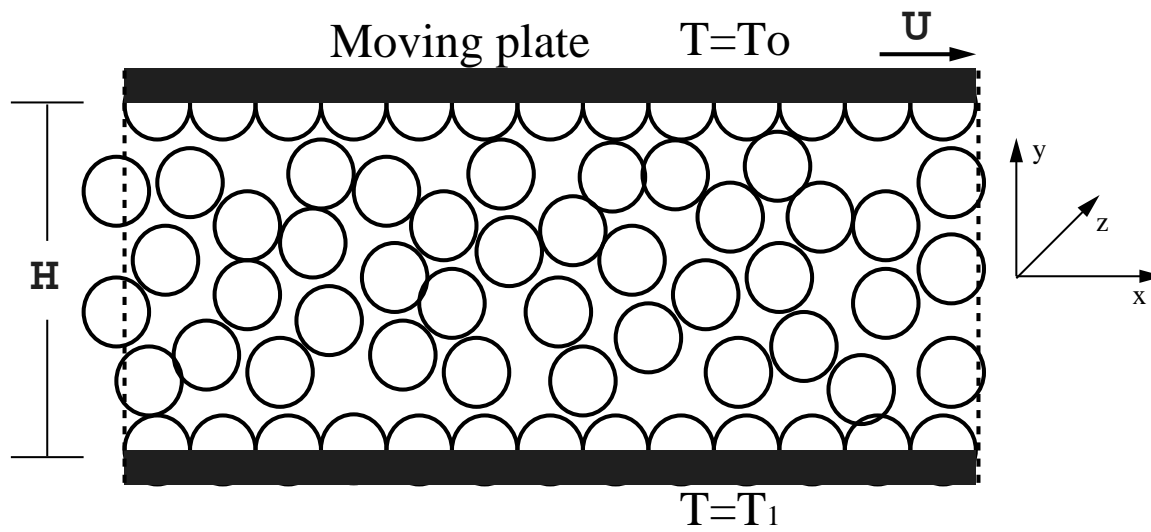
Figure 5.1 Schematic of a simple Couette flow with periodic boundaries and heat transfer exchange at the walls. To impose a shear rate (U/H), the top wall is set in motion with velocity U, in the positive x direction. Heat flows in the y direction, from the bottom wall to the top of the cell.
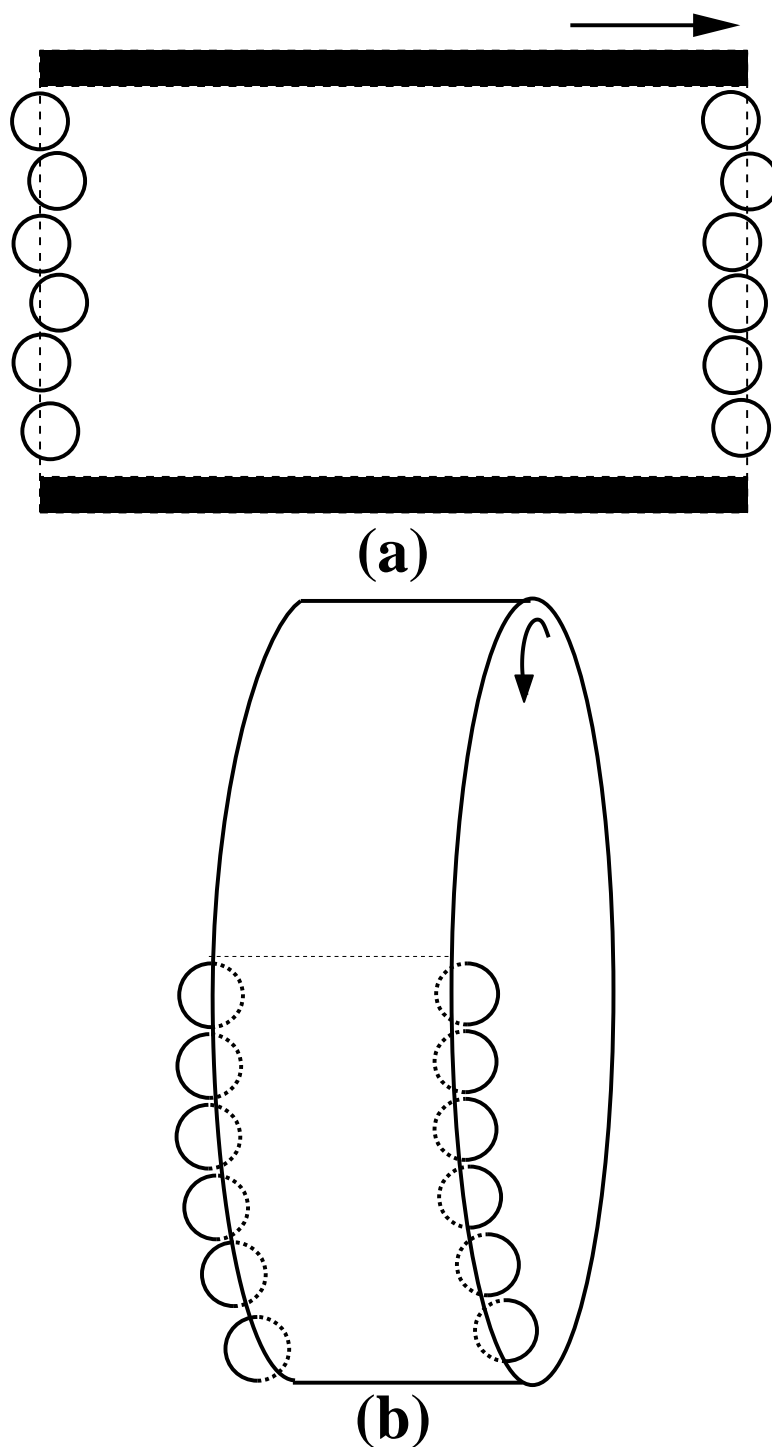
Figure 5.2   Schematic of periodic boundaries (a) Couette cell (b) rotating tumbler. Periodic boundaries emulate a system which is periodically repeated many times, thus allowing to model an infinitely long system with a reduced number of particles.

2000-2500 particles at the interior of the cell and 462 particles forming the wall. The effect of different solid fractions ν is considered by changing the number of particles inside the domain while keeping the separation between walls fixed. The parameters used in the simulation are given in Table 5.1.

Table 5.1 Parameters used in the shear cell simulations. The material properties are those of soda-lime glass.

Parameter	Value
Density	2600 kg/m^3
Poisson ratio	0.25
Young's Modulus	6.6×10^{10} Pa
Particle diameter	3.0×10^{-3} m
Thermal Diffusivity	5.1×10^{-7} m^2/s
Number of particles	2500-3000
Cell length	$20d_p$ m
Cell height	$10d_p$ m
Cell width	$10d_p$ m
Friction coefficient	0.29

5.1.1 Flow behavior

Following Lun [141], the solid fraction in this work is defined as the ratio of the volume occupied by the particles in flow to the total volume of the cell, excluding the volume of the particles in the walls. Cells with three different initial solid fractions, 0.72, 0.70 and 0.66 are generated using the procedure described in Section 5.1. All three cells are subjected to shearing under constant volume (separation between walls is fixed). A typical transverse profile of the averaged void fraction is shown in Figure 5.3. The oscillations in $< \epsilon >$ have a wavelength of roughly a particle diameter. These results agree with those of Louge *et al.*[139]. The lower void fraction area at the center of the cell ($y/H \approx 0.5$) indicates the region with higher mobility inside the cell.
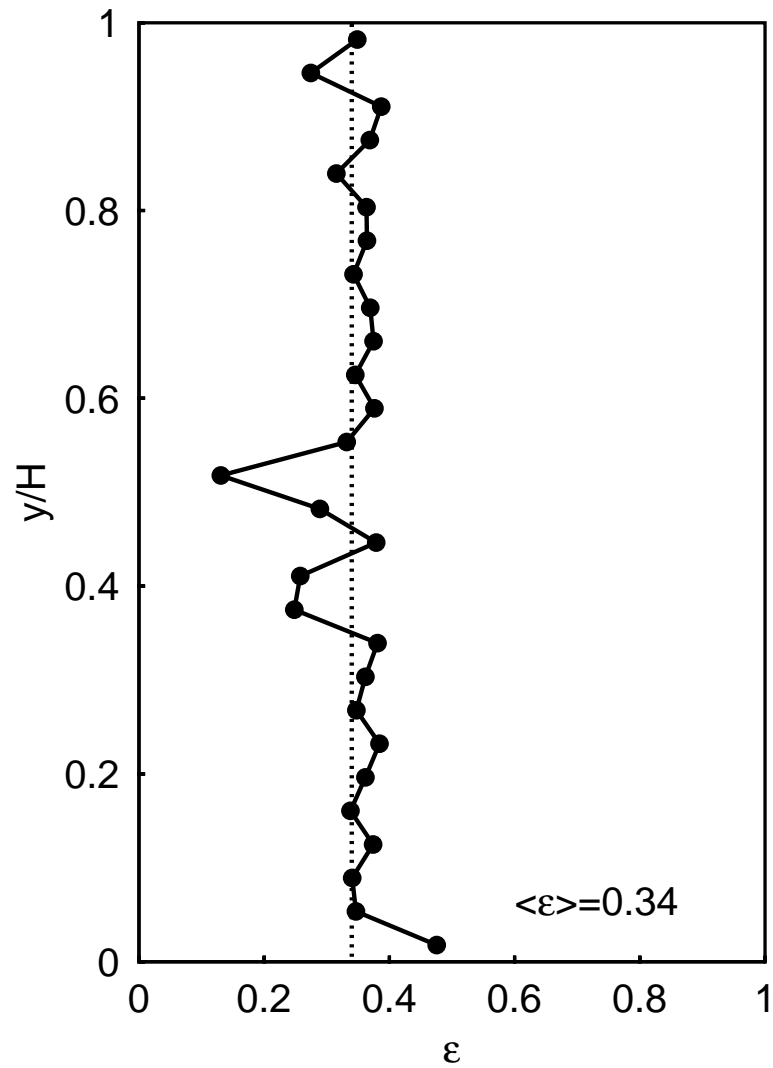
Figure 5.3 Averaged void fraction in a shear cell. The lower void fraction area at the center of the cell ($y/H \approx 0.5$) indicates the region with higher mobility inside the cell – e.g., highest granular temperature (Υ).

Typical velocity, granular temperature and temperature profiles developed in the simple shear flow at two different solid fractions are illustrated in Figure 5.4. The velocity profiles indicate a statistical steady-state that compares fairly well with the theoretical solution proposed by Haff [17] for steady-state Couette flow with no gravity, (represented by the gray line). The granular temperature profiles in Figure 5.4 illustrate the high-shear zones at the center of the cell, which correspond to a lower solid fraction (see Fig. 5.3) and high granular temperatures. The dimensionless granular temperature is given by $\Upsilon/(d_pU/H)^2$. It is worth noting that, in theories regarding rapid granular flows, the granular temperature plays exactly the same role as the thermodynamic temperature plays in kinetic theory of gases. Thus, it not surprising to see that the larger granular temperature correspond with the system whose mobility is higher, in this case the cell with lower solid fraction, $\nu = 0.66$. These results compare well with the heuristic theoretical model proposed by Haff.

5.1.2 Heat transfer studies

Heat transport studies carried out in shear cells are relatively scarce. A notable exception is the study by Wang and Campbell [120]. In this study, it was experimentally found that in relatively dilute rapid flows, the bulk shear motion improves the internal transport of both heat and momentum. Also, they find that both the apparent thermal conductivity and viscosity increase linearly with the imposed shearing rate, suggesting that similar internal mechanisms drive both transport processes (i.e., momentum and heat). Momentum is transported both by particle collisions and by random motion of the particles; however, since heat transfer is a slow process, little heat is conducted during short contact times and only advection of the particles seems to be important. Therefore, at large particle concentrations, Wang and Campbell found that there is almost no shear-induced enhancement of the effective thermal conductivity due to the limited mobility of the particles which in turn hinders the particles' self-diffusivity and ultimately the mixing process.
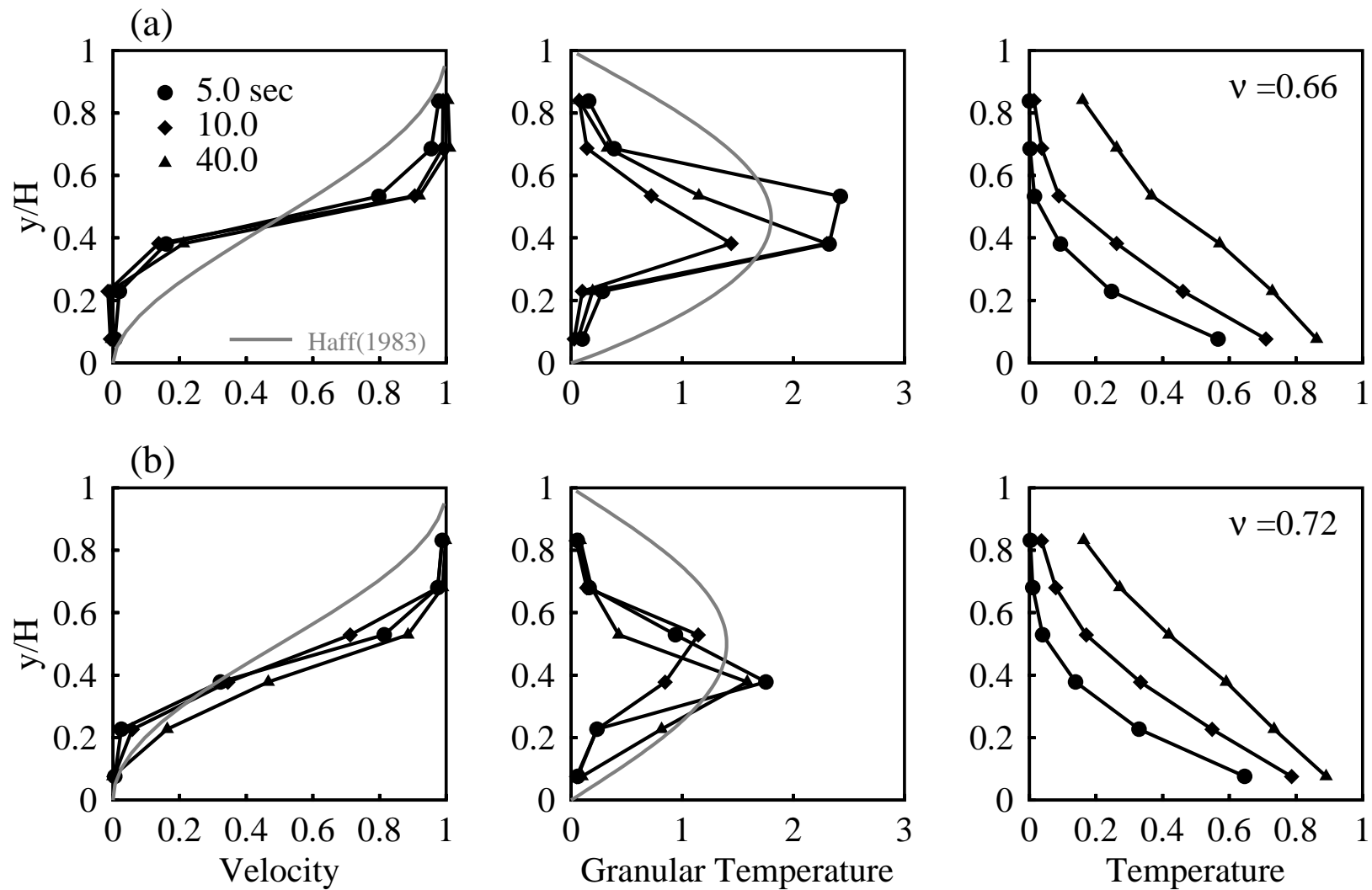
Figure 5.4 Typical velocity, granular temperature and temperature profiles in a simple shear flow at a constant shear rate $U/H = 50s^{-1}$, with overall $\nu = 0.7$ and $H/d_p = 10$.

Wang and Campbell fit their experimental data with an expression of the form

$$k_{eff} = k_o + b_k \frac{U}{H}, \tag{5-1}$$

where the value of k_o (as determined by extrapolation of the experimental data at zero shear rate (U/H)), is noted by the authors to have questionable physical meaning; in particular, it does not represent the conductivity of the static bed. Nevertheless, for each material tested, k_o was found to increase with solid fraction, indicating that this constant still reflects the expected increase in effective conductivity in a static bed as the solid fraction is increased. Thus, they conclude that the relation in Equation 5-1 between the effective thermal conductivity and the shear rate is not valid down to zero shear rates, although it correctly fits the experimental data at high shear rates.

Figure 5.5 illustrates TPD measurements of the normalized effective conductivity in the Couette cell as a function of the shear rate at three different values of the solid fraction ν. The conductivity has been normalized using the effective conductivity of the static bed with the highest solid fraction ($\nu = 0.72$). For the three densities considered, the effective conductivity goes through two distinct regions of behavior. At high shear rates, an increasing linear region is observed which qualitatively confirms the conclusions and observations reached earlier by Wang and Campbell [120]. At low shear rates, a decaying nonlinear region not previously reported is observed. As suggested by Wang and Campbell [120], Figure 5.5 shows that as the solid fraction is increased from $\nu = 0.66$ to $\nu = 0.72$ the particles achieved a smaller degree of mobility (lower granular temperature) and therefore the rate of enhancement of the conductivity is limited. In fact, at the highest solid fraction ($\nu = 0.72$) the shear rate has almost no effect on the thermal conductivity. The behavior observed at low shear rates seems to provide an explanation for the discrepancies observed in k_o as discussed by Wang and Campbell [120]. Note that the normalized effective conductivity in

Figure 5.5, at zero shear rate is a function of the solid fraction and in fact, increases with solid fraction.

Since the main mechanisms of heat transfer considered here are particle-particle contact and convection of the particles (i.e. the heat carried by particles as they follow their random paths) it is reasonable to assume that the effective conductivity should be dominated by conduction at low shear rates and by convection at higher shear rates. Therefore, this new behavior can be explained in the following manner: at low shear rates "stress chains" – the conduction paths for heat transfer – are frequently broken due to the shear, dramatically affecting the conductivity when compared with that of the static bed. At high shear rates, the increased granular temperature results in a higher self-diffusion coefficient for the particles (see Eqn. 2-30) and therefore the rate of enhancement of the conductivity is increased. It is possible to propose a semi-empirical correlation that describes this behavior by combining a "pure" conductive component with a convective (diffusive) component as

$$k_{eff} = k_{oe} + k_{sh} \tag{5-2}$$

where k_{oe}, is the effective conductivity of the static bed and $k_{sh} = \rho c_p D$, is the effective conductivity due to the mass diffusion. Note that Equation 5-2 is similar in spirit to the correlation proposed by Wang and Campbell [120] (see Eq. 5-1).

A suitable description of the conductive component of the effective conductivity for the case of a *static* bed may be obtained from Jagota and Hui [96] (see Eqn. 2-16). For the case of a sheared bed, we must modify this expression to account for the variation of the
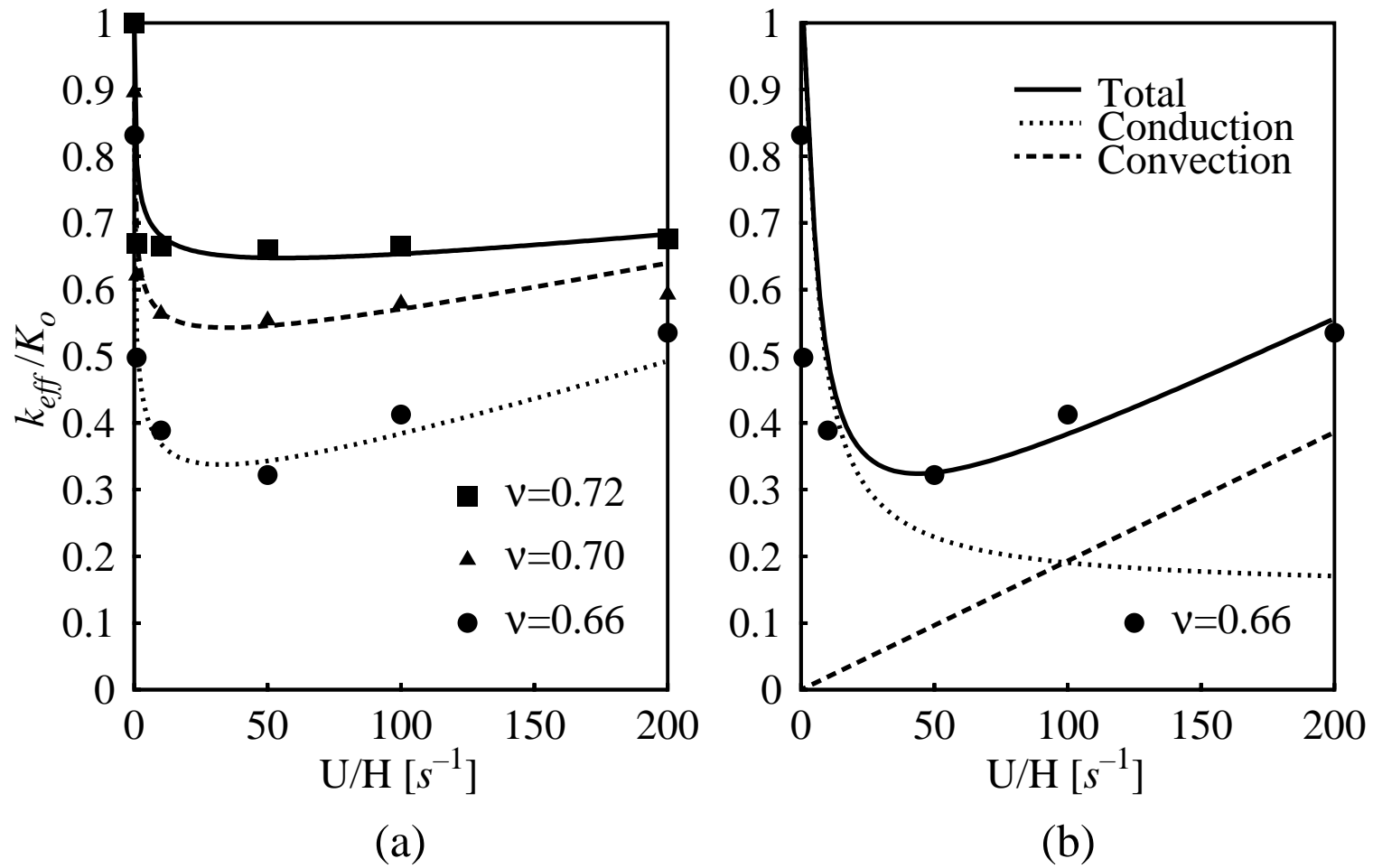
Figure 5.5 Effective conductivity in a simple shear flow (a) Normalized effective conductivity (b) shear rate dependence of the different contributions to the effective conductivity in a simple shear flow determined by Eq. 5-6

number of contacts with shear rate. This expression for the effective conductivity tensor, K_{ij}, is given by

$$K_{ij} = \frac{3\bar{Z}k_s(1-\epsilon)}{\pi} \left(\frac{a}{r}\right) F_{ij} \left[1 - e^{-\frac{c_1\alpha}{(U/H)d_p^2}}\right], \tag{5-3}$$

where $\bar{Z}\left[1 - e^{-\frac{c_1\alpha}{(U/H)d_p^2}}\right]$ is the effective average coordination number, ϵ is the void fraction, and F_{ij} is the fabric tensor as discussed in Section 2.2. By combining Eqs. 5-3 and 2-30, the effective conductivity for simple shear flow is

$$k_{eff} = \frac{3\bar{Z}k_s\nu}{\pi} \left(\frac{a}{r_p}\right) F_{ij} \left[1 - e^{-\frac{c_1\alpha}{(U/H)d_p^2}}\right] + c_2\rho c_p \frac{d_p\sqrt{\pi\Upsilon}}{8(1+e)\nu g(\nu)} \tag{5-4}$$

where c_1 and c_2 are constants that need to be estimated from fitting experimental or computational data. In this work, the form of the radial distribution function is taken from Savage [118] as,

$$g(\nu) = \frac{(16 - 7\nu)}{16(1 - \nu/\nu_\infty)^2}, \tag{5-5}$$

where ν_∞ is the solids fraction corresponding to closest packing ($\nu_\infty = 0.74$). Replacing $\Upsilon^{1/2}$ in Equation 5-4 in terms of S and du/dy from Equation 2-28 an expression in terms of shear rate is given by

$$k_{eff} = \frac{3\bar{Z}k_s\nu}{\pi} \left(\frac{a}{r_p}\right) F_{ij} \left[1 - e^{-\frac{c_1\alpha}{(U/H)d_p^2}}\right] + c_2\rho c_p \frac{d_p^2\sqrt{\pi}(U/H)}{8(1+e)\nu g(\nu)S} \tag{5-6}$$

For a granular flow, the value of the constant S – which is a function of e, the coefficient of restitution and ν the solid fraction – typically varies from ≈ 1.0–4.0 [119, 133, 137]. For

a steady simple shear flow, an extensive review of similar relations is provided by Lun *et al.* [133]. Here we use a relation between S and e of the form

$$S = 24 \left(\frac{\nu}{\nu_\infty} \right)^{\frac{2}{3}} \frac{1-e}{1+e} \tag{5-7}$$

Equation 5-6 can be expressed in a compact form as

$$k_{eff} = \frac{3\bar{Z}k_s\nu}{\pi} \left(\frac{a}{r_p} \right) F_{ij} \left[1 - e^{-\frac{c_k}{(U/H)}} \right] + b_k \frac{U}{H} \tag{5-8}$$

where the constants c_k and b_k are given by

$$c_k = \frac{c_1 \alpha}{d_p^2} \tag{5-9}$$

and

$$b_k = c_2 \rho c_p \frac{d_p^2 \sqrt{\pi}}{8(1+e)\nu g(\nu)S} \tag{5-10}$$

respectively.

Equation 5-6 contains several parameters which include material properties, averaged properties for static beds and the constants c_1 and c_2, which are treated as fitting parameters. While estimates of the averaged properties for static beds are possible both from experimental observations and/or simulations (see Section 4), the constants c_1 and c_2, and their dependence on the system parameters are unknown. Equation 5-6 is plotted in Figure 5.5(b). It can be seen that the variation of the effective conductivity with shear rate at a constant value of the solid fraction has the same general shape as the estimated values from the TPD simulations. In fact, the computationally estimated values can be closely fitted using the correlation.

In spite of this good "agreement", many questions remain to be solved. First the physical meaning and nature of the constants c_1 and c_2, in particular their functionality with variables such as solid fraction, coefficient of restitution, etc. As pointed out by Hsiau and Hunt [134] any underestimation of $g(\nu)$ will result in an overprediction of the diffusivity and, unfortunately, an appropriate radial distribution function for dense systems has not been examined in the literature. In addition, as the solid fraction increases, the assumptions on which the kinetic theory is built – and hence the origin of our convective term in Equation 5-6 – come into question as binary collisions become less common. Finally, the use of an isotropic granular temperature may not be valid.

Figure 5.6 illustrates the variation of the constant b_k in Equation 5-10 with solid fraction ν. It is interesting to notice that in agreement with the observations of Wang and Campbell [120], as the solid fraction increases the value of b_k, which corresponds to the shear-induced enhancement of the effective conductivity in Equation 5-8, effectively goes to zero. The inset in Figure 5.6 illustrates the values of the constant b_k used in the fitting of the effective conductivity in Figure 5.5.

As a further point to consider, the distribution of particle contacts, for the cells considered in this study, is shown in Figure 5.7 using a second order representation of the fabric tensor [26, 85]. It can be seen that as the shear rate is increased from the static case U/H=0 to 0.8, 50 and 100 the system becomes less anisotropic, an indication that some type of internal reordering takes place as the shearing is increased. Shear-induced ordering in a dense Couette flow has also been reported by Zamankhan *et al.* [217] as well as Campbell and Brennen [137]. As evidenced by the curves shown in Figure 5.7, the distribution of contact orientations changes during shearing, leading to a decreased structural anisotropy. This observation has also been confirmed by the computer simulated experiments of Zhang and Campbell [136] and Campbell and Brennen [137] on uniformly shearing flows at low
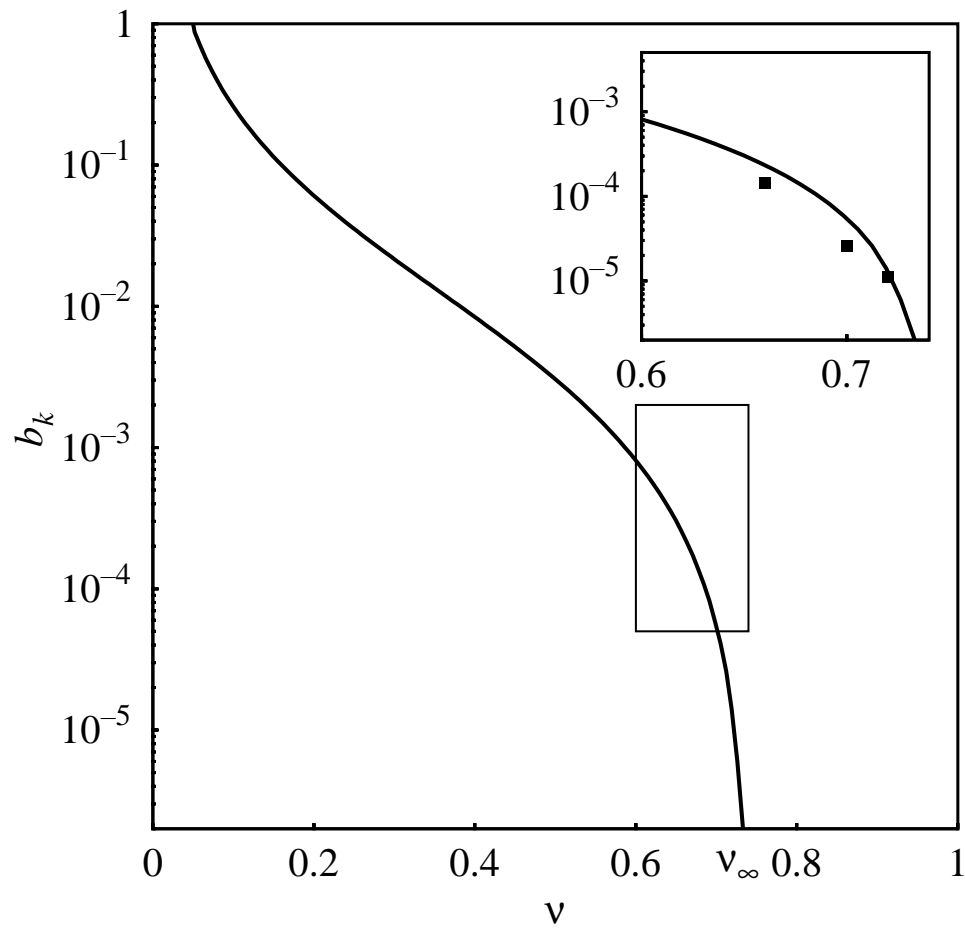
Figure 5.6 Variation of the constant b_k in Equation 5-10 with solid fraction ν. The inset figure on the upper right shows the values of b_k used in the curve fitting in Figure 5.5.

concentrations. These studies demonstrated the formation of a "layered" microstructure oriented in the direction of the flow that influences the angle of collision between particles and which might be related to the results in Figure 5.7.

5.2 Tumblers

In a three dimensional rotating container avalanches move material from the upper part of the surface to the lower, and mixing occurs only during the avalanche. Several studies have dealt with mixing in rotating containers [117, 128, 148, 154, 155, 156, 157]. These investigations have demonstrated that the movement of solids in a rotating cylinder, such as rotary kilns, rotary coolers or dryers, can be resolved into two components, i.e. flow in the axial direction caused by the inclination of the cylinder and flow in the radial direction imparted by rotation. Theories exist that allows the prediction of the flow in the cascading layer and the solid-body rotation region, yet heat transfer in these devices is not fully understood despite the fact that a considerable amount of experimental and theoretical work has been carried out [103, 117, 128, 148, 154, 155, 156, 157].

Figure 5.8 illustrates the coordinate system and the numerical setup used in the simulation of the rotating tumbler. As in the case of the simple shear cell (Section 5.1), the numerical experiments consist of a mono-disperse system of perfectly smooth spheres bounded by a cylindrical wall of immobile particles with periodic boundaries in the z direction (see Figure 5.2 (b)). The wall of the drum is rotated at a constant angular velocity Ω. A typical initial condition for the rotating tumbler simulations is obtained by allowing a bed of particles arranged in a randomly perturbed lattice to settle under the action of gravity using a traditional isothermal PD simulation (particle mechanics only). From this initial configuration, a prescribed angular velocity is imposed simultaneously with setting the wall at a high temperature (T=T_1). The temperature of the particles is initiated, in all cases, at
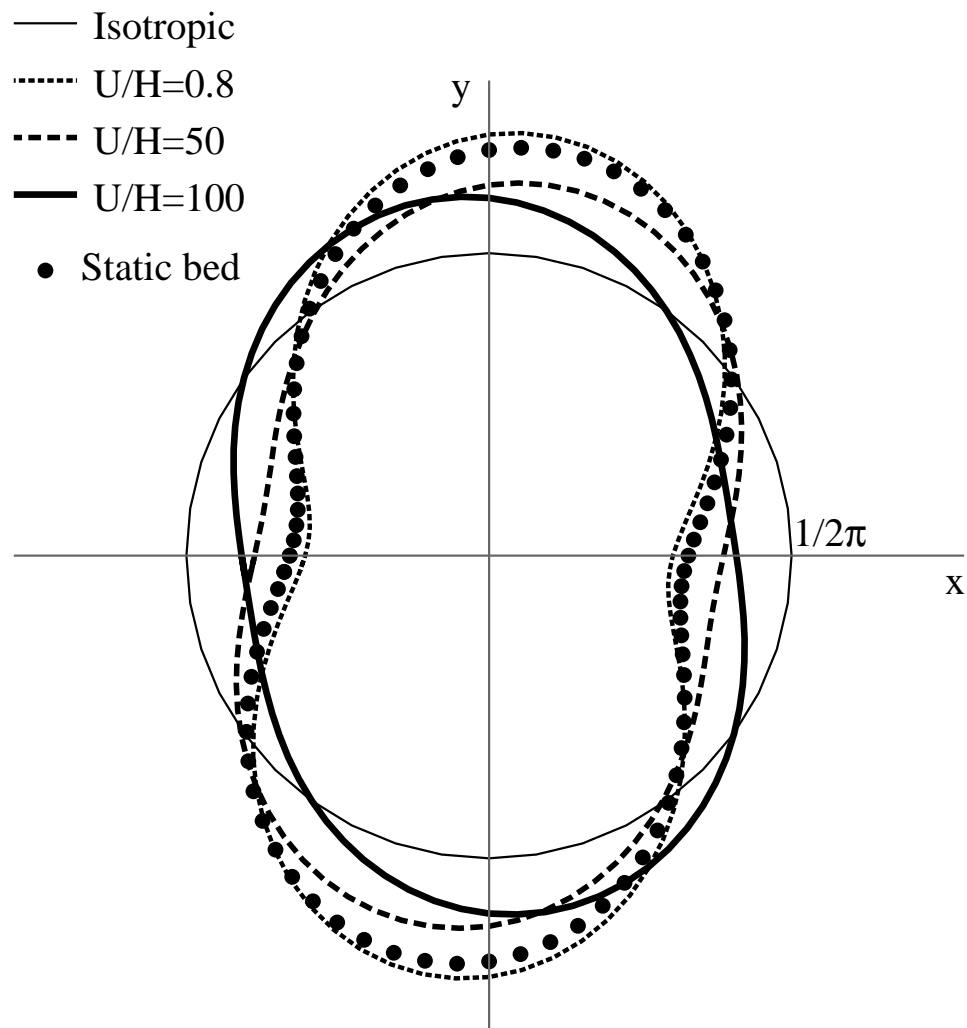
Figure 5.7 Shear-induced anisotropy in a simple shear flow. A plot of the contact distribution anisotropy and its variation with shear rate U/H. The main consequence of shear-induced anisotropy is its effect on the preferred orientation of the contact between particles.

a lower and constant value (T=T_o). The simulation is allowed to proceed for approximately 5 - 10 revolutions based on the rotation rate prescribed. Then, the temperature profiles, rate of mixing and the heat transfer coefficient at the wall are determined as a function of time.

The parameters used in the simulation and the properties of the material are similar to those used for simple shear flows (Section 5.1).

5.2.1 Flow behavior

As discussed earlier, for a rotating tumbler in the rolling regime, the particles within the tumbler rotate with the drum as a solid-body until the material surface reaches some critical angle – the dynamic angle of repose. At this point the material flows down the surface of the bed where it is again entrained in the solid-body region. As the rotation continues this process is repeated and mixing of particles occurs only in the cascading region. A schematic representation of this process is shown in Figure 5.9. This figure shows a tagging experiment in which a rectilinear grid pattern is imposed on selected particles and the evolution of this pattern – as result of the flow – is followed in time at a rotation rate of 15 revolutions per minute. It is easy to visualize in Figure 5.9 the rigid body rotation of the particles near the cylinder wall as well as the flow taking place along the free surface.

Figure 5.10(a) shows a schematic of the bed motion. The dynamic angle of repose of the 3 mm glass beads as determined from this Figure is approximately 24.5^o at a rotation velocity of 6 revolutions per minute. This value compares well with the experimentally observed value of 26.5^o reported by Ding *et al.* [103].

The shear layer δ in Figure 5.10, consists of two regions, a constant shear region near the free surface and a variable shear rate region that serves as transition to the rigid body
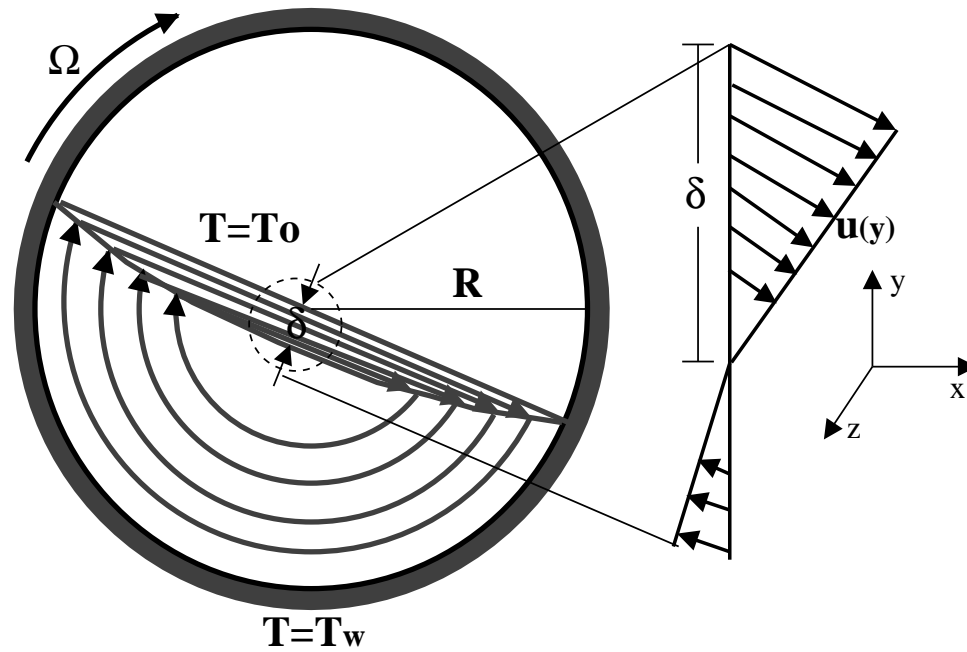
Figure 5.8 Schematic of the flow field in a rotating cylinder with heat exchange at the wall, showing the definition of the shear layer thickness δ. The shear layer defines the region within the bed where the main motion of the particles is taking place, and defines the boundary from the region of solid-body rotation. Representative streamlines are also shown.

Ω=15 rpm
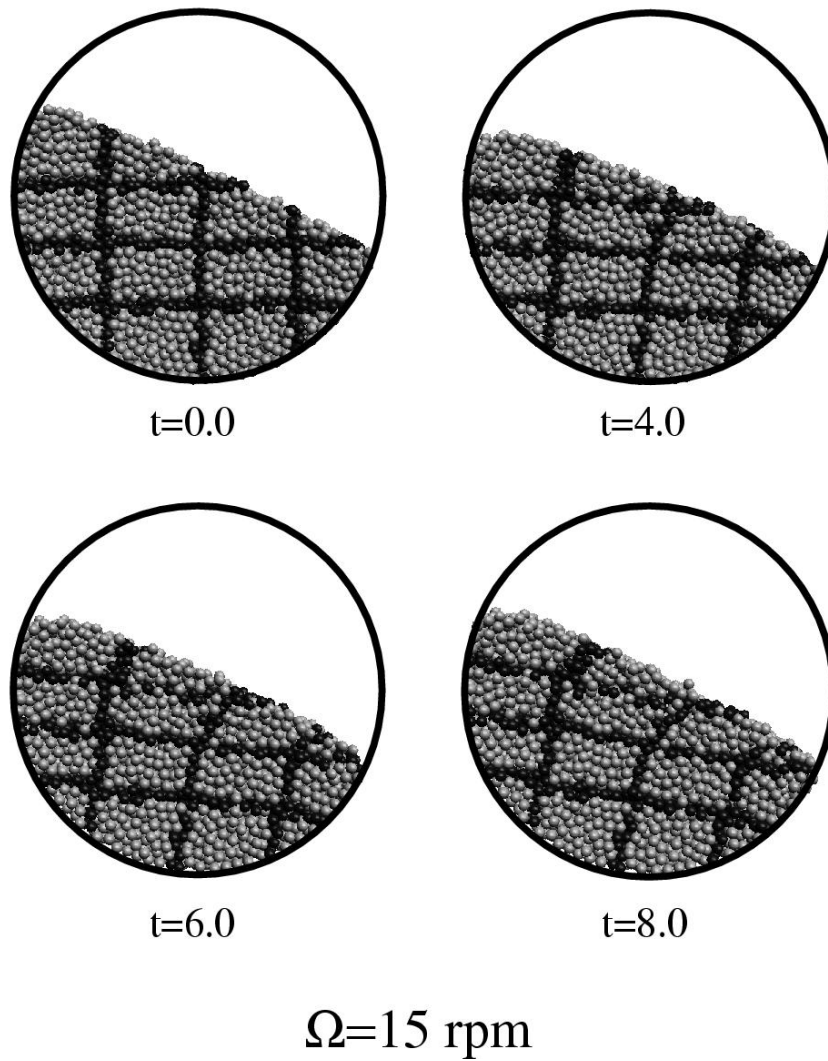
Figure 5.9 Evolution of a rectilinear grid pattern during flow in a rotating tumbler, time in seconds. Tagged particles in a rectilinear grid are imposed and the evolution of this pattern –as result of the flow, is followed in time. The regions of solid-body rotation and free flow are clearly visible.
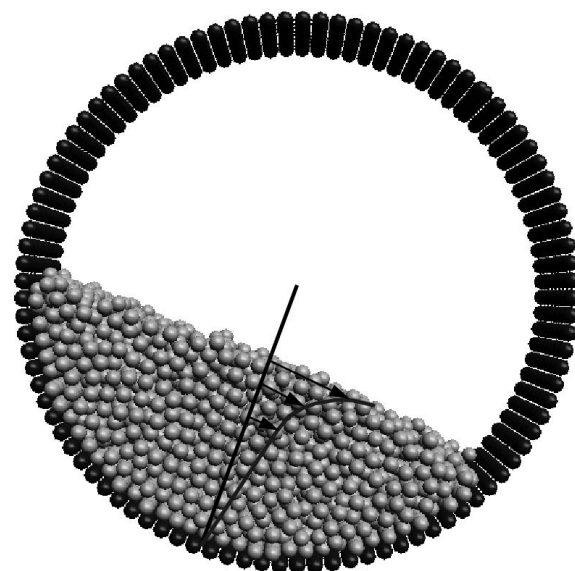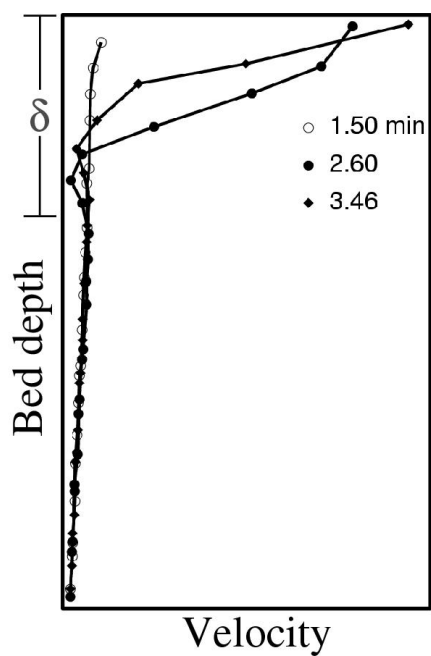
Figure 5.10 (a) Schematic view of the bead motion with the corresponding evolution of the velocity profiles (b). The velocity profiles in (b) are based on a moving frame of reference as illustrated in (a).

rotation zone. These results agree with those reported by Nakagawa *et al.* [161] from experimental observations using Magnetic Resonance Imaging (MRI) experimental techniques.

5.2.2 Transverse mixing

The dynamics of mixing for a rotating tumbler in the rolling regime are analyzed by the advection of tracer particles by the flow. Identical particles of different colors are initially placed in two halves of the drum, and their distribution after a given mixing time is analyzed. Particles in the passive region of the drum undergo solid-body rotation; particles in the cascading layer experience linear motion due to shear, and diffusion-like (random) motion takes place due to interparticle collisions. For a quantitative determination of the rate of mixing, the intensity of segregation (I_s) is calculated from

$$I_s = \left[\frac{1}{N-1} \sum_{i=1}^{N} (\phi_i - <\phi>)^2 \right]^{1/2} \tag{5-11}$$

where (ϕ_i) are concentrations at a set of N uniformly distributed points in the bed. The concentration at a given point is calculated as the fraction of black (or white) particles in a box of specified size centered on the point. The intensity of segregation as described by Equation 5-11 depends on the filling of the drum ($f = \frac{1}{2\pi} \left[\frac{\pi\phi}{180} - \sin(\phi) \right]$) and the rotation rate which affects both the diffusion coefficient and the average velocity of the particles in the shear layer [148]. The average velocity in the cascading layer determines the residence time of the particles in the layer relative to the passive region.

Figure 5.11 illustrates the average circulation time in a tumbler with given radius and angle of repose at different filling degrees.

The difference in circulation times as a function of radial position results in convective mixing of the particles. The diffusive mixing in the bed is determined by both the diffusivity
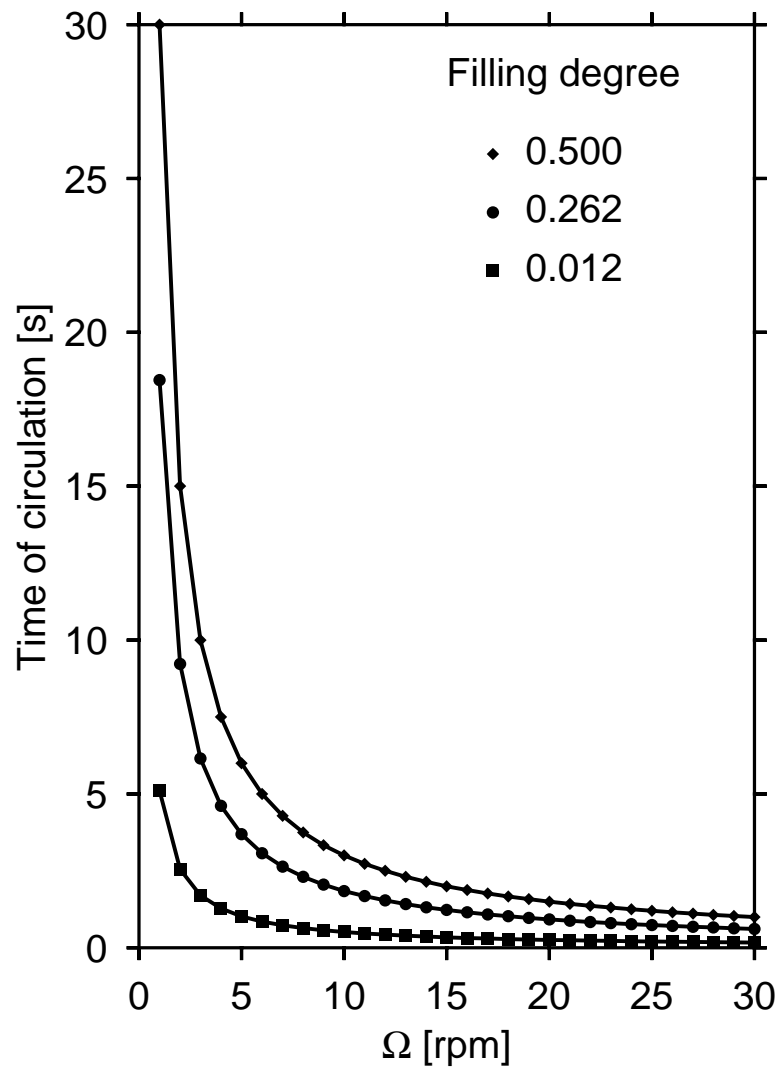
Figure 5.11 Circulation time as a function of rotation rate and the degree of filling f. The degree of filling refers to the fraction of the tumblers's diameter that is covered by material.

in the shear layer as well as the circulation time – which determines the number of passes through the shear layer.

Figure 5.12 shows the time evolution of the mixing process in a typical computational mixing experiment. The initially segregated system ($I_s = 0.5$) is mixed to an increasing extent with time ($I_s \rightarrow 0$) as $t \rightarrow \infty$. The intensity of segregation calculated from Equation 5-11 at different rotations rate are shown in Figure 5.13. In all cases there is an exponential decay in the intensity of segregation which can be fitted to an Equation of the form

$$I_s = ce^{(-2\pi k_{mix}t)}. \tag{5-12}$$

The fitted lines are shown as solid lines in Figure 5.13. A mixing rate constant, k_{mix}, can then be determined by fitting these curves to Equation 5-12. The values are tabulated in Table 5.2. In general, the mixing rate increases with rotation rate and with decreasing the fill level of the drum. An optimum filling level at which the effectiveness of mixing is maximized has been predicted by McCarthy [158]. These observations agree well with those of Khakhar et al. [148], Lehmberg et al. [128], Hogg and Fuerstenau [156, 157].

Table 5.2 Computational rates of mixing, $k_{mix}[s^{-1}]$

Ω [rpm]	f=0.50	f=0.37
5	1.11×10^{-3}	0.02898
10	1.27×10^{-3}	0.04992
15	1.37×10^{-3}	0.05993

5.2.3   Analysis of heat conduction

The general problem of heat transfer encountered in a rotating tumbler is a very common one in chemical engineering [218]. There is a region which presents resistance to transfer
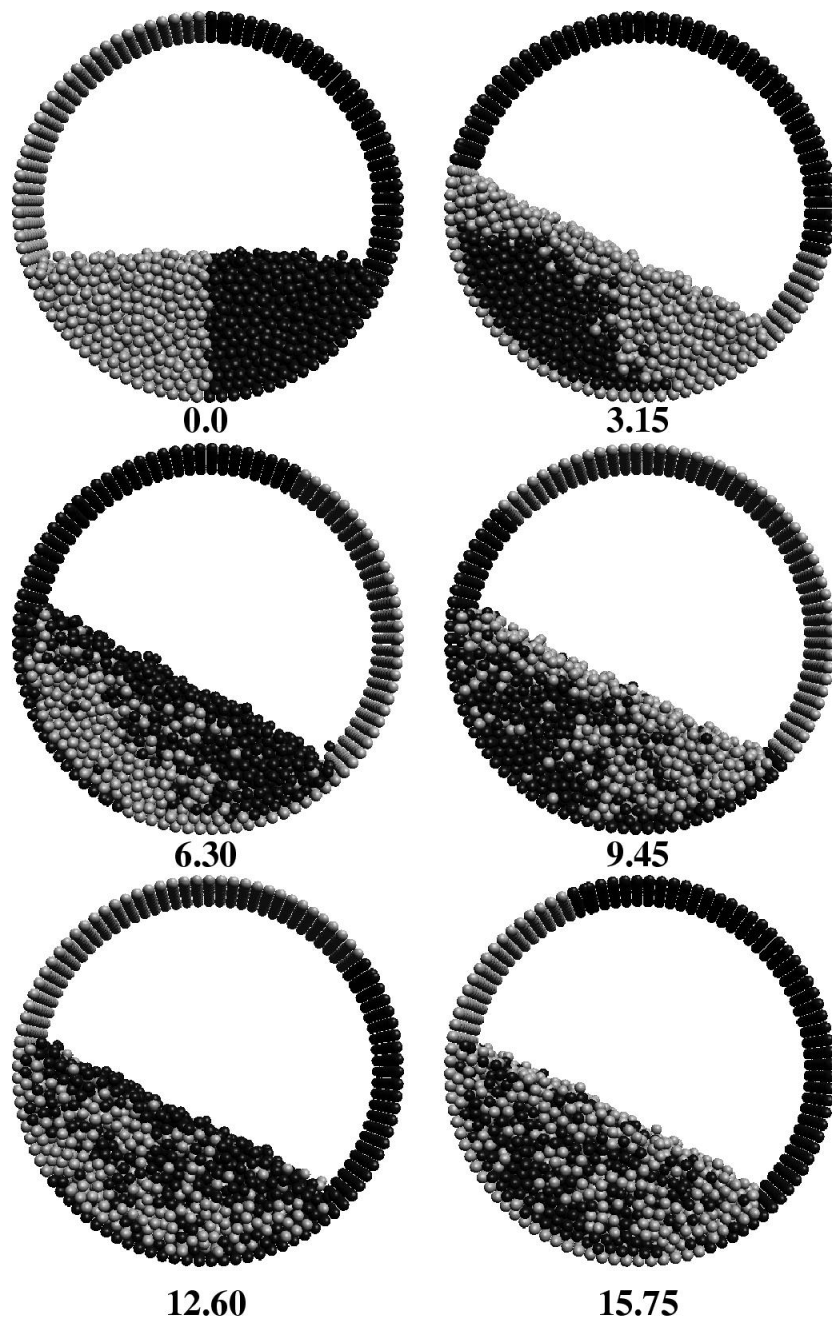
Figure 5.12 Typical time evolution of the mixing process in a rotating drum in the rolling regime ($\Omega = 15rpm$), time in seconds. The dynamics of mixing in the simulation is visualized and quantified by the advection of tracer particles of two colors by the flow.
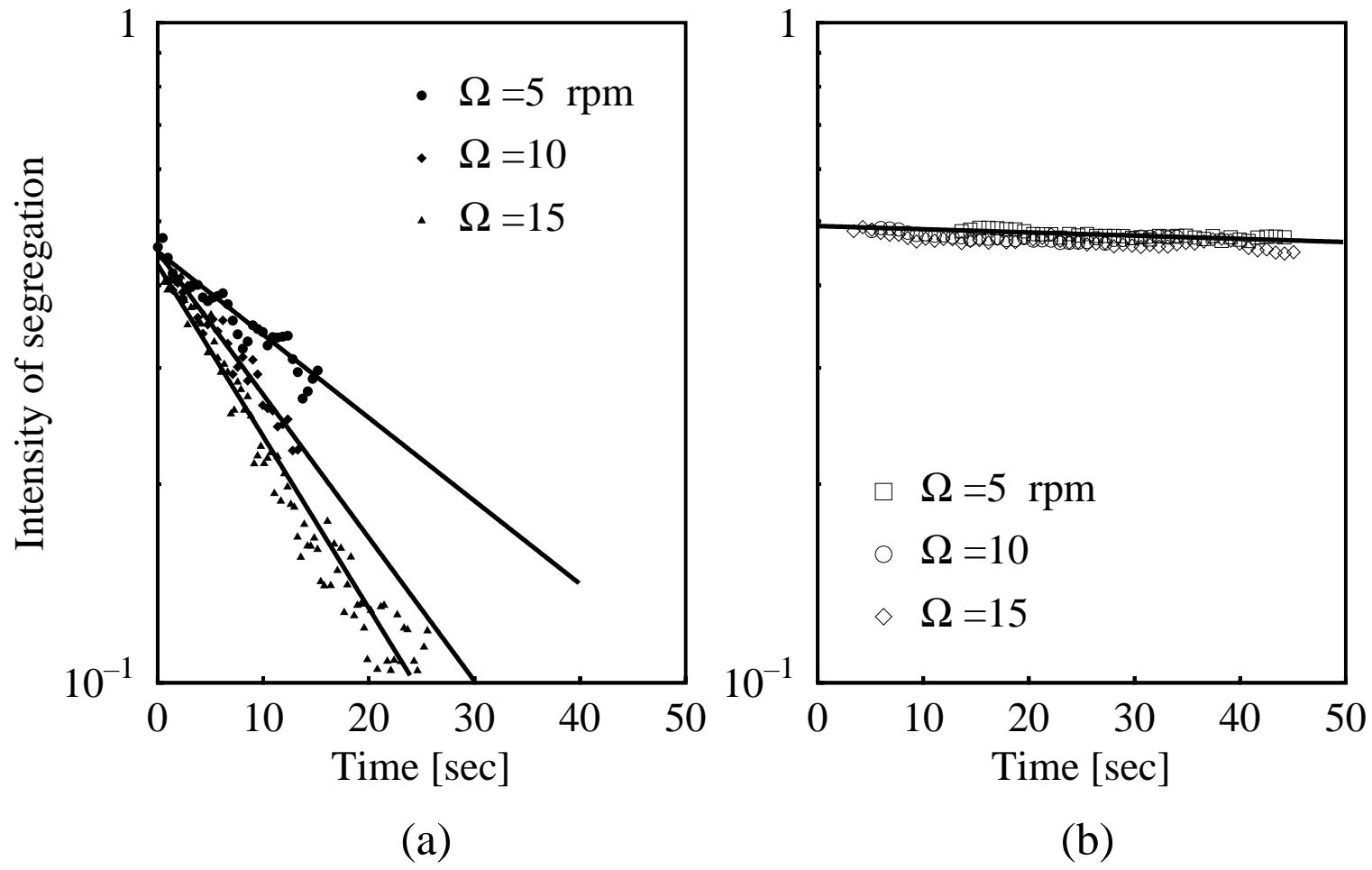
Figure 5.13 Variation of the intensity of segregation with different rotation rates at constant filling degree (a) $f = 0.37$ (b) $f = 0.5$. For a half filled tumbler $f = 0.5$, the circulation time of the material in the bed is independent of radial position thus mixing takes place at a very low rate. In contrast, for less than hall filled drums $f \to 0$, the circulation time varies with radial position and therefore mixing is more rapid [158].

and fresh matter and/or energy is supplied or taken away from the boundary to this region by the constant renewal of material at the boundaries. Differences in contact time at different locations of the bed would clearly lead to different resistances to heat transfer throughout the system. The above observation suggests that it might not be permissible to make assumptions that a continuous description with uniform thermal properties is able to describe the transport process when flow conditions give rise to different contact times at the boundary. Traditionally, heat transfer in rotating drums has been modeled by means of a heat transfer coefficient (h_w) between the wall of the drum and the bed of particles. The heat transfer coefficient (h_w) is usually determined based on penetration theory arguments – a continuous approach – which are outlined below. When particles at temperature T_o move into contact with the wall at a temperature T_w and gain heat by unsteady heat conduction, the rate of heat transfer at the wall q_w, is given by

$$q_w = h_w A(T_w - T_o) \tag{5-13}$$

where A is the area of particles in contact with the wall. The heat transfer coefficient h_w from the wall to the particles bed is then given by [127, 128]

$$h_w = 2\sqrt{\frac{k_{eff}(\rho C_p)_b)}{\pi t_c}} \tag{5-14}$$

where k_{eff} is the effective thermal conductivity of the bed of particles, $(\rho C_p)_b$ is the heat capacity of the bulk, and t_c is the time of contact between the wall and the particles which can be linked to the rotational rate of the drum (Ω) by

$$t_c = \frac{\beta}{2\pi\Omega} \tag{5-15}$$

where β defines the arc of length of material in contact with the wall. Comparison is made between predictions based on this model, TPD simulations results and experimental data below. This approach holds true as long as the following assumptions are valid (1) the effective thermal conductivity can be used to describe the heat flow by conduction through the bed from the heated surface, (2) all the heat flow is normal (unidirectional) to the heater surface, (3) the size of the system is sufficiently large that it can be approximated as a semi-infinite medium with constant properties. This analysis has inspired several experimental methodologies for evaluation of h_w from temperature measurements. One of these methods, proposed by Ito *et al.* [126], relates the transient change of the temperature in the shear layer to the heat transfer coefficient at the wall using the theoretically derived expression

$$\ln \frac{T_w - <T_c(t)>}{T_w - T_o} = \frac{t}{t_c} \ln \left(1 - \frac{h_w A t_c}{c_p w} \right) \tag{5-16}$$

where w is the weight of the particles in the bed and $<T_c(t)>$ is an average temperature far enough from the wall. According with Equation 5-16, h_w can be estimated from the plots of $(T_w - <T_c(t)>)/(T_w - T_o)$ vs. t as determined from experiments or from simulations. A simplified correlation for estimating h_w has been also derived by Wes et al. [127] based on penetration theory grounds. Note that the expression derived by Wes et al. [127] is a first order approximation to that obtained by Ito *et al.* [126].

Bed motion in a partially filled drum can be characterized by different modes, depending on the properties of the material and the rotation rate (see Sec. 2.4.4). The snapshots in Figure 5.14 illustrate a typical flow in the rolling regime, characterized by the flatness of the surface with no airborne particles. Figure 5.14 shows a series of snapshots (essentially a contour plot, color-coded by temperature) of the temperature evolution in a typical computational heat transfer experiment in a rotating tumbler at a given rotation rate. The

parameters in the simulation are taken directly from the literature and consist solely of the material properties of soda-lime glass.

In granular flows undergoing heat transfer, particles act as local source and sinks for heat. In the absence of radiant heat transfer and interstitial fluids, the particles in the bulk exchange heat by particle-particle conduction, and due to the nature of the flow they may stay in the bulk of the bed long enough to come to the same temperature as their neighbors depending on the rotation rate. When, due to the natural circulation patterns inside the drum, the particles come in proximity of the wall, initially, there is a steep local gradient between the particles and the wall and heat transfers rapidly. Later in the process, the heat flux is reduced due to a decreased driving force. Figure 5.15 illustrates the temperature evolution for a particle close to the wall Figure 5.15 (a) and one in the bulk Figure 5.15 (b). The longer the particles stay in contact with the wall, the faster their temperature approaches that of the wall with the consequent reduction in the local heat transfer rate. Notice, however, that the bulk temperature of the bed follows a logarithmic functionality (see Figure 5.16). Accordingly, high rates of heat transfer and high heat transfer coefficients are to be expected under conditions in which there is a rapid exchange between particles in the bulk and those close to the wall. This fact particularly illustrates the importance of the heat capacity and the effect of solids mixing in achieving good heat transfer in a rotating drum. The best possible operating conditions, therefore are those in which the bulk of the bed is kept isothermal due to the rapid solid circulation and mixing and the local temperature gradient is maximum near the wall. Hence, particles mixing is a key factor in the heat transfer within a rotating tumbler.

In evaluating the wall to particle heat transfer coefficient, it is important to select the relevant driving force. Figure 5.17 compares profiles of temperature as a function of time used in the estimation of h_w, using different temperatures to define the driving force. It can
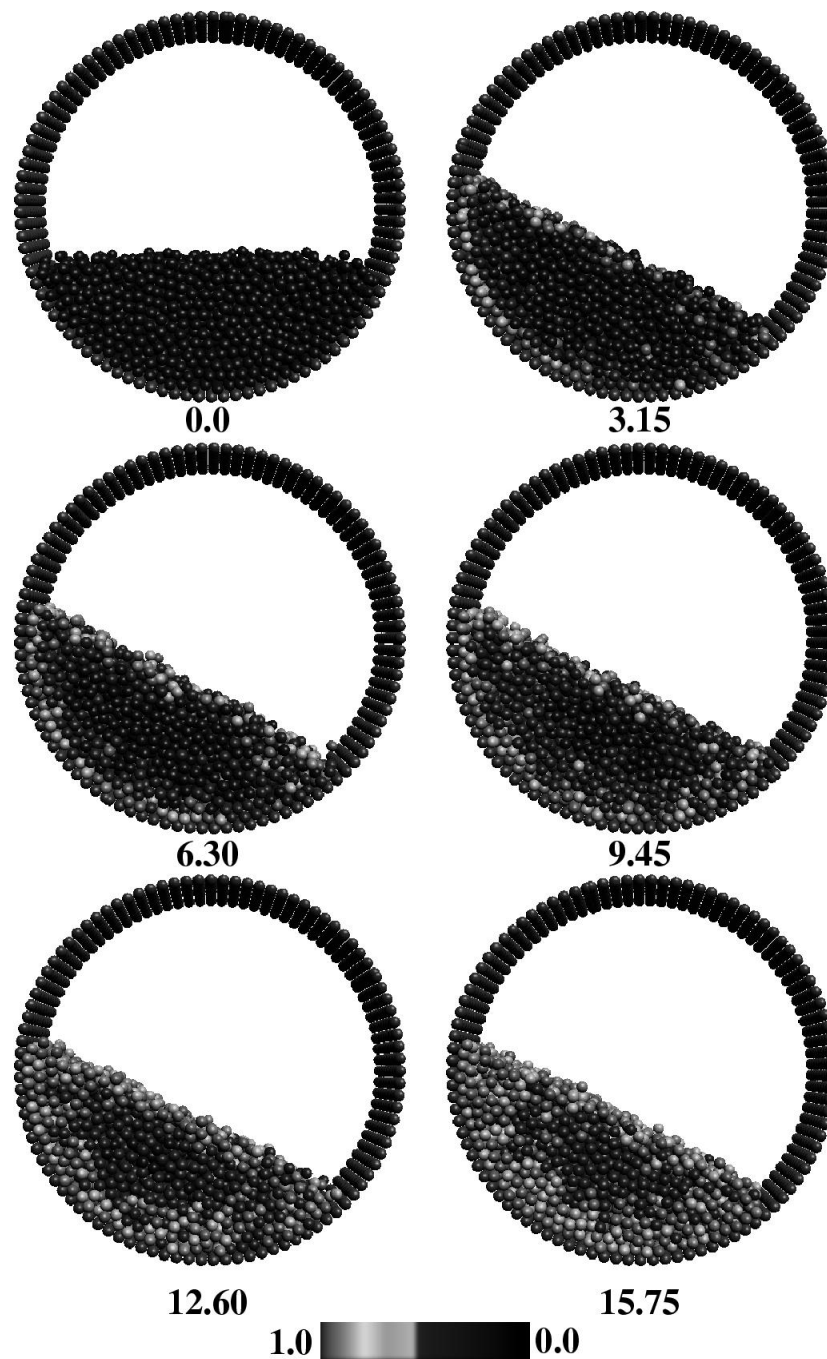
Figure 5.14   Typical time evolution of the temperature in a rotating drum at 15 rpm, time in seconds. Particles close to the wall perform more circuits, and travel through the shear layer more often than particles in the bulk. It follows that sharp temperature gradients are observed between the wall and the center of bed. Notice the striations that take place where particles in the shear layer mix with particles in the bulk.
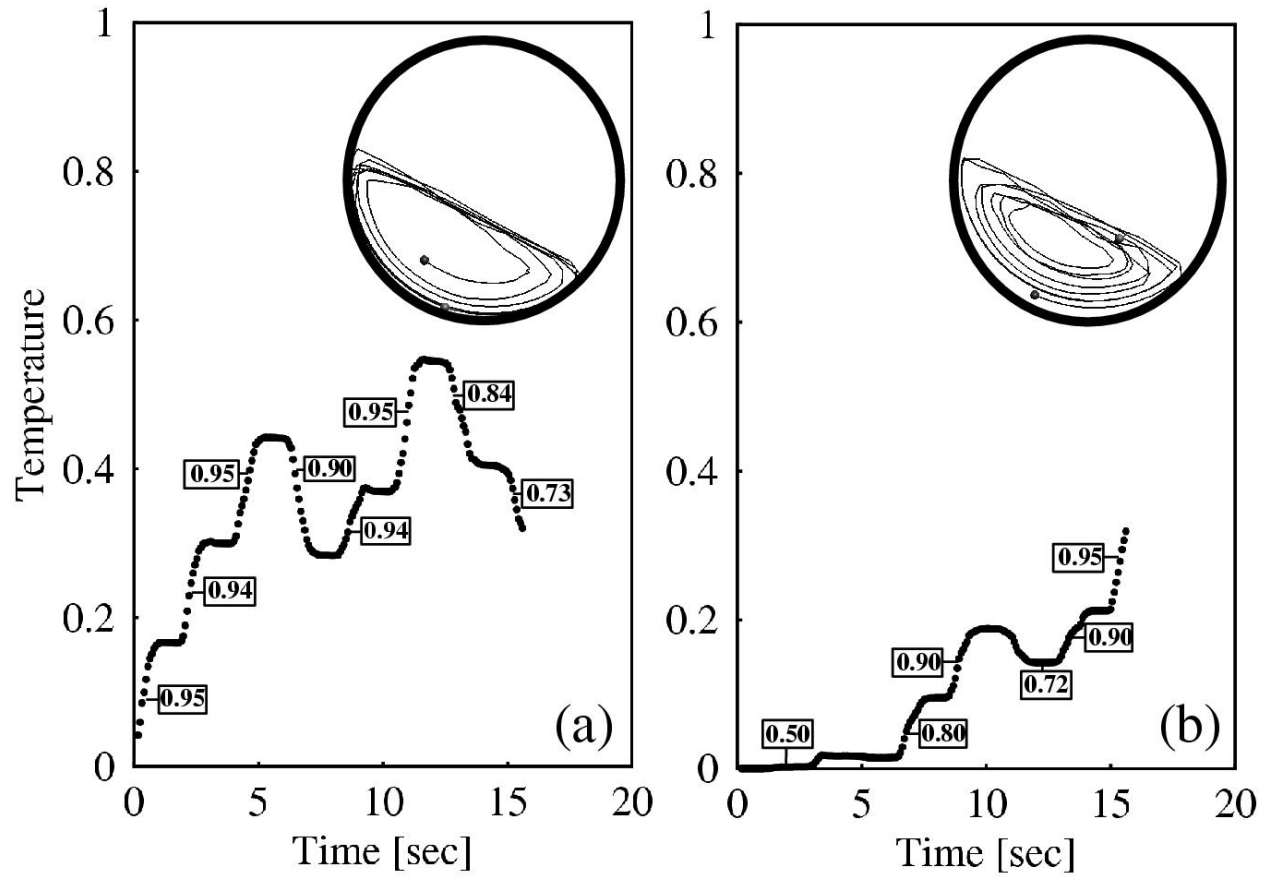
Figure 5.15 Temperature evolution of a particle (a) close to the wall (b) in the bulk. The insets illustrate the particle path (numbers represent relative radial positions). The evolution of temperature for individual particles is highly non-linear, regardless of the position within the bed. In contrast, the overall temperature evolution of the bed follows a logarithmic functionality.
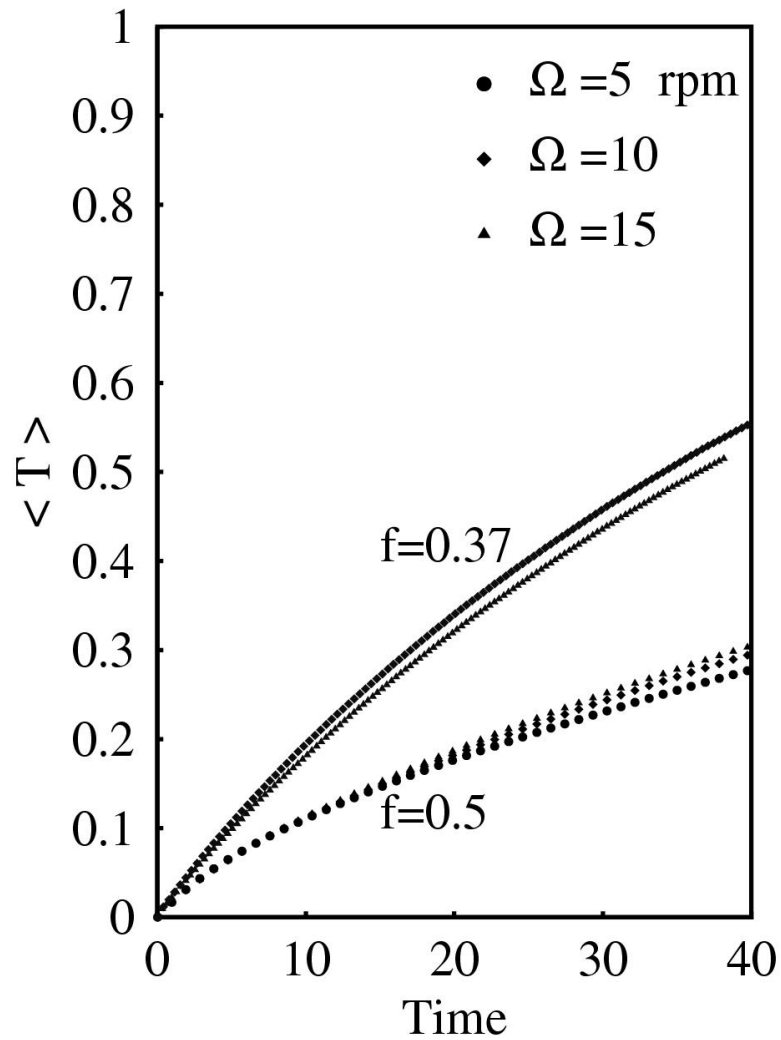
Figure 5.16 Variation of the bulk temperature in a rotating tumbler at two different extents of filling. The bulk temperature within the drum varies in a logarithmic fashion, although the local temperature evolution of individual particles is highly nonlinear. The rate of change is dependent on the fill level f.
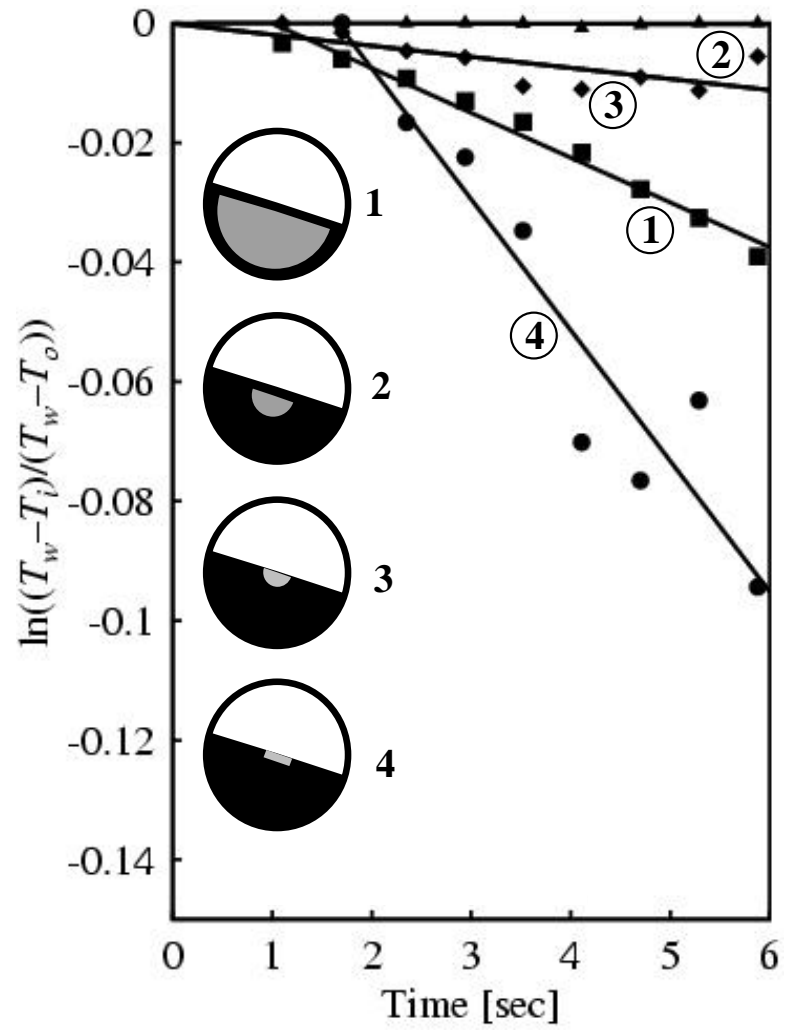
Figure 5.17 Profiles of temperature based in different driving force definitions.

be observed that dramatically different values of the slope and therefore the heat transfer coefficient at the wall, can be obtained for each of the cases considered. Following the definition for the driving force previously used by Ito *et al.* [126], the relevant temperature driving force used in the estimation of the heat transfer coefficient is illustrated on the insets of Figure 5.17 under numeral 3.

Figure 5.18 illustrates plots obtained from TPD simulation, based on Equation 5-16 for different rotational speeds and a filling degree $f = 0.5$, using glass particles. In this Figure, the linearity is quite good and can be used to estimate the heat transfer coefficients from the slope of the plots as

$$h_w = \frac{(c_p w) \left[1 - e^{(slope)t_c}\right]}{A t_c}, \qquad (5\text{-}17)$$

a similar procedure has been used for a fill level $f = 0.37$.

Figure 5.19 illustrates the calculated heat transfer coefficient, using Eq. 5-17, at two different extents of filling of the drum as a function of the rotation rate, using the methodology outlined above. While the mixing rate slowly increases with increasing rotation rate, it was shown in Figure 5.13 that the rate of mixing is strongly dependent on the fill level. The rate of mixing for a half filled drum (f=0.5) is slow (Table 5.2), while those at f=0.37 are an order of magnitude higher. The effect of the mixing rate can be seen clearly in Figure 5.19. The values of the heat transfer coefficient in the case of slow mixing (f=0.5) monotonically increases, but saturates at high values of the rotation rate. The same trend is observed for the faster mixing case (f=0.37). The bulk temperatures at the same extents of filling also illustrate the same behavior (see Figure 5.16). Experimental observations by Nakagawa *et al.* [161] have shown that the thickness of the flowing layer increases monotonically with rotation rate but with an ever decreasing rate, indicating the fact that the mass flux along the free surface is not linearly proportional to the rotation rate.
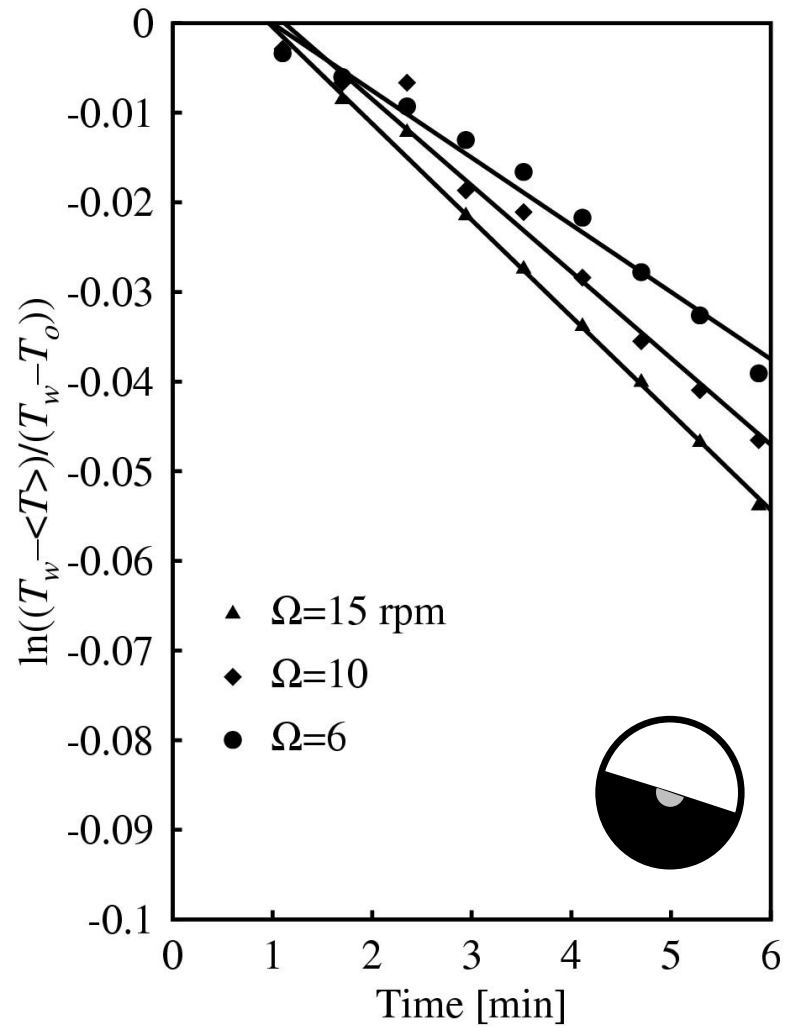
Figure 5.18 Profiles of temperature used in the calculation of h_w.

Increasing the rotation rate therefore can be expected to increase the volume of the material or the number of particles in the shear layer. However, due to the fact that the drum loading is a function of the total drum cross-section, the chord length and the drum radius beyond a specific degree of filling the heat transfer coefficient is relatively insensitive to drum rotation rate although the number of particles sheared increases. At this stage, increasing the outer wall speed would not force more particles into the shear layer. Thus, the heat transfer coefficient in rotating drums is dependent on the extent of filling as found above. The predictions based on TPD simulations at moderate to high rotations rates are lower than those from conventional penetration theory, and therefore are in better agreement with the experimental observations. The explanation comes from realizing that convective mixing plays an important role in heat redispersion. The heat transfer coefficient cannot be represented only as a function of the contact time – as in conventional penetration theory approximations –, the extent of filling also needs to be considered.

Qualitatively, the results in Figure 5.19 are consistent with the experimental observations of Ito et al. [126], Wes et al. [127] and Lehmberg et al. [128]. The lines in Figure 5.19 represent the theoretical solution obtained from Eq. 5-14 and Eq. 5-15. The results presented here show that that heat transfer through the solid phase is the dominant mechanism in supplying heat to the bed. Note that the values of h_w in Figure 5.19 as calculated from TPD represent roughly 80% of the experimentally measured values which also include the contribution of the gas phase. In general, these observations indicate that the physical mechanisms for the heat transfer process have been correctly incorporated into the the computational model and that it functions essentially as intended.
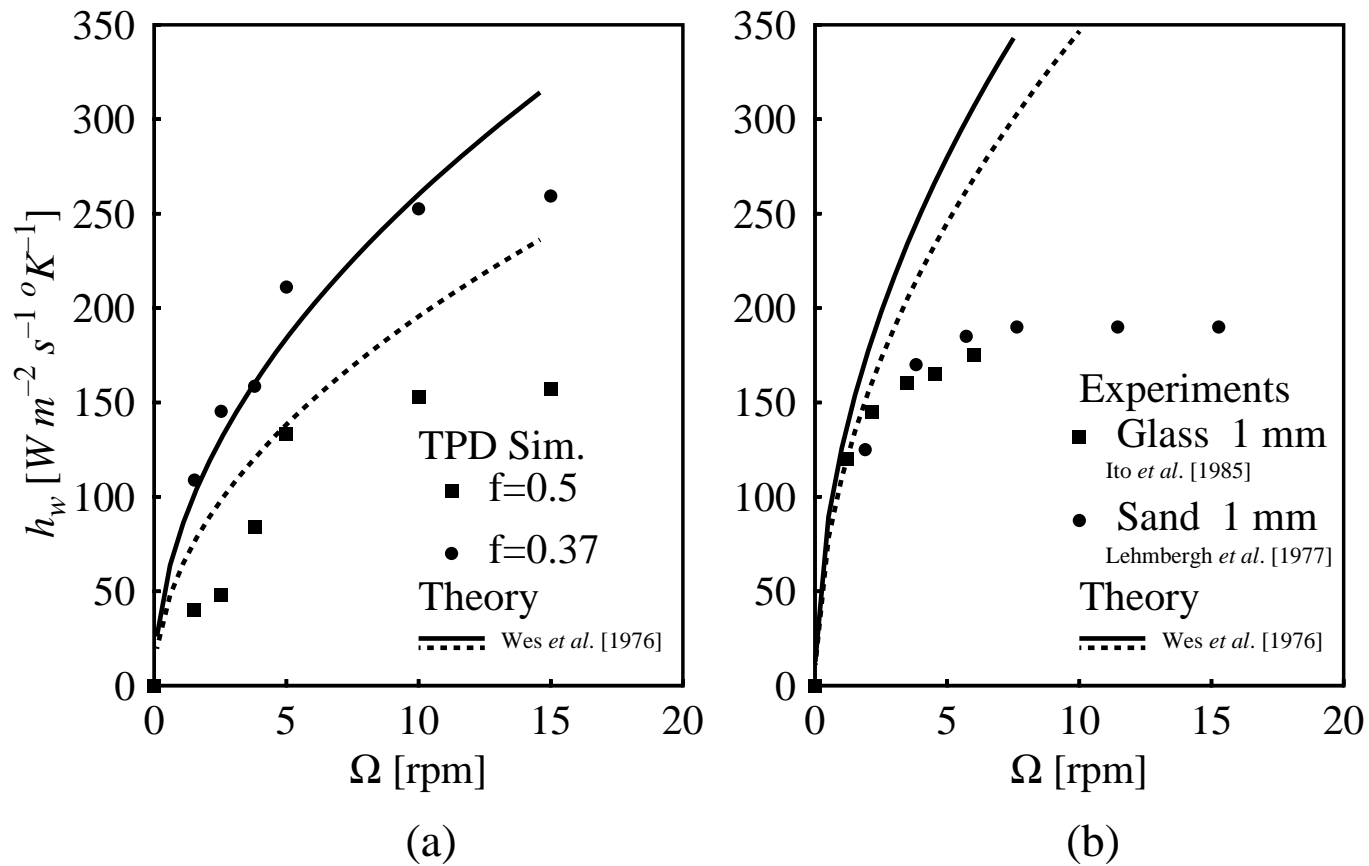
Figure 5.19 Comparison of the heat transfer coefficient as determined from TPD, experiments and theoretical models based on penetration theory (Eq. 5-14). (a) TPD simulations (b) Experimental data.

6.0   SUMMARY AND OUTLOOK

Granular media are frequently encountered in different fields of science and industry. These materials exhibit a vast array of unusual phenomena, and their physicochemical and transport properties are of interest in the analysis, design and optimization of industrial processes and in the understanding of natural phenomena. A primary cause of much of this behavior can be traced to the unique nature of particle-particle interactions.

This dissertation addresses heat conduction in granular systems under static and slow flow conditions with the ultimate goals of providing some insight into the fundamentals of this process as well as developing computational tools for further study. A novel multi-scale, modeling technique – Thermal Particle Dynamics (TPD) – has been developed and used to examine heat conduction through static beds and slow granular flows of granular materials under vacuum conditions and in the presence of stagnant fluids.

In this work, a general picture of heat conduction in granular media for simple configurations such as static beds of particles under vacuum conditions and in the presence of stagnant fluids and for slow granular flows in a simple shear cell and a rotating drum has been developed. In its simplest form – elastic, perfectly contacting particles under vacuum – TPD is capable of capturing details of particle-level temperature profiles which have not been previously reported, without requiring adjustable parameters. Results of both experiments and a microstructurally-based continuum model compare well with those obtained from TPD simulations.

6.1   Static particle beds

It is found that by matching the microstructure of an experimental system only qualitatively, quantitatively accurate estimates of effective properties are possible. In this sense,

the TPD technique is quite useful as a test-bed of new and existing theories of granular conductivity. In fact, even these simple results suggest that an important consideration has been missing from previous granular conduction studies – the stress distribution in the particle bed.

We find that stress and contact heterogeneities – due primarily to the existence of localized "chains" of particles which support the majority of an imposed load (stress chains) – may cause dramatic changes in the way that heat is transported by conduction. While these stress chains serve to augment heat flow along their axis, they effectively hamper perpendicular heat flow. This tends to create regions within a particle bed which are thermally isolated from their surroundings, possibly supporting previous claims that particle packing has a strong influence on the size and location of reactor hot spots [219]. Moreover, non-uniformities in both temperature and heat flow, similar to those found during combustion synthesis of powdered ceramics [220] or for electrical conduction during varistor failure [221], occur over length scales which would be difficult, if not impossible, to capture in even the most rigorous of effective medium approximations [10]. These non-uniformities could certainly have a profound effect on a variety of materials processing operations and require more investigation. However, our results indicate that with a reasonable choice of the relevant parameters, the effective medium theories can provide a good approximate description of the effective properties in static granular media.

An interesting trend is seen when the anisotropy of the conductivity is examined. For low compressive loads, when the width of the distribution of contact force magnitudes is large, both TPD and the fabric tensor-based effective conductivity expression [96] exhibit relatively strong anisotropy. This effect seems to decrease as the compressive load is increased. A similar effect is present when the aspect ratio of the bed is varied or when the geometry of the bounding walls is changed. This suggest that the microstructure of a granular bed can

be altered by changing the bed geometry or the imposed load and, as in traditional materials processing, the effective properties can be *tuned* via these changes in microstructure.

It has been demonstrated that for $k_s/k_f \gg 1$, TPD provides good qualitative and quantitative agreement between measured and calculated values of the effective conductivity for a wide variety of materials and for packed beds at different loads in the presence of both liquid and/or gases. In general, the values predicted from TPD seem to deviate more from the experimental observations as the ratio k_s/k_f gets smaller. This behavior is not surprising since the model is built on the assumption that $k_s/k_f \gg 1$ (so that heat transfer between non-contacting particles may be ignored) and the heat storage capacity of the fluid is ignored. However, it is important to note the wide range of conductivities over which the model has been successfully applied, as well as the variety of fluids that have been used. Therefore, the present model can be used – within its limitations – to predict the results for a variety of measurements. The combination of TPD with a CFD technique using a similar approximation as that described by Hunt [9]; and/or by Li and Mason [174] for binary collition-dominated flows, could be used as a starting point for simulating systems without any restrictions on the ratio k_s/k_f.

6.2 Granular flows

We underline some preliminary results on heat conduction in slowly flowing granular media. We have shown that in simple shear flows the microstructural evolution – creation and loss of conduction paths – plays a very important role in granular media under flow. Our results indicate that at low shear rate the heat transfer process is dominated by conduction while at higher shear rates the convection of the particles seems to take over. At intermediate shear rates, a balance between conduction and convection is established. A

qualitative comparison with experimental observations by Wang and Campbell [120] indicate a reasonable agreement.

In rotating drums, due to the fact that the particle circulation patterns will change with changes in scale and arrangement of internals, no simple correlation between the heat transfer and mixing can be drawn. However, some trends of dependence have been observed when the transfer coefficient is linked to the degree of filling which determines the circulation time and therefore the degree of mixing. The rate of heat transfer is higher for shallower beds ($f \to 0$) which can be attributed to a higher rate of mixing as indicated by the k_{mix} values determined. Increasing the rotation rate and therefore the shear rate in the active layer improves mixing and therefore an enhanced heat transfer coefficient at the wall is observed with increasing rotation rate. These observations are in agreement with experimental observations by Boateng and Barr [102].

In both the systems considered here – systems where the motion is induced and relatively slow – stress chain dynamics (formation and collapse) and collision frequency play a significant role. In general, the two characteristic variables controlling the heat transfer process – namely, the effective conductivity in simple shear flow and the heat transfer coefficient at the wall in the rotating drum – increase with shear rate (increase in granular temperature). Though this was not studied in detail, the mechanisms by which the heat transport process takes place in these two systems appears to be similar: at low shear rates conduction through particle contacts dominates due to lasting contacts; as the shear rate increases, convective mixing caused by an increased granular temperature enhances the transport of heat and therefore the effective conductivity increases proportionally.

6.3 Outlook

In Section 4.2.5, we underline the possible importance of the bounding geometry on the contact distribution anisotropy but the physical mechanisms involved remain unclear. These preliminary results raise many fundamental questions and call for further investigation. At first, a more complete study is required to understand how this effects can be exploited with purposes of *tuning* the effective properties of the bed. Then, a question arises as to how these effects would be in 3D situations. Note that these observations might have important practical consequences in many instances where transport through the solid phase is essential for the process (for example, the cooling of exothermal packed bed reactors).

A binary mixture of granular materials of different size or density in a horizontal rotating cylinder is known to segregate [222, 223]. In the case of axial segregation, the components separate into bands of relatively pure single concentrations along the rotational axis of the drum. In addition to axial segregation, all granular mixtures also display radial segregation. For a mixture of different sized particles, the smaller particles form a radial core before axial segregation takes place. The same phenomenon occurs for a mixture of particles with different density. Few studies have been performed on the effects of segregation on heat transfer. Experimental observations and numerical results by Boateng and Barr [102] suggests that in strongly segregated systems, significant temperature differences exist whithin the bed. Some interesting questions arise about these transport phenomena. First, how the two phenomena of radial and axial segregation affect the heat transport. Can one of these factors or both enhance or hinder the heat transfer process. Second, the role of the cascading layer in assisting the heat redispersion. Although it has been thought that segregation and remixing – in dry systems – are driven primarily by surface effects, the experimental observations of Hill [223] suggest that there are structures beneath the surface (within the bulk) which may prove to be important for heat conduction. Similar experimental obser-

vations have been reported by Jain *et al.* [224] for granular slurries. Also, the interplay between segregation and heat transfer may produce new and interesting results as the time scales for heat transfer are different from those for the onset of segregation.

As presented in this work, the TPD method considers only conduction through beds of identical, elastic, smooth particles in a vacuum or in the presence of a stagnant fluid; however, this method is eminently extensible. Differing contact mechanics, and therefore contact conductance, can be included as are the effects of variations in particle mechanical and thermal properties. Further, polidispersity in size, shape and properties should be explored as well. Finally, incorporating into TPD the effects of fluid flow under conditions of granular flow may allow the analysis of more industrially relevant problems.

BIBLIOGRAPHY

BIBLIOGRAPHY

[1] Reynolds O. On the dilatancy of media comprised of rigid particles in contact. with experimental illustration. *Phil. Mag. J. Sci.*, 20:469–481, 1881.

[2] Ngadi A. and J. Rajchenbach. Intermittencies in the compression process of a model granular medium. *Phy. Rev. Lett.*, 80:273–276, 1998.

[3] Rege N. V. *Computational Modeling of Granular Materials*. PhD thesis, Massachusetts Institute of Technology, 1996.

[4] Wu Y. and R. J. Friauf. A model for including thermal conduction in molecular dynamics simulations. *J. Appl. Phys.*, 65:4714–4718, 1989.

[5] Lukes J. R., D. Y. Li, X.-G. Liang, and C.-L. Tien. Molecular dynamics study of solid thin-film thermal conductivity. *J. of Heat Transfer*, 122:536–543, 2000.

[6] Kincaid J. M., E.G.D. Cohen, and E. Hernandez. Nanoscale heat transfer on the picosecond time scale. *Fluid Phase Equilibria*, 183–184:389–397, 2001.

[7] Keblinski P., S. R. Phillpot, S.U.S. Choi, and J. A. Eastman. Mechanisms of heat flow in suspensions of nano-sized particles (nanofluids). *Int. J. Heat Mass Transfer.*, 45:855–863, 2002.

[8] Furmansky P. Effective macroscopic description for heat conduction in heterogeneous media. *Int. J. Heat Mass Transfer.*, 35:3047–3058, 1992.

[9] Hunt M. L. Discrete element simulations for granular material flows: Effective thermal conductivity and self-diffusivity. *Int. J. Heat Mass Transfer*, 40:3059–3068, 1997.

[10] Zhuang X., Didwania A. K., and J. D. Goddard. Simulation of the quasi-static mechanics and scalar transport properties of ideal granular assemblages. *J. Comp. Phys.*, 121:331–346, 1995.

[11] L. Bocquet, E. Charlaix, S. Ciliberto, and J. Crassous. Moisture-induced ageing in granular media and the kinetics of capillary condensation. *Nature*, 396:735–737, 1998.

[12] D. Hornbaker, R. Albert, I. Albert, A.-L. Barabási, and P. Schiffer. What keeps sandcastles standing. *Nature*, 387:765–767, 1997.

[13] Liu C. H., Nagel S., Shechter D., Coppersmith S., Majumdar S., Narayan O., and T. Witten. Force fluctuations in bead packs. *Science*, 269:513–515, 1995.

[14] Metcalfe G., Shibrot T., McCarthy J. J., and J. M. Ottino. Avalanche mixing of granular materials. *Nature*, 374:39–41, 1995.

[15] Patton J. S., Sabersky R. H., and C. E. Brennen. Convective heat transfer to rapidly flowing granular materials. *Int. J. Heat Mass Transfer*, 29:1263–1269, 1986.

[16] Massoudi M. and T. X. Phuoc. Flow and heat transfer due to natural convection in granular materials. *Int. J. Non-Lin. Mech.*, 34:347–359, 1999.

[17] Haff P.K. Grain flow as a fluid-mechanical problem. *J. Fluid Mech.*, 134:401–430, 1983.

[18] Thornton C. and D. J. Barnes. Computer simulated deformation of compact granular assemblies. *Acta Mech.*, 64:45–61, 1986.

[19] Jaeger H. M., Nagel S. R., and R. P. Behringer. The physics of granular material. *Physics Today*, April:32–38, 1996.

[20] Wittmer J. P., P. Claudin, M. E. Cates, and J. P. Bouchaud. An explanation for the stress minimum in sand piles. *Nature*, 382:336–338, 1996.

[21] C. H. Liu and S. Nagel. Sound in granular material: Disorder and nonlinearity. *Phys. Rev. B*, 48:15646–15650, 1993.

[22] C. Thornton, K. K. Yin, and M. J. Adams. Numerical simulation of the impact fracture and fragmentation of agglomerates. *J. Phys. D*, 29:424–435, 1996.

[23] Howell D. W. and R. P. Behringer. Fluctuations in granular media. *Chaos*, 9:559–572, 1999.

[24] Quintanilla J. and S. Torquato. Microstructure functions for a model of statistically inhomogeneous random media. *Physical Review E*, 55:1558–1565, 1997.

[25] Torquato S. Thermal conductivity of disordered heterogeneous media from microstructure. *Reviews in Chemical Engineering*, 4:151–204, 1987.

[26] Oda M. A mechanical and statistical model of granular material. *Soils and Foundations*, 14:13–27, 1974.

[27] Sahimi M. and T. T. Tsotsis. Transient diffusion and conduction in heterogeneous media: Beyond the classical effective-medium approximation. *Ind. Eng. Chem. Res.*, 36:3043–3052, 1997.

[28] W. W. M. Siu and S. H.-K. Lee. Transient temperature computation for a system of multiply contacting spheres in a 180-degree orientation. *J. Heat Trans.*, 121:739–742, 1999.

[29] Goddard J. D. History effects in transient diffusion through heterogeneous media. *Ind. Eng. Chem. Res.*, 31:713–721, 1992.

[30] Bauer R. and E.U. Schlünder. Effective radial thermal conductivity of packings in gas flow. part ii. thermal conductivity of the packing fraction without gas flow. *International Chemical Engineering*, 18:189–204, 1978.

[31] Cheng G. J., Yu A.B., and P. Zulli. Evaluation of effective thermal conductivity from the structure of a packed bed. *Chem. Eng. Sci.*, 54:4199–4209, 1999.

[32] Logtenberg S.A. and A. G. Dixon. Cfd studies of the effects of temperature-dependent physical properties on fixed bed heat transfer. *Ind. Eng. Chem. Res.*, 37:739–747, 1998.

[33] D.J. Gunn, M.M. Ahmad, and M.N. Sabri. Radial heat transfer to fixed beds of particles. *Chem. Eng. Sci.*, 42:2163–2171, 1987.

[34] Brenner H. and D. A. Edwards. *Macrotransport Processes*. Butterworth-Heinemann, Boston, 1993.

[35] Bird R.B., Stewart W.E., and E.N. Lightfoot. *Transport Phenomena*. John Wiley & Sons, New York, 1960.

[36] Slattery J. C. *Advanced Transport Phenomena*. Cambridge, Cambridge, 1999.

[37] Batchelor G. K. and R. W. O'Brien. Thermal or electrical conduction through a granular material. *Proc. R. Soc. Lond.*, 355:313–333, 1977.

[38] Kirkpatrick S. Percolation and conduction. *Rev. Mod. Phy.*, 45:574–588, 1973.

[39] Lee T. Y. R. and R. E. Taylor. Thermal diffusivity of dispersed materials. *J. of Heat Transfer*, 100:720–724, 1978.

[40] Kerrisk J. F. Thermal diffusivity of heterogeneous materials. *J. Appl. Phys.*, 42:267–271, 1971.

[41] Kerrisk J. F. Thermal diffusivity of heterogeneous materials ii: Limits of the steady state approximation. *J. Appl. Phys.*, 43:112–117, 1972.

[42] Truong H. V. and G. E. Zinsmeister. Experimental study of heat transfer in layered composites. *Int. J. Heat Mass Transfer.*, 21:905–909, 1978.

[43] Quintard M., Kaviany M., and S. Whitaker. Two-medium treatment of heat transfer in porous media: numerical results for effective properties. *Advances in Water Resources*, 20:77–94, 1997.

[44] Maurer M. J. and H.A. Thompson. Non-fourier effects at high heat fluxes. *J. of Heat Transfer*, pages 284–286, 1973.

[45] Baumeister K. J. and T. D. Hamill. Hyperbolic heat conduction equation: A solution for the semi-infinite body problem. *J. of Heat Transfer*, pages 543–548, 1969.

[46] Taitel Y. On the parabolic, hyperbolic and discrete formulation of the heat conduction equation. *Int. J. Heat Mass Transfer.*, 15:369–371, 1972.

[47] Luikov A. V. Application of irreversible thermodynamics methods to investigation of heat and mass transfer. *Int. J. Heat Mass Transfer.*, 9:139–152, 1966.

[48] Batycky R. P. and H. Brenner. On the need for fictitious initial conditions in effective medium theories of transient nonconservative transport phenomena. some elementary unsteady-state heat conduction examples. *Chem. Eng. Comm.*, 152-153:173–187, 1996.

[49] Batycky R. P. and H. Brenner. Thermal macrotransport processes in porous media. a review. *Advances in Water Resources*, 20:95–110, 1997.

[50] Joseph D. D. and L. Preziosi. Heat waves. *Rev. Mod. Phy.*, 61:41–73, 1989.

[51] Marchioro M. and A. Prospereti. Heat conduction ina non-uniform composite with spherical inclusions. *Proc. R. Soc. Lond.*, A455:1483–1508, 1999.

[52] Mukasyan A. S., Rogachev A. S., and A. Varma. Mechanisms of reaction wave propagation during combustion synthesis of advanced materials. *Chem. Eng. Sci.*, 54:3357–3367, 1999.

[53] Antonishin N. V., Simchenko L. E., and V. V. Lushchikov. Discrepancy between theoretical and experimental data on non-steady heat conduction in disperse systems. *Journal of Engineering Physics*, 13:296–303, 1967.

[54] Hwang S., Mukasyan A. S., and A. Varma. Mechanisms of combustion wave propagation in heterogeneous reaction systems. *Combustion and Flame*, 115:354–363, 1998.

[55] Dunmead S. D. and Z. A. Munir. Temperature profile analysis in combustion synthesis: I, theory and background. *J. Am. Ceram. Soc.*, 75:175–179, 1992.

[56] Dunmead S. D. and Z. A. Munir. Temperature profile analysis in combustion synthesis: Ii, experimental observations. *J. Am. Ceram. Soc.*, 75:180–188, 1992.

[57] Moyne C., Didierjean S., Amaral Souto H.P., and O. T. da Silveira. Thermal dispersion in porous media: one-equation model. *Int. J. Heat Mass Transfer.*, 43:3853–3867, 2000.

[58] Brenner H. Dispersion resulting from flow through spatially periodic porous media. *Phil. Trans. R. Soc. Lond. A*, A297:81–133, 1980.

[59] Aris R. On the dispersion of a solute in a fluid flowing through a tube. *Proc. R. Soc. Lond.*, A235:67–77, 1956.

[60] Horn F.J.M. Calculation od dispersion coefficients by means of moments. *AIChEJ*, 17:613–620, 1971.

[61] Brenner H. A general theory of taylor dispersion phenomena. *PhysicoChem. Hydrodyn.*, 1:91–423, 1980.

[62] Taylor G. I. Dispersion of soluble matter in solvent flowing slowly through a tube. *Proc. R. Soc. Lond.*, A219:186–203, 1953.

[63] Taylor G. I. The dispersion of matter in turbulent flow through a pipe. *Proc. R. Soc. Lond.*, A223:446–468, 1954.

[64] Tzou D. Y. The generalized lagging response in samall-scale and high-rate heating. *Int. J. Heat Mass Transfer.*, 38:3231–3240, 1995.

[65] Tzou D. Y. and J. K. Chen. Thermal lagging in random media. *J. of Therm. and Heat Transfer*, 12:567–574, 1998.

[66] Özişik M. N. and D. Y. Tzou. On the wave theory in heat conduction. *J. of Heat Transfer*, 116:526–535, 1994.

[67] Sangani A. S. and A. Acrivos. The effective conductivity of a periodic array of spheres. *Proc. R. Soc. London Series A*, 386:263–275, 1983.

[68] Bonnecaze R. T. and J. F. Brady. The effective conductivity of random suspensions of spherical particles. *Proc. R. Soc. Lond.*, A 432:445–465, 1991.

[69] Lee Y. M., Haji-Sheikh A., Fletcher L. S., and G. P. Peterson. Effective thermal conductivity in multidimensional bodies. *Journal of Heat Transfer*, 116:17–27, 1994.

[70] Maxwell J. C. *A treatise on elasticity and magnetism.* Pergamon Press, Oxford, 1904.

[71] Kaviany M. *Principles of Heat Transfer in Porous Media.* Springer-Verlag, New York, 1995.

[72] Cheng P. and C-T. Hsu. Heat conduction. In D. B. Ingham and I. Pop, editors, *Transport phenomena in porous media*, pages 57–76. Pergamon, Amsterdam, 1998.

[73] Tavman I. H. Effective thermal conductivity of granular porous materials. *Int. Comm. Heat Mass Transfer*, 23:169–176, 1996.

[74] Dutta A. and R. A. Mashelkar. Thermal conductivity of structured liquids. *Advances in Heat Transfer*, 18:161–239, 1987.

[75] Slavin A.J., Londry F.A., and J. Harrison. A new model for the efective thermal conductivity of packed beds of solid spheroids. *Int. J. Heat Mass Transfer.*, 43:2059–2073, 2000.

[76] Molerus O. Heat transfer in moving beds with a stagnant interstitial gas. *Int. J. Heat Mass Transfer.*, 40:4151–4159, 1997.

[77] Buonanno G. and A. Carotenuto. The effective thermal conductivity of a porous medium with interconnected particles. *Int. J. Heat Mass Transfer.*, 40:393–405, 1997.

[78] Buonanno G. and A. Carotenuto. The effective thermal conductivity of packed bed of spheres for a finite contact area. *Numerical Heat Transfer, Part A*, 37:343–357, 2000.

[79] Zinchenko A. Z. Effective conductivity of loaded granular materials by numerical simulation. *Phil. Trans. R. Soc. Lond. A*, 356:2953–2998, 1998.

[80] Wu A. K. C. and S.H.-K. Lee. Sphere packing algorithm for heat transfer studies. *Numerical Heat Transfer, Part A*, 37:637–651, 2000.

[81] Siu W.W. and S.H. Lee. Effective conductivity computation of a packed bed using constriction resistance and contact angle effects. *Int. J. Heat Mass Transfer.*, 43:3917–3924, 2000.

[82] P. Furmanski. Effective macroscopic description for heat conduction in heterogeneous materials. *Int. J. Heat Mass Transfer.*, 35:3047–3058, 1992.

[83] Rothenburg L. and R. J. Bathurst. Analytical study of induced anisotropy in idealized granular materials. *Géotechnique*, 39:601–614, 1989.

[84] Oda M. and H. Nakayama. Yield function for soil with anisotropic fabric. *J. Eng. Mech.*, 115:89–104, 1989.

[85] Kanatani K-I. Distribution of directional data and fabric tensors. *Int. J. Engng. Sci.*, 22:149–164, 1984.

[86] Satake M. Constitution of mechanics of granular materials through the graph theory. In S.C. Cowin and M. Satake, editors, *U.S.-Japan Seminar in Continuum Mechanics and Statistical Approaches in the Mechanics of Granular Materials*, pages 47–62. 1978.

[87] Subhash G., Nemat-Nasser S., Mehrabadi M. M., and H. M. Shodja. Experimental investigaction of fabric-stress relations in granular materials. *Mechanics of Materials*, 11:87–106, 1991.

[88] Chang C. S, Chao S. J., and Y. Chang. Estimates of elastic moduli for granular material with anisotropic random packing structure. *Int. J. Solids Structures*, 32:1989–2008, 1995.

[89] McGreavy C., Foumeny E.A., and K.H. Javed. Characterization of transport properties for fixed bed in terms of local bed structure and flow distribution. *Chem. Eng. Sci.*, 41:787–797, 1986.

[90] Haughey D.P. and S.G. Beveridge. Structural properties of packed beds: A review. *Can. J. Chem. Eng*, 47:130–140, 1969.

[91] Mariani N.J, Bressa S., Mazza G., Martinez O., and G. Barreto. A bem formulation for evaluating conductive heat transfer rates in particulate systems. *Numerical Heat Transfer, B*, 31:459–476, 1997.

[92] Froment G. F. and K. B. Bischoff. *Chemical Reactor Analysis and Design.* John Wiley & Sons, New York, 1990.

[93] Bauer R. and E.U. Schlünder. Effective radial thermal conductivity of packings in gas flow. part i. convective transport coefficient. *International Chemical Engineering*, 18:181–188, 1978.

[94] Lemcoff N.O., Pereira S.I., and O.M. Martinez. Heat transfer in packed beds. *Reviews in Chemical Engineering*, 6:229–292, 1990.

[95] Zhuang X. *Computer Simulation and Experiments on the Quasi-Static Mechanics and Transport Properties of Granular Material.* PhD thesis, University of California, San Diego, 1993.

[96] Jagota A. and C. Y. Hui. The effective thermal conductivity of a packing of spheres. *J. Appl. Mech.*, 57:789–791, 1990.

[97] Kuo C.Y, Frost J. D., and J. A. Chameau. Image analysis determination of stereology based fabric tensors. *Geotechnique*, 48:515–525, 1998.

[98] Kanatani K-I. Stereological determination of structural anisotropy. *Int. J. Engng. Sci.*, 22:531–546, 1984.

[99] Argento C. and D. Bouvard. Thermal conductivity of granular media. In C. Thornton, editor, *Powders & grains*, pages 129–134. A.A. Balkema, Rotterdam, 1993.

[100] Borkink J.G. and K.R. Westerterp. Influence of tube particle diameter on heat transport in packed beds. *AIChEJ*, 38:703–715, 1992.

[101] Roux S., Stauffer D., and H.J. Herrman. Simulation of disordered systems of cylinders.i. geometrical behaviour. *J. Physique*, 48:341–345, 1987.

[102] Boateng A. A. and P. V. Barr. A thermal model for the rotary kiln including heat transfer within the bed. *Int. J. Heat Mass Transfer.*, 39:2131–2147, 1996.

[103] Ding Y. L., R. N. Foster, J. P. Seville, and D. J. Parker. Scaling relationships for rotating drums. *Chem. Eng. Sci.*, 56:3737–3750, 2001.

[104] Yovanovich M. M. Thermal contact resistance across elastically deformed spheres. *J. Spacecraft Rockets*, 4:119, 1967.

[105] Holm R. *Electrical Contacts: Theory and Application.* Springer-Verlag, New York, 1967.

[106] Chan C. K. and C. L. Tien. Conductance of packed spheres in vacuum. *Journal of Heat Transfer*, pages 302–308, 1973.

[107] Duncan A. B., Peterson G.P., and L.S. Fletcher. Effective thermal conductivity within packed beds of spherical particles. *J. of Heat Transfer*, 111:830–836, 1989.

[108] Sridhar M. R. and M. M. Yovanovich. Elastoplastic contact conductance model for isotropic conforming rough surfaces and comparison with experiments. *Journal of Heat Transfer*, 118:3–9, 1996.

[109] Lambert M. A. and L. S. Fletcher. Thermal contact conductance of spherical rough metals. *Journal of Heat Transfer*, 119:684–690, 1997.

[110] Majumdar A. and C. L. Tien. Fractal network model for contact conductance. *Journal of Heat Transfer*, 113:516–525, 1991.

[111] Greenwood J. A. and J.H. Tripp. The elastic contact of rough spheres. *Journal of Applied Mechanics*, March:153–159, 1967.

[112] Peterson G. P. and L. S. Fletcher. Measurement of the thermal conductance and thermal conductivity of anodized aluminium coatings. *Journal of Heat Transfer*, 112:579–585, 1990.

[113] Marotta E. E. and L. S. Fletcher. Thermal contact conductance for aluminum and stainless-steel contacts. *Journal of Thermophysics and Heat Transfer*, 12:374–381, 1998.

[114] Lambert M. A. and L. S. Fletcher. Review of models for thermal contact conductance of metals. *Journal of Thermophysics and Heat Transfer*, 11:129–140, 1997.

[115] Sridhar M. R. and M. M. Yovanovich. Review of elastic and plastic contact conductance models: Comparison with experiment. *Journal of Thermophysics and Heat Transfer*, 8:633–640, 1994.

[116] Schlünder E.U. Heat transfer to moving spherical packings at short contact times. *International Chemical Engineering*, 20:550–554, 1980.

[117] Boateng A. A. and P. V. Barr. Granular flow behaviour in the transverse plane of a partially filled rotating cylinder. *J. Fluid Mech.*, 330:233–249, 1997.

[118] Savage S. B. Analyses of slow high-concentration flows of granular materials. *J. Fluid Mech.*, 377:1–26, 1998.

[119] Campbell C. S. Self-diffusion in granular shear flows. *J. Fluid Mech.*, 348:85–101, 1997.

[120] Wang D. G. and C. S. Campbell. Reynolds analogy for shearing granular material. *J. Fluid Mech.*, 244:527–546, 1992.

[121] Natarajan V. V. R. and M. L. Hunt. Heat transfer in verticle granular flows. *Exp. Heat Trans.*, 10:89–107, 1997.

[122] Sullivan W. N. and R. H. Sabersky. Heat transfer to flowing granular media. *Int. J. Heat Mass Transfer*, 18:97–107, 1975.

[123] Spelt J. K., Brennen C. E., and R. H. Sabersky. Heat transfer to flowing granular material. *Int. J. Heat Mass Transfer*, 25:791–796, 1982.

[124] Muchowski E. Heat transfer from the bottom of vibrated vessels to packing of spheres at atmospheric pressure and under vacuum. *International Chemical Engineering*, 20:564–576, 1980.

[125] Wunschmann J. and E. U. Schlünder. Heat transfer from heated surfaces to spherical packings. *International Chemical Engineering*, 20:555–563, 1980.

[126] Ito N., Obata K, and T. Hakuta. Heat transfer from the wall to a particle bed in a rotary drum. *Kagaku Kogaku Ronbunshu*, 9:628–634, 1983.

[127] Wes G. W., A. A Drinkenburg, and S. Stemerding. Heat transfer in a horizontal rotary drum reactor. *Powder Technol.*, 13:185–192, 1976.

[128] Lehmberg J., M. Hehl, and K. Schügerl. Transverse mixing and heat transfer in horizontal rotary drum reactors. *Powder Technol.*, 18:149–163, 1977.

[129] Natarajan V. V. R. and M. L. Hunt. Kinetic theory analysis of heat transfer in granular flows. *Int. J. Heat Mass Transfer.*, 41:1929–1944, 1998.

[130] Kubie J. Heat transfer between gas fluidized beds and inmersed surfaces. *Int. J. Heat Mass Transfer.*, 28:1345–1353, 1985.

[131] Sun J. and M. M. Chen. A theoretical analysis of heat transfer due to particle impacts. *Int. J. Heat Mass Transfer*, 31:969–975, 1988.

[132] Chou C.-S. The steady inhomogeneous rapid granular shear flow of nearly elastic spheres. *Physica A*, 287:127–152, 2000.

[133] Lun C. K., S. B. Savage, D. J. Feffrey, and N. Chepurniy. Kinetic theories for granular flow:inelastic particles in couette flow and slightly inelastic particles in a general flow field. *J. Fluid Mech.*, 140:223–256, 1984.

[134] Hsiau S. S. and M. L. Hunt. Kinetic theory analysis of flow-induced particle diffusion and thermal conduction in granular material flows. *J. Heat Trans.*, 115:541–548, 1993.

[135] Campbell C. S. Rapid granular flows. *Annu. Rev. Fluid Mech.*, 22:57–92, 1990.

[136] Zhang Y. and C. S. Campbell. The interface between fluid-like and solid-like behaviour in two-dimensional granular flows. *J. Fluid Mech.*, 237:541–568, 1992.

[137] Campbell C. S. and C. E. Brennen. Computer simulations of granular shear flows. *J. Fluid Mech.*, 151:167–188, 1985.

[138] Karion A. and M. L. Hunt. Wall stresses in granular couette flows of mono-sized particles and binary mixtures. *Powder Technol.*, 109, 2000.

[139] Louge M. Y., J. T. Jenkins, and M. A. Hopkins. Computer simulations of rapid granular shear flows between parallel bumpy boundaries. *Phys. Fluids A*, 2:1042–1044, 1990.

[140] Sch*ddoto*llmann S. Simulation of a two-dimensional shear cell. *Phys. Rev. E*, 59:889–899, 1999.

[141] Lun C. K. Granular dynamics of inelastic spheres in couette flow. *Phys. Fluids*, 8:2868–2883, 1996.

[142] Lun C. K. Kinetic theory for granular flow of dense, slightly inelastic, slightly rough spheres. *J. Fluid Mech.*, 233:539–559, 1991.

[143] Savage S. B. and D. J. Jeffrey. The stress tensor in a granular flow at high shear rates. *J. Fluid Mech.*, 110:255–272, 1981.

[144] Miller B., C. O'Hern, and R. P. Behringer. Stress fluctuations for continuously sheared granular materials. *Phy. Rev. Lett.*, 77, 1996.

[145] Schwartz O. J., Horie Y., and M. Shearer. Discrete element investigation of stress fluctuations in granular flow at high strain rates. *Phys. Rev. E*, 57, 1998.

[146] Zamankhan P. and T. Tynjälä. stress fluctuations in continuously sheared dense granular materials. *Phys. Rev. E*, 60, 1999.

[147] Antony S. J. Evolution of force distribution in three-dimensional granular media. *Phys. Rev. E*, 63, 2000.

[148] Khakhar D. V., McCarthy J. J., Shinbrot T., and J. M. Ottino. Transverse flow and mixing of granular materials in a rotating cylinder. *Phys. Fluids*, 9:31–43, 1997.

[149] Khakhar D. V., McCarthy J. J., and J. M. Ottino. Radial segregation of granular materials in rotating cylinders. *Phys. Fluids*, 9:3600–3614, 1997.

[150] McCarthy J. J., Shinbrot T., Metcalfe G., Wolf J. E., and J. M. Ottino. Mixing of granular materials in slowly rotated containers. *AIChEJ*, 42:3351–3363, 1996.

[151] McCarthy J. J. and J. M. Ottino. Particle dynamics simulation: A hybrid technique applied to granular mixing. *Powder Technol.*, 97:91–99, 1998.

[152] Heydenrych M. D. *Modeling of rotary kilns*. PhD thesis, University of Twente, 2001.

[153] Mellman J. The tranverse motion of solids in rotating cylinders-forms of motion and transition behavior. *Powder Technol.*, 118:251–270, 2001.

[154] Boateng A. A. and P. V. Barr. Modelling of particle mixing and segregation in the transverse plane of a rotary kiln. *Chem. Eng. Sci.*, 51:4167–4181, 1996.

[155] Mu J. and D. D. Perlmutter. The mixing of granular solids in a rotary cylinder. *AIChEJ*, 26:928–934, 1980.

[156] Hogg R. and D. W. Fuerstenau. Transverse mixing in rotating cylinders. *Powder Technol.*, 6:139–147, 1972.

[157] Hogg R., G. Mempel, and D. W. Fuerstenau. The mixing of trace quantities into particulate solids. *Powder Technol.*, 2:223–228, 1968/69.

[158] McCarthy J. J. *Mixing, segregation, and flow of granular materials*. PhD thesis, Northwestern University, 1998.

[159] Savage S. B. Disorder, diffusion and structure formation in granular flow. In D. Bideau and A. Hansen, editors, *Disorder and granular media*, pages 255–285. Elsevier Science, Amsterdam, 1993.

[160] Hsiau S.-S. andY. M. Shieh. Effect of solid fraction on fluctuations and self-diffusion of sheared granular flows. *Chem. Eng. Sci.*, 55:1969–1979, 2000.

[161] Nakagawa N., S.A. Altobelli, A. Caprihan, E. Fukushima, and E.K Jeong. Non-invasive measurements of granular flows by magnetic resonance imaging. *Experiments in fluids*, 16:54–60, 1993.

[162] ed. C. Thornton. Special issue of numerical simulations of discrete particle systems. *Powder Technol.*, 109, 2000.

[163] Tai Q. M. and M. H. Sadd. A discrete element study of the relationship of fabric to wave propagational behaviours in granular material. *Int. J. Numer. Anal. Meth. Geomech.*, 21:295–311, 1997.

[164] Bardet J. P. Introduction to computational granular mechanics. In B. Cambou, editor, *Behavior of granular materials*, pages 99–169. Springer-Verlag, 1998.

[165] Ng T-T. Small-strain response of random arrays of spheres using dem. *J. Eng. Mech.*, 122:239–244, 1996.

[166] Kaneko Y., Shiojima T., and M. Horio. Dem simulation of fluidized beds for gas-phase olefin polymerization. *Chem. Eng. Sci.*, 54:5809–5821, 1999.

[167] Mikami T., Kamiya H., and M. Horio. Numerical simulation of cohesive powder behavior in a fluidized bed. *Chem. Eng. Sci.*, 53:1927–1940, 1998.

[168] Tsuji Y., Kawaguchi T., and T. Tanaka. Discrete particle simulation of two-dimensional fluidized bed. *Powder Technology*, 77:79–87, 1993.

[169] Yen K.Z.Y. and T.K. Chaki. A dynamic simulation of particle rearrangement in powder packings with realistic interactions. *J. Appl. Phys.*, 71:3164–3173, 1992.

[170] Cundall P. A. and O. D. L. Strack. A discrete numerical model for granular assemblies. *Géotechnique*, 29:47–65, 1979.

[171] Tsuji Y., Tanaka T., and T. Ishida. Lagrangian numerical simulation of plug flow of cohesionless particles in a horizontal pipe. *Powder Technol.*, 71:239–250, 1992.

[172] Nase S.T., Vargas W.L., and J. J. McCarthy. Discrete characterization tools for wet granular media. *Powder Technology*, 116:214–223, 2001.

[173] K. Kuwagi, T. Mikami, and M. Horio. Numerical simulation of metallic solid bridging particles in a fluidized bed at high temperature. *Powder Technol.*, 109 (1):27–40, 2000.

[174] Li J. and D. J. Mason. A computational investigation of transient heat transfer in pneumatic transport of granular particles. *Powder Technol.*, 112:273–282, 2000.

[175] Johnson K. L. *Contact Mechanics*. Cambridge University Press, Cambridge, 1987.

[176] Hertz H. Ueber die berhrungfester elastischer korper. *J. renie ange. Math.*, 92:1–15, 1881.

[177] Mindlin R. D. Compliance of elastic bodies in contact. *J. Appl. Mech.*, 16:256–270, 1949.

[178] McCarthy J. J. and J. M. Ottino. Particle dynamics simulation: A hybrid technique applied to granular mixing. *Powder Technol.*, 97:91–99, 1998.

[179] Thornton C. and C. W. Randall. Applications of theoretical contact mechanics to solid particle system simulation. In M. Satake and J. T. Jenkins, editors, *Micromechanics of Granular Material*, pages 133–142. Elsevier Science Publishers, Amsterdam, 1988.

[180] Fletcher L. S. Recent developments in contact conductance heat transfer. *Journal of Heat Transfer*, 110:1059–1070, 1988.

[181] Vargas W. L. and J. J. McCarthy. Heat conduction in granular materials. *AIChEJ*, 47:1052–1059, 2001.

[182] Vargas W. L. and J. J. McCarthy. Unsteady heat conduction in granular media. In *Mat. Res. Soc. Symp. Proc.*, volume 627, pages BB3.9.1–BB3.9.6, 2000.

[183] Masamune S. and J. M. Smith. Thermal conductivity of beds of spherical particles. *I & EC Fundamentals*, 2:136–143, 1963.

[184] Kunii D and J. M. Smith. Heat transfer characteristics of porous rocks. *AIChEJ*, 6:71–77, 1960.

[185] Okazaki M. Heat and mass transport properties of heterogeneous materials. *Drying'85*, pages 84–96, 1985.

[186] Kennard E. H. *Kinetic theory of gases.* McGraw Hill, N.Y., 1938.

[187] Rose W. Volumes and surface areas of pendular rings. *J. Appl. Phys.*, pages 687–691, 1958.

[188] Munjiza A. and K. R. F. Andrews. Nbs contact detection algorithm for bodies of similar size. *Int. J. Numer. Meth. Engng.*, 43:131–149, 1998.

[189] Vargas W. L. and J. J. McCarthy. Stress effects on the conductivity of particulate beds. submitted to Chem. Eng. Sci., 2001.

[190] Vargas W. L. and J. J. McCarthy. Conductivity of granular media with stagnant interstitial fluids via thermal particle dynamics simulation. submitted to Int. J. Heat Mass Transfer, 2001.

[191] Reid R. C, Prausnitz J. M., and B. E. Poling. *The properties of gases and liquids.* McGraw Hill, N.Y., 1987.

[192] Shackelford J. F. *Introduction to materials science for engineers.* Macmillan, N.Y., 1985.

[193] Vargaftik N B., Filippov L.V., Tarzimanov A., and E. Totskii. *Handbook of thermal conductivity of liquids and gases.* CRC Press, London, 1994.

[194] Le Neindre B., Tufeu R., Bury P., Johannin P., and B. Vodar. The thermal conductivity coefficients of some noble gases. In C. Y. Ho and R. E. Tylor, editors, *Thermal Conductivity*, pages 75–100. Plenum Press, N.Y., 1969.

[195] Zharkova G. M. Temperature field visualization using liquid crystal method. *Experimental Heat Transfer*, 4:83–92, 1991.

[196] Dabiri D. and M. Gharib. Digital particle image thermometry: The method and implementation. *Experiments in fluids*, 11:77–86, 1991.

[197] Akino N., Kunigi T., Ichimiya K., Mitsushiro K., and M. Ueda. Improved liquid crystal thermometry excluding human color sensation. *J. of Heat Transfer*, 111:558–565, 1989.

[198] Ichimiya K., Akino N., and T. Kunigi. A fundamental study of the heat transfer and flow situation around spacers. *Int. J. Heat Mass Transfer.*, 33:2451–2462, 1990.

[199] Bejan A. *Convecttive Heat Transfer*. Wiley, N.Y., 1984.

[200] Peterson D., Hu S.H., Richards C.D., and R.F. Richards. The measurement of droplet temperature using thermochromic liquid crystals. *30th National Heat Transfer Conference*, 1995.

[201] Fortner B. and T.E. Meyer. *Number by Colors*. Springer-Verlag, New York, 1997.

[202] Thornton C. Force transmission in granular media. *KONA*, 15:81–90, 1997.

[203] B. Cambou. From global to local variables in granular materials. In C. Thornton, editor, *Powders & grains*, pages 129–134. A.A. Balkema, Rotterdam, 1993.

[204] Thornton C. and S. J. Anthony. Quasi-static deformation of particulate media. *Phil. Trans. R. Soc. Lond. A*, 356:2763–2782, 1998.

[205] Kolb E., T. Mazozi, E. Clement, and J. Duran. Force fluctuations in a vertically pushed granular column. *Eur. Phys. J. B.*, 8:483–491, 1999.

[206] Rossmanith H. P. and A. Shukla. Photoelastic investigation of dynamic load transfer in granular media. *Acta Mechanica*, 42:211–225, 1982.

[207] Janssen H. Tests on grain pressure silos. *Zeits. d. Vereins Deutsch Ing.*, 39:1045–1049, 1895.

[208] Mueth D. M, Jaeger H. J., and S. R. Nagel. Force distribution in a granular medium. *Phys. Rev. E*, 57:3164–3169, 1998.

[209] Masamune S. and J. M. Smith. Thermal conductivity of porous catalyst pellets. *J. of Chem. Eng. Data*, 8:54–58, 1963.

[210] Zeng S. Q., Hunt A., and R. Greif. Mean free path and apparent thermal conductivity of a gas in a porous medium. *J. of Heat Transfer*, 117:758–761, 1995.

[211] Hadley G. R. Thermal conductivity of packed metal powders. *Int. J. Heat Mass Transfer.*, pages 909–920, 1986.

[212] Pratt A. W. Heat transmission in low conductivity materials. In R. P. Tye, editor, *Thermal Conductivity*, pages 312–313. Academic Press, London, 1969.

[213] Büssing W. and H.J. Bart. Thermal conductivity of unsaturated packed beds – comparison of experimental results and estimation methods. *Chem. Eng. and Processing*, 36:119–132, 1997.

[214] Crane R. A. and R. I. Vachon. A prediction of bounds on the effective thermal conductivity of granular materials. *Int. J. Heat Mass Transfer.*, pages 711–723, 1977.

[215] Prasad V., Kladias N., Bandyopadhaya A., and Q. Tian. Evaluation of correlations for stagnant thermal conductivity of liquid-saturated porous beds of spheres. *Int. J. Heat Mass Transfer.*, pages 1793–1796, 1989.

[216] Nozad I., Carbonell R. G., and S. Whitaker. Heat conduction in multiphase flows-ii. *Chem. Eng. Sci.*, pages 857–863, 1985.

[217] Zamankhan P., Tafreshi H. V., Polashenski W., Sarkomaa P., and C. L. Hyndman. Shear induced diffusive mixing in simulations of dense couette flow of rough, inelastic hard spheres. *J. of Chem. Phy.*, 109:4487–4491, 1998.

[218] Botterill J. S. M. *Fluid-bed heat transfer*. Academic Press, N.Y., 1975.

[219] Balakotaiah V., Christoforatou E.L., and D.H. West. Transverse concentration and temperature nonuniformities in adiabatic packed bed catalytic reactors. *Chem. Eng. Sci.*, 54:1725–1734, 1999.

[220] Varma A., Rogachev A. S., Mukasyan A. S., and S. Hwang. Combustion synthesis of advanced materials: Principles and applications. *Adv. Chem. Eng.*, 24:79–226, 1998.

[221] Vojta A., Wen Q., and D. R. Clarke. Influence of microstructural disorder on the current transport behavior of varistor ceramics. *Computational Material Science*, 6:51–62, 1996.

[222] Nakagawa N., S.A. Altobelli, A. Caprihan, and E. Fukushima. Nmri study: axial migration of radially segregated core of granullar mixtures in a horizontal rotating cylinder. *Chem. Eng. Sci.*, 52:4423–4428, 1997.

[223] Hill K. M., A. Caprihan, and J. Kakalios. Bulk segregation in rotated granular material measured by magnetic resonance imaging. *Phy. Rev. Lett.*, 78:50–53, 1997.

[224] Jain N., J. D. Khakhar, R. M. Lueptow, and J. M. Ottino. Self-organization in granular slurries. *Phy. Rev. Lett.*, 86:3771–3774, 2001.